The effect of small modifications in primary sequence of antimicrobial peptides on their membrane activities

by

Amy M.Won

A thesis submitted to the Faculty of Graduate and Postdoctoral Affairs in partial fulfillment of the requirements for the degree of

Doctor of Philosophy

in

Chemistry

Carleton University
Ottawa, Ontario

Library and Archives Canada

Published Heritage Branch

395 Wellington Street
Ottawa ON K1A 0N4
Canada

Bibliothèque et Archives Canada

Direction du Patrimoine de l'édition

395, rue Wellington
Ottawa ON K1A 0N4
Canada

Your file Votre référence
ISBN: 978-0-494-93703-7

Our file Notre référence
ISBN: 978-0-494-93703-7

ABSTRACT

The continuous unnecessary and inappropriate usage of antibiotics has resulted in emergence of antibiotic resistant bacterial pathogens. Antimicrobial peptides are believed to be one of the best alternatives to treat these resistant strains. However, the unknown mechanism of action is one main reason that hinders their clinical usage. In this thesis, four projects were undertaken to allow further understanding of the effect that various parameters have on the peptide/lipid interaction using Langmuir-Blodgett monolayer techniques, atomic force microscopy, leakage assay, ultra-violet resonance Raman Spectroscopy, antimicrobial assay, X-ray photoemission electron microscopy, and scanning transmission X-ray microscopy.

In the first project, tryptophan containing peptide pEM-2 (Chapter 3) demonstrated that electrostatic interactions play a crucial role in the initial recognition and binding of the peptide; however, more parameters besides ionic attraction are involved in membrane rupturing activity. The data further support the correlation between the number of tryptophans and the antimicrobial activity and other derivatives similar to pEM-2. In the second project (Chapter 4), using the smallest naturally found linear alpha-helical antimicrobial peptide anoplin the effects of deamidation and enantiomer substitution on the interaction with model membrane were investigated. The study showed the importance of amidation in anoplin and that its action is non-specific. The third project (Chapter 5) used two other derivatives of anoplin to demonstrate that not only charge, but also peptide helicity and amphipathicity affect membrane lytic activity of anoplin. Latarcin 2a was investigated in the last project (Chapter 6) for hinge property examination. Through single amino acid substitution, the more rigid derivative latarcin 2aG11A exhibited increased

cytolytic activity. Both latartcin 2a derivatives induce membrane reorganization by reducing line tension of the liquid ordered phase upon peptide addition, visualized via *in situ* AFM.

ACKNOWLEDGEMENTS

My deepest and most sincere gratitude is to my supervisor Dr. Anatoli Ianoul. I have been amazingly fortunate to have an advisor who offered me the freedom to explore on my own and at my own pace. At the same time thank you, Anatoli, for providing guidance and support patiently and understandingly for me to recover from stumbles. Furthermore, thank you for demonstrating and mentoring me to think outside the box for good science!

I am truly indebted and thankful to my beloved mother for her strength, support, motivation, and love!

I am gratefully and sincerely thank the course instructors, and comprehensive and thesis defense committees Dr. Maria DeRosa, Dr. David Miller, Dr. Zoya Leonenko, Dr. Linda J. Johnston, Dr. James Cheetham, Dr. Robert Burk, Dr. Sean Barry, Dr. P.R. Sundararajan, Dr. Bill Willmore, and Dr. Kent Storey for your challenges, guidance, encouragements and inspiration to broaden my view to become a better scientist.

Special thanks to Dr. Tyler Avis, Bryan Quan, Graham Galway, Fred Casselman, and Harrison Westwick for the extensive training, insightful discussion, and accessibility. Special thanks to Adam Bottomley, Iryna Buznytska, Stahs Pripotnev, Annamaria Ruscito, and Graham Galway for the awesome English 101. Special thanks to undergraduates Grace Idiong, Sorin Gustin, Akpawa Akuvi, Stahs Pripotnev, Annamaria Ruscito, Morin Khan, Steven Tshakatumba, and Altaf Mahmud for their assistance in this dissertation.

Truthful thanks to the rest of the Ianoul group members, friends and family for the much needed laugh, companionship, and support. Especially to Gary Sy for accompanying me all the experiments took place during late nights and weekends.

Last but not least, a big thanks to the Department of Chemistry, this dissertation would not have taken place as smoothly if it wasn't for all the valuable conversation and accessibility.

These studies were funded by Natural Science and Engineering Research Council (Ianoul A.), Canadian Foundation for Innovation (Ianoul A.), Early Researcher Award (Ianoul A.), Carleton University (Ianoul A. and Won A.), and Ontario Graduate Scholarship (Won A.).

TABLE OF CONTENTS

Abstract.....ii

Acknowledgements.....iv

List of Tables.....xi

List of Figures.....xii

List of Videos.....xx

List of Publications.....xxii

List of Conferences.....xxiii

List of Abbreviation.....xxv

Chapter 1 Introduction

1.1 Antibiotic resistant pathogens.....1

1.2 Antimicrobial peptides.....2

1.2.1 Parameters of antimicrobial peptides.....2

1.2.2 Proposed mechanism of actions of antimicrobial peptides.....5

1.3 The challenges and limitations of peptide drug development.....7

1.4 Model membranes.....9

1.5 Thesis objectives.....12

1.6 References.....15

Chapter 2 Experiments

2.1 Chemical.....23

2.2 Langmuir Blodgettry.....21

2.2.1 Pressure-area isotherm.....21

2.2.2 Critical micelle concentration.....23

2.2.3 Kinetic adsorption and critical pressure of insertion.....24

2.3 Liposome preparation.....25

2.4 Leakage assay.....27

2.5 Phosphate assay.....29

2.5.1 Ashed by KNO_3 and reduced by Fiske & Subbarow reagent.....29

2.5.2 Ashed by $HClO_4$ and reduced by Fiske & Subbarow reagent.....29

2.5.3 Ashed by H_2SO_4 and reduced by Ascorbic acid.....30

2.6 Atomic force microscopy.....30

2.6.1 Imaged monolayers of peptide, lipid, and peptide/lipid mixtures in air.....30

2.6.2 Imaged supported lipid bilayers in solution.....31

2.7 UVRR spectroscopy.....32

2.7.1 Sample preparations for Chapter 4.....32

2.7.2 Sample preparations for Chapter 5.....33

2.7.3 UVRR spectra collection.....33

2.8 X- ray spectromicroscopy.....34

2.9 Antimicrobial assay.....35

2.10 References.....36

Chapter 3 The effect of antimicrobial peptide pEM-2 on the interactions with phospholipid mono- and bilayers

3.1 Introduction.....39

3.2 Results and Discussion.....40

3.2.1 Monolayers of pEM-2.....40

3.2.2 Kinetics of pEM-2 binding to lipid monolayers.....42

3.2.3 Interaction of pEM-2 with DPPC monolayer.....46

3.2.4 Interaction of pEM-2 with DPPG monolayer.....47

3.2.5 The effect of calcium ions on pEM-2/lipid interaction.....53

3.2.6 Leakage assay.....54

3.3 References.....57

Chapter 4 The effects of deamidation and L- to D- amino acid substitution on the activity and membrane interactions of antimicrobial peptide anoplin

4.1 Introduction.....62

4.2 Results and Discussion.....63

4.2.1 Antimicrobial assay.....63

4.2.2 Raman spectra of anoplin derivatives in aqueous PBS, D_2O and TFE.....64

4.2.3 Interactions of anoplin derivatives with lipid vesicles.....67

4.2.4 Monolayers of anoplin derivatives with DPPC, DPPG and *E. coli* total lipid extract.....72

4.2.5 Kinetic of anoplin binding to a lipid monolayer.....82

4.2.6 Leakage assay.....87

4.3 Contribution.....91

4.4 References.....91

Chapter 5 Investigating the effect of point mutation on the secondary structure and membrane interaction of antimicrobial peptide anoplin

5.1 Introduction.....95

5.2 Results and Discussion.....96

5.2.1 Single and multiple amino acid substitutions change surface/membrane activity of anoplin.....97

5.2.2 UVRR spectroscopy probes conformational difference of anoplin Derivatives.....103

5.2.3 Membrane lytic activity of anoplin derivatives.....114

5.3 Contributions.....117

5.4 References.....118

Chapter 6 Investigating the hinge property of latarcin 2a on lipid model membranes

6.1 Introduction.....123

6.2 Results and Discussion.....127

6.2.1 Single amino acid replacement changes surface activity of latarcin 2a.....127

6.2.2 Single amino acid replacement changes molecular surface area and lipid/peptide monolayer morphology.....130

6.2.3. Deletion of the hinge region does not affect membrane-rupturing activity.....142

6.2.4 Supported lipid bilayers.....145

6.2.4.1 Raft domains in supported lipid bilayers visualized by atomic force Microscopy.....145

6.2.4.2 Peptides reduce line tension and reorganize morphology of supported lipid bilayer.....146

6.2.4.3 Peptide oligomerization may contribute to the different mode of action.....154

6.2.4.4 Ltc2aG11A induced membrane thinning.....156

6.2.4.5 Cholesterol attenuated the effect of the peptides.....158

6.2.4.6 Proposed mechanisms of action.....159

6.3 Contributions.....162

6.4 References.....162

Chapter 7 Conclusions and future direction.....169

7.1 Conclusions and implication.....169

7.2 Suggestions and future direction.....170

LIST OF TABLES

Table 1.1: The sequence and properties of the studied antimicrobial peptides.....12

Table 2.1: Model membrane composition in mole percentage.....26

Table 4.1: Antimicrobial activities of anoplin and derivative toward *E. coli* and *B. subtilis*.....64

Table 5.1: Properties of anoplin and derivatives.....98

Table 5.2: Assignment of the UVRR amide bands of anoplin derivatives in PBS and 50% TFE.....112

Table 5.3: Relative area of the peaks corresponding to α-helix, β-sheet, and random coil in anoplin, Ano8K and Ano1K5V8K as percentages of total amide I area in PBS and 50% TFE.....112

LIST OF FIGURES

Figure 1.1: Structural factor determinants on antimicrobial activity of an AMP.....2

Figure 1.2: Proposed mechanisms of actions of antimicrobial peptides: (A) barrel-stave model, (B) carpet model, (C) toroidal model, (D) molecular electroporation model, and (E) sinking raft model.....10

Figure 1.3: The membrane composition of (a) mammalian membrane and (b) bacterial membrane.....11

Figure 1.4: Structures of (A) pEM-2, (B) Ano-NH_2, (C) Ano-8K, (D) Ano-1K5V8K, (E) ltc2a, and (F) ltc2aG11A built in Molecular Operating Environment. Red, white, and blue represents hydrophobic, neutral, and hydrophilic surface, respectively.....13

Figure 2.1: Schematic diagram of pressure-area isotherm and various phase of a phospholipid.....21

Figure 2.2: Schematic diagram of pressure increases as the number of phospholipid molecules saturate air-water interface.....23

Figure 2.3: Schematic diagram of surface pressure change with time as injected peptide adsorp to a lipid monolayer.....24

Figure 2.4: Structure of (A) DPPC, (B) DPPG, (C) DOPC, (D) DOPG, (E) DOPE, (F) 18:1 CL, (G) Chol, ovine wool, and (H) egg SPM.....26

Figure 2.5: Structures of (A) CF and (B) calcein.....28

Figure 2.6: Schematic diagram of fluorescence signal increased as encapsulated dye that self-quench at high concentration leaks out from the liposomes subsequent to the addition of AMP or Triton X-100.....28

Figure 2.7: (A) Sealed liquid cell with sample holder (MP4LCNTF, NT-MDT, Russia) (B) cantilever on the glass pedestal for liquid imaging (NT-MDT, Russia).....31

Figure 2.8: (A) Standard curved of *E. coli* and *B. subtilis* culture in MHB and (B) MIC determination of Ano-NH_2 and Ano-OH on *B. subtilis* in a 96 well microtiterplate.....36

Figure 3.1: (A) LB compression-expansion isotherm cycles of pEM-2 monolayer of different peptide concentrations. (B) Area per nanomolar as a function of surface pressure. Average data calculated for different pEM-2 concentrations as presented.....43

Figure 3.2: Selected AFM topography image of 420 nM pEM-2 monolayer transferred at 15 mN/m.....44

Figure 3.3: Relative increase of the area of DPPG, DPPC, or *E. coli* monolayer compressed to (A) 7.5 mN/m and (B) 30 mN/m as a function of time after pEM-2 was injected into the subphase. Final pEM-2 concentration was 400 nM.....45

Figure 3.4: (A) Effect of different pEM-2 concentrations on the compression isotherms of a DPPC/pEM-2 monolayer. (B) Relative area increase at different pressures calculated from the isotherms shown in Fig 3.4A.....48

Figure 3.5: Selected AFM topography images of DPPC/pEM-2 monolayers transferred at 30 mN/m in the absence or presence of calcium chloride.....49

Figure 3.6: (A) Effect of increasing pEM-2 concentration on the compression-expansion isotherm cycles of DPPG/pEM-2 monolayer. (B) Relative area increase at different pressure calculated from Fig 3.6 A isotherms.....51

Figure 3.7: Selected AFM topography images of DPPG/pEM-2 monolayers transferred at 30 mN/m in the absence or presence of calcium chloride.....52

Figure 3.8: Calcein fluorescence signal increase measured about 15 min after the addition of pEM-2 into DPPC, DPPG, *E. coli* model, *S. aureus* model, and *B. subtilis* model vesicles.....56

Figure 4.1: UVRR spectra of Ano-OH, Ano-NH_2, and D-Ano-NH_2 in PBS.....65

Figure 4.2: The effect of temperature on the UVRR spectra of (A) Ano-NH_2 and (B) Ano-OH.....69

Figure 4.3: UVRR specta of Ano-NH_2, (B) D-Ano-NH_2, and (C) Ano-OH in 30% TFE for both amidated derivatives or 40% TFE for Ano-OH and PBS. Contributions from TFE subtraction are marked by asterisks.....70

Figure 4.4: UVRR spectra of (A) Ano-NH_2, (B) D-Ano-NH_2, and (C) Ano-OH in PBS, 1:6 DPPG, and 1:6 DPPC. Contributions from the lipids are marked by asterisks.....71

Figure 4.5: LB isotherm cycles for monolayer of (A) DPPC (blue), DPPG (red) and *E. coli* total lipid extract (green), and (B) Ano-NH_2 (black), Ano-OH (grey) and D-Ano-NH_2 (beige) at air/water interface.....73

Figure 4.6: Selected AFM topography images and cross sections of (A) Ano-NH_2 at 15 mN/m, (B) Ano-OH at 20 mN/m, and (C) D-Ano-NH_2 at 15 mN/m.....74

Figure 4.7: First compression of anoplin, (A) DPPC and DPPC/anoplin 50/50 mol% mixtures, and (B) DPPG and DPPG/anoplin 50/50 mol% mixtures monolayers.....76

Figure 4.8: LB isotherm cycles of (A) DPPC/anoplin 50:50 mol% mixtures and (B) DPPG/anoplin 50:50 mol% mixtures monolayers.....77

Figure 4.9: Selected AFM topography images and corresponding cross sections of single lipid monolayer and 50:50 mol% lipid/peptide mixtures deposited at 30 mN/m.....80

Figure 4.10: X-PEEM images of (A-C) DPPC/Ano-NH_2 and (D-F) DPPC/Ano-OH 50:50 mol% mixtures.....81

Figure 4.11: X-PEEM images of (A-C) DPPG/Ano-NH_2 and (D-F) DPPG/Ano-OH 50:50 mol% mixtures.....81

Figure 4.12: (A) Langmuir isotherm cycles of *E. coli* total lipid extract and *E. coli*/peptide (20 μL 1mg/mL/10uL 1mg/mL). Selected AFM topography images of (A inserted) *E.coli*, (B) *E.coli*/Ano-NH_2 and (C) *E. coli*/Ano-OH deposited at 30 mN/m.....83

Figure 4.13: Increase of the surface pressure at constant area for monolayer of (A) DPPC, (B) DPPG and (C) *E. coli* total lipid extract after injecting 21.5 μM anoplin derivatives under lipid monolayer.....84

Figure 4.14: Increase of the surface pressure at constant area for (A) lipid monolayers after injecting 5 μL PBS (inserted: 100 μL PBS) under lipid monolayer, and (B) PBS after injecting 80 nM of peptides under the interface.....86

Figure 4.15: CF fluorescence signal increase after addition of anoplin into (A) DPPC, (B) DPPG, (C) *E. coli* model, (D) *S. aureus* model, and (E) *B. subtilis* model vesicles.....90

Figure 5.1: Helical wheel diagram of anoplin, Ano8K, and Ano1K5V8K. Eisenberg consensus hydrophobicity scale was used.....98

Figure 5.2: Peptide-induced pressure changes as a function of peptide concentration in the subphase for anoplin derivatives.....100

Figure 5.3: Insertion of anoplin derivatives into (A) DPPC and (B) DPPG monolayers..102

Figure 5.4: Relative increase of the pressure of (A) DPPC and (B) DPPG monolayers after inserting anoplin derivatives.....103

Figure 5.5: Peak fitting of UVRR spectra of anoplin in (A) PBS and (B) 50% TFE. Original spectrum (thick) is shown on top of the fitted trace (dashed) with individual fitted peaks (thin) and baseline (flat) below.....107

Figure 5.6: Peak fitting of UVRR spectra of Ano-8K in (A) PBS and (B) 50% TFE. Original spectrum (thick) is shown on top of the fitted trace (dashed) with individual fitted peaks (thin) and baseline (flat) below.....108

Figure 5.7: Peak fitting of UVRR spectra of Ano-1K5V8K in (A) PBS and (B) 50% TFE. Original spectrum (thick) is shown on top of the fitted trace (dashed) with individual fitted peaks (thin) and baseline (flat) below.....109

Figure 5.8: CF fluorescence signal increase after the addition of anoplin derivatives (Ano – black circles; Ano8K – grey squares; Ano1K5V8K – beige triangels) into (A) DPPC, (B) DPPG, (C) mammalian model, (D) *E. coli* model, (E) *S. aureus* model, and (F) *B. subtilis* model vesicles.....116

Figure 6.1: Helical net diagrams for ltc2a and lytc2aG11A. Eisenberg consensus hydrophobicity scale was used.....124

Figure 6.2: (A) Peptide induced variations of the surface pressure as a function of peptide concentration in the subphase for ltc2a derivatives. (B) Insertion of ltc2a derivatives into DPPC (left) and DPPG (right) monolayers.....132

Figure 6.3: Kinetics of ltc2a derivatives inserting into (A) DPPC and (B) DPPG monolayers at different initial pressure.....133

Figure 6.4: Compression isotherms for ltc2a derivatives and 50:50% molar ratio mixtures with (A) DPPC and (B) DPPG.....134

Figure 6.5: Compression and expansion isotherm cycles of (A) DPPC and DPPG, (B) ltc2a and ltc2a G11A, (C) DPPC and 50:50% molar ratio mixtures, and (D) DPPG and 50:50% molar ratio mixtures monolayers.....137

Figure 6.6: Selected AFM topography images of (A) ltc2a and (B) ltc2aG11A monolayer deposited at 30 mN/m.....138

Figure 6.7: Selected AFM topography images and corresponding cross sections of 50:50% peptide/lipid molar ratio mixture monolayers deposited at 30 mN/m.....140

Figure 6.8: Selected X-PEEM images of (A-C) DPPG/ltc2a and (D-F) DPPG/ltc2aG11A 50:50 mol% mixtures.....141

Figure 6.9: Selected X-PEEM images of (A-C) DPPC/ltc2a and (D-F) DPPC/ltc2aG11A 50:50 mol% mixtures.....141

Figure 6. 10: CF fluorescence signal increase after the addition of ltc2a (solid circles) and ltc2a G11A (opened squares) in (A) DPPC, (B) DPPG, (C) mammalian model, and (D) raft model vesicles.....144

Figure 6. 11: CF fluorescence signal increase after the addition of ltc2a (solid circles) and ltc2a G11A (opened squares) in (A) *E. coli* model, (B) *S. aureus* model, and (C) *B. subtilis* model vesicles.....145

Figure 6.12: AFM images (10 × 10 μm^2) of raft SLBs (A) before and (B) after the addition of 0.28 mM Triton X-100.....147

Figure 6.13: RepresentativeAFM images (10 × 10 μm^2) of raft SLBs before and after the addition of (A-D) ltc2a and (E-H) ltc2aG11A in 150 mM NaCl medium.....150

Figure 6. 14: Representative AFM images (10 × 10 μm^2) of raft SLBs before and after the addition of (A-D) ltc2a and (E-G) ltc2aG11A in deionized water.....151

Figure 6.15: Representative AFM images (10 × 10 μm^2) of raft SLBs before and after the addition of (A-D) 0.6 μM ltc2a and (E-H) 0.6 μM ltc2aG11A in 150 mM NaCl medium.....152

Figure 6.16: Representative AFM images (10 × 10 μm^2) of raft SLBs before and after the addition of (A-D) 0.6 μM ltc2a and (E-H) 0.6 μM ltc2aG11A in deionized water.....153

Figure 6.17: Representative AFM images (10 × 10 μm^2 expect 5 × 5 μm^2 for D) of raft SLBs (A) before and after the addition of (B) 0.6 μM ltc2a and (C, D) 0.6 μM ltc2aG11A in deionized water.....156

Figure 6.18: Representative AFM images (5 × 5 μm^2) of DOPC/SPM 50/50 mol% SLBs before and after the addition of (A-D) 0.6 μM ltc2a and (E-H) 0.3 μM ltc2aG11A in deionized water.....160

Figure 6.19: Proposed mechanisms of action of ltc2a (left) and ltc2aG11A (right) in deionized water and in 150 mM NaCl solution.....161

LIST OF VIDEOS

Video 6.1: Morphology changes of raft SLBs after the addition of ltc2aG11A from 0.3 to 0.9 μM in 150 mM NaCl medium. Time after the peptide addition as well as the concentration are indicated. Scale bar represents 2 μm.

Video 6.2: Morphology changes of raft SLBs after the addition of ltc2a from 0.3 to 0.9 μM in 150 mM NaCl medium. Time after the peptide addition as well as the concentration are indicated. Scale bar represents 2 μm.

Video 6.3: Morphology changes of raft SLBs after the addition of ltc2aG11A from 0.3 to 0.9 μM in deionized water. Time after the peptide addition as well as the concentration are indicated. Scale bar represents 2 μm.

Video 6.4: Morphology changes of raft SLBs after the addition of ltc2a from 0.3 to 0.9 μM in deionized water. Time after the peptide addition as well as the concentration are indicated. Scale bar represents 2 μm.

Video 6.5: Morphology changes of raft SLBs after the addition of 0.6 μM ltc2aG11A in 150 mM NaCl medium. Time after the peptide addition as well as the concentration are indicated. Scale bar represents 2 μm.

Video 6.6: Morphology changes of raft SLBs after the addition of 0.6 μM ltc2a in 150 mM NaCl medium. Time after the peptide addition as well as the concentration are indicated. Scale bar represents 2 μm.

Video 6.7: Morphology changes of raft SLBs after the addition of 0.6 μM ltc2aG11A in deionized water. Time after the peptide addition as well as the concentration are indicated. Scale bar represents 2 μm.

Video 6.8: Morphology changes of raft SLBs after the addition of 0.6 μM ltc2a in deionized water. Time after the peptide addition as well as the concentration are indicated. Scale bar represents 2 μm.

LIST OF PUBLICATIONS

- **Won, A.**; Rucito, A.; Ianoul, A. Imaging the membrane activity of bioactive peptide latarcin 2a. *Biochimica et Biophysica Acta – Biomembrane* **2012**, *1818*, 3072 - 3080.
- Idiong, G.; **Won, A.**; Ruscito, A.; Leung, B.O.; Hitchcock, A.O.; Ianoul, A. Investigating the effect of a single glycine to alanine substitution on interactions of antimicrobial peptide ltartcin 2a with a lipid membrane. *European Biophysical Journal* **2011**, *40*, 1087-1100.
- Leung, B.O.; Hitchcock, A.P.; **Won, A.**; Ianoul, A.; Scholl, A. Imaging interactions of cationic antimicrobial peptides with model lipid monolayers using X-ray spectromicroscopy. *European Biophysical Journal* **2011**, *40*, 805-810.
- **Won, A.**; Pripotnev, S.; Ruscito, A.; Ianoul, A. Effect of point mutations on the secondary structure and membrane interactions of antimicrobial peptide anoplin. *Journal of Physical Chemistry B* **2011**, *115*, 2371-2379.
- **Won, A.**; Khan, S.; Gustin, S.; Akpawu, A.; Seebun, D.; Avis, T.J.; Leung, B.O.; Hitchcok, A.O.; Ianoul, A. Investigating the effects of L- to D- amino acid substitution and deamidation on the activity and membrane interactions of antimicrobial peptide anoplin. *Biochimica et Biophysica Acta – Biomembrane* **2011**, *1808*, 1592-1600.
- Pripotnev, S.; **Won, A.**; Ianoul, A. The effects of L- to D- isomerisation and C-terminus deamination on the secondary structure of antimicrobial peptide anoplin in aqueous and membrane mimicking environment. *Journal of Raman Spectroscopy* **2010**, *41*, 1355-1359.
- **Won, A.**; Ianoul, A. Interaction of antimicrobial peptide from C-terminus of myotoxin II with phospholipid mono- and bilayers. *Biochimica et Biophysica Acta – Biomembranes* **2009**, *1788*, 2277-2283.

LIST OF CONFERENCES - ORAL/POSTER

Oral: **Won, A.**, Ruscito, A., Ianoul, A. Interaction between lytic peptide latarcin 2a and supported lipid bilayers studied by *in situ* atomic force microscopy. 14th International Scanning Probe Microscopy Conference. Toronto, ON. Jun 15-18, 2012.

Poster: **Won, A.**, Ruscito, A., Ianoul, A. Interaction between lytic peptide latarcin 2a and supported lipid bilayers studied by *in situ* atomic force microscopy. Ottawa-Carleton Chemistry Institute Day. Ottawa, ON. May 18, 2012.

Chemical Biophysics Symposium 2012, Toronto, ON. Apr 13-15, 2012.

Poster: **Won, A.**, A., Ianoul, A. Interaction between lytic peptide latarcin 2a and supported lipid bilayers studied by *in situ* atomic force microscopy. Biophysical Society 56th Annual Meeting. San Diego, CA. Feb 25-29, 2012.

Poster: **Won, A.**, Pripotnev, S., Ruscito, A., Ianoul, A. Effect of single and multiple amino acid substitutions on the membrane binding and lytic activity of antimicrobial peptide anoplin. The 94th Canadian Chemistry Conference. Montreal, QC. Jun 5-9, 2011.

Poster: **Won, A.**, Pripotnev, S., Ruscito, A., Ianoul, A. Effect of single and multiple amino acid substitutions on the membrane binding and lytic activity of antimicrobial peptide anoplin. Biophysical Society 55th Annual Meeting. Baltimore, MA. Mar 5-9, 2011.

Oral: **Won, A.**, Pripotnev, S., Ruscito, A., Ianoul, A. Effect of single and multiple amino acid substitutions on the membrane binding and lytic activity of antimicrobial peptide anoplin. Joint Australia-Croatia Workshop on Antimicrobial Peptides. Split, Croatia. Aug 8-13, 2010.

Poster: Idiong, G., **Won, A.**, Pripotnev, S., Ianoul, A. Interactions of antimicrobial peptide latarcin with model cell membrane. The 93rd Canadian Chemistry Conference. Toronto, ON. May 29-Jun 2, 2010.

Poster: **Won, A.**, Khan, M., Gustin, S., Akpawu, A., Pripotnev, S., Ianoul, A. Effect of L- to D-peptide isomerisation on the activity of antimicrobial peptide anoplin. The 93rd Canadian Chemistry Conference. Toronto, ON. May 29-Jun 2, 2010..

Oral: **Won, A.**; Khan, S.; Gustin, S.; Akpawu, A.; Seebun, D.; Avis, T.J.; Leung, B.O.; Hitchcok, A.O.; Ianoul, A. Effect of L- to D-peptide substituion on the activity of antimicrobial peptide anoplin. Ottawa-Carleton Chemistry Institute Day. Ottawa, ON. May 21, 2010.

Poster: Idiong, G., **Won, A.**, Pripotnev, S., Ianoul, A. Interactions of antimicrobial peptide latarcin with model cell membrane. Biophysical Society 54th Annual Meeting. San Francisco, CA. Feb 20-24, 2010.

Poster: **Won, A.**, Khan, M., Gustin, S., Akpawu, A., Pripotnev, S., Ianoul, A. Effect of L- to D-peptide isomerisation on the activity of antimicrobial peptide anoplin. Biophysical Society 54th Annual Meeting. San Francisco, CA. Feb 20-24, 2010.

Oral: **Won, A.**, Ianoul, A. Deamidation modifies membrane binding properties of antimicrobial peptide anoplin. The 92th Canadian Chemistry Conference. Hamilton, ON. May 30, Jun 3, 2009.

Oral: **Won, A.**, Ianoul, A. Deamidation modifies membrane binding properties of antimicrobial peptide anoplin. Ottawa-Carleton Chemistry Institute Day. Ottawa, ON. May 15, 2009.

Poster: **Won, A.**, Ianoul, A. Deamidation modifies membrane binding properties of antimicrobial peptide anoplin. Biophysical Society 53rd Annual Meeting. Boston, MA. Feb 28-Mar 4, 2009.

Poster: **Won, A.**, Ianoul, A. Molecular mechanism of pEM-2 activity. Biophysical Society 53rd Annual Meeting. Boston, MA. Feb 28-Mar 4, 2009.

Poster: **Won, A.**, Ianoul, A. Molecular mechanism of pEM-2 activity. The 91st Canadian Chemistry Conference. Edmonton, AB. May 24 - 28. 2008.

LIST OF ABBREVIATIONS

AFM: atomic force microscopy

AMP: antimicrobial peptide

Ano-OH: deamidated anoplin

D-Ano-NH_2: anoplin composed with D-enantiomer of amino acid residues

Ano8K: anoplin-8K

Ano1K5V8K: anoplin-1K5V8K

B. subtilis: *Bacillus subtilis*

CD: circular dichroism

CMC: critical micelle concentration

CPI: critical pressure of insertion

D_2O: deuterium oxide

Chol: cholesterol

DMPC: 1,2-dimyristoyl-*sn*-glycero-3-phosphocholine

DOPC: 1,2-dioleoyl-*sn*-glycero-3-phosphocholine

DOPE: 1,2-dioleoyl-*sn*-glycero-3-phosphoethanolamine

DOPG: 1,2-dioleoyl-*sn*-glycero-3-phospho-(1'-*rac*-glycerol)

DPPC: 1,2-dipalmitoyl-*sn*-glycero-3-phosphocholine

DPPG: 1,2-dipalmitoyl-*sn*-glycero-3-phospho-(1'-*rac*-glycerol) (sodium salt)

CFU: colony forming unit

CL: cardiolipin

EC_{50}: half maximal effective concentration or medium efficacious concentration

E. coli: *Escherichia coli*

L_d: liquid disordered phase

L_o: liquid ordered phase

LB: Langmuir Blodgett

LC: liquid condensed phase

LD_{50}: medium lethal dose

LE: liquid expanded phase

ltc 1: latarcin 1

ltc 2a: latarcin 2a

ltc 2aG11A: latarcin 2aG11A

MC: Monte Carlo

MD: molecular dynamics

MIC: minimum inhibitory concentration

MHA: mueller hinton agar

MHB: mueller hinton broth

mM: millimolar

NMR: nuclear magnetic resonance

nm: nanometer

PBS: phosphate buffer saline

PTFE: polytetrafluoroethylene

S. aureus: *Staphylococcus aureus*

SDS: sodium dodecyl sulfate

SLB: supported lipid bilayer

SM: sphingomyelin

STXM: scanning transmission X-ray microscopy

TFE: 2,2,2-trifluoroethanol

Tris: tris(hydroxymethyl)aminomethane

μM: micromolar

μm: micrometer

UVRR: ultra violet resonance Raman

X-PEEM: X-ray photoemission electron microscopy

CHAPTER 1 INTRODUCTION

1.1 ANTIBIOTIC RESISTANT PATHOGENS

The emergence of multidrug resistant pathogens has been a rising health concern around the globe.[1-8] The resistance has developed for the last 60 years, especially in hospitals and other health care settings.[3-5] Since synthetic antibiotics have been developed for a specific site of action, their unnecessary and inappropriate usages have promoted the development of resistant pathogens.[3,8] The main mechanisms of antibiotic resistance include reduction of cellular uptake, active cellular efflux, modification or overproduction of specific target site of action, enzyme inactivation of antibiotics, or metabolic bypass.[3,5,8,9]

The three major areas of concern of resistant pathogens are multidrug/methicillin resistant *Staphylococcus aureus* (MRSA); drug resistant respiratory pathogens such as *Streptococcus pneumoniae* and *Mycobacterium tuaberculosis*; and multidrug resistant Gram negative bacilli such as *Pseudomonas aeruginosa*, *Acinetobacter baumannii*, and *Klebsiella pneumoniae*.[2,7] It was estimated that 60-70% of *S. aureus* isolated in hospitals are MRSA.[4] The U.S. Centres for Disease Control and Prevention estimated (in 2002) that more than 90,000 deaths in the U.S. are caused by bacterial infection annually.[4] In the Canadian health care system, the overall medical cost for antibiotic resistance was estimated to be approximately 200 million (CAD) per year.[5] Moreover, Dantas et. al showed that more than 70% of tested antibiotics were the sole carbon source for hundreds of isolated soil bacteria.[10] Thus the discovery and development of new therapeutic agents

to perform safer and more effective antimicrobial action have attracted a great deal of attention .

1.2 ANTIMICROBIAL PEPTIDES

Antimicrobial peptides (AMPs) are ancient host defense effector molecules in the innate immunity of both plants and animals and thus are also known as host defense peptides.[11-14] Bacteria have been exposed to AMPs for millions of years, however, wide spread resistance has not yet been reported, thus making AMPs one of the best candidates to combat antibiotic resistant pathogens.[1]

1.2.1 Parameters of antimicrobial peptides

AMPs are generally composed of 9 to 100 amino acid residues with overall positive charge from +2 to +9 and contain at least 30% of hydrophobic amino acid residues at neutral pH.[11,14] The interaction between an AMP and the membrane cannot be explained by a specific primary sequence but rather by a combination of various physicochemical and structural characteristics such as charges, hydrophobicity, hydrophobic moment, polar angle, and conformation (Fig 1.1).[1,14,16]

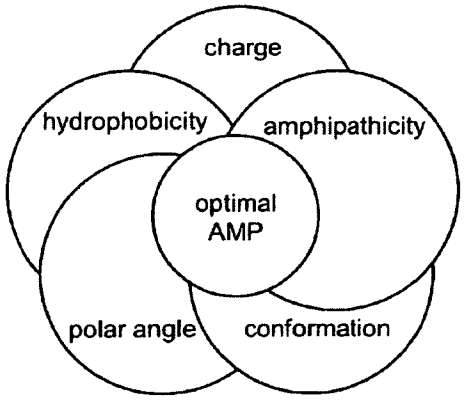

Figure 1.1: Structural factor determinants on antimicrobial activity of an AMP.[14]

The polar hydrophilic residues, arginine and lysine, generally contribute to cationicity of an AMP. Phospholipid bilayers are the basic component of all biomembranes. The composition, however, varies between biomembranes of prokaryotes and eukaryotes. For instance, the outer leaflet of human erythrocytes is predominantly composed of zwitterionic phosphatidylcholine and sphingomyelin, whereas the outer leaftlet of prokaryotic cells mainly consists of anionic phosphatidyglycerol and cardiolipin.[14,17,18]

The membrane asymmetry leads to overall transmembrane potential of bacterial pathogens in the range of -130 to -150 mV versus of mammalian in the range of -90 to -110 mV.[14] In addition, outer membranes of Gram-positive bacteria are composed of negatively charged teichoic and lipoteichoic acids, while those of Gram–negative bacteria are composed of anionic lipopolysaccharides.[19] Therefore, overall selectivity of AMPs is the result of cationic peptides being electrostatically attractive to the net negatively charged bacterial membrane rather than net neutral mammalian membrane. Furthermore, the presence of sterols discriminates mammalian from fungal and bacterial cell membranes.[11-14] Cholesterol and ergosterol within mammalian and fungal membranes, respectively, stabilize the lipid bilayer and hinder the binding and insertion of AMPs.[11-14]

The hydrophobic residues contribute to peptides' hydrophobicity, which is defined by the magnitude of a peptide transfer from an aqueous phase into a hydrophobic phase that is the capacity of a peptide to insert into membrane lipid bilayers.[11-14,16] If the overall hydrophobicity is too low, a peptide can dissolve sufficiently in aqueous solution at high concentration but will not be able to pass through the hydrophobic core of lipid bilayers.

On the other hand, high hydrophobicity will promote self-association of peptides and prevent peptide dissolve at desired concentration for target transporting.

Numerous hydrophobicity scales have been derived theoretically and/or developed experimentally based on different aspects of peptide hydrophobicity.[20-23] One of the most commonly used is the consensus scale derived by Eisenberg et al. that combined five scales by averaging the normalized hydrophobicity of each amino acid residue.[21] Eisenberg et al. then further assessed peptide properties with hydrophobic moment by incorporating the derived hydrophobicity into the helical wheel diagram suggested by Schiffer and Edmundson.[24, 25]

The hydrophobic moment — a measurement of peptide amphipathicity — is the average of vectorial sums of amino acids within an ideal helix.[14,16,24] Peptides with high hydrophobic moment values often attain high permeabilizing and hemolytic activities. However, the hydrophobic moment does not directly correlate to peptides' action due to two factors. First, the hydrophobic and hydrophilic residues often do not evenly distribute throughout a peptide; thus some regions contain higher or lower hydrophobic moment.[16] Second, membrane bound peptides do not fold into ideal helices — often less than 100% — as it is assumed in the hydrophobic moment calculation.[16] Thus, hydrophobicity is more frequently used to assess peptide activity.

AMPs are often unstructured or randomly coiled in solution and fold into according secondary structure when contacting membranes or in membrane mimetic environment.[11,12,14] The two largest conformation categories are α-helical and β-sheet peptides whereas the majority of the remaining peptides are those rich in one or more residues, often being tryptophan, arginine, and proline.[14,26] The permeabilizing efficiency

of a peptide with an α-helical conformation often associates with its helicity. For example, peptides with amidated C-terminus — enables intramolecular NH-CO hydrogen bonding — frequently possess higher activity than their deamidated derivative.[16,27,28] Peptides with helix-hinge-helix conformations have also been reported with lower activity than their single helix derivatives.[29,30]

Membrane binding requires the hydrophobic surface of the peptide to penetrate into membrane cores composed of apolar acyl chains, and the hydrophilic surface of the peptide to persist in contact with the membrane surface composed of polar head groups. Thus it is expected that the relative portions of hydrophobic and hydrophilic facets — known as the polar angle — can predict the membrane binding and perturbation of a peptide.[14,16] Previous studies suggested that peptides with a smaller polar angle that contained larger hydrophobic facets had higher permeabilizing efficiency and formed pores in the membrane faster.[14] These pores, however, have shorter half-life in comparison to those formed by peptides with larger polar angle.[14]

1.2.2 Proposed mechanisms of action of antimicrobial peptides

Over 1200 AMPs have been discovered but the mechanisms of actions are still not understood[15] — several databases are available with detailed summaries.[31,32] As discussed previously, it is known that cationic AMPs selectively bind to the anionic pathogenic membrane through a long-range electrostatic interaction. AMPs displace divalent ions from lipopolysaccharside or lipoteichoic acids, destabilize this network and allow translocation of AMPs into anionic plasma membrane.[33] Upon membrane binding, peptides lie in a parallel position on the membrane that is often referred to as S state

where the peptide is inactive.[13] However, membrane organization is altered upon peptide association resulting in membrane thinning, line tension reduction and curvature adaptation.[1,33] As the numbers of AMP molecules increase in the local environment and reach their threshold concentration, peptides self associate and/or form complexes with neighboring lipid molecules; as a result, peptides reorient themselves into their active state, the I state which is frequently perpendicular to the lipid bilayer.[13] Various models have been proposed to explain membrane disruption and permeabilization by AMPs.

In the barrel-stave model (Fig 1.2 A), peptides self-associate and channel through the lipid bilayer in a barrel-like ring around the pore.[13,14,34,35] To undergo barrel-stave mechanisms, the AMPs must contain sufficient hydrophobic facets to channel through the lipid core and self-associate, and sufficient length to transverse the lipid bilayer — a minimum of 22 and 8 amino acid residues for α-helical and β-sheet peptides, respectively.[34]

In the carpet model (Fig 1.2 B), peptides cover the membrane surface in a carpet-like manner. The high density of peptide accumulation alters membrane structure and its barrier property.[13,14,34,35] At the threshold concentration, peptides form transient pores within the membrane and allow peptide transfer to the inner leaflet for further binding. Subsequently, the membrane disintegrates through formation of peptide/lipid micelle configuration.

In the toroidal pore model (Fig 1.2 C), peptide binding causes the lipid monolayer to fold inwards and form a channel lined with both inserted peptides and hydrophilic headgroups of lipids.[13, 14, 35] This model has been suggested as the intermediate step of the carpet model or other proposed mechanisms.[34] For example in the two-state model,[36]

incorporation of peptides into the outer leaflet of the membrane below the critical peptide/lipid ratio causes asymmetric area stretching and membrane thinning in a peptide concentration-dependent manner. Above the critical peptide/lipid ratio, peptides insert into lipid bilayers and induce pore formation while membrane thickness remains the same as before peptide addition. The molecular electroporation model (Fig 1.2 D) demonstrates that an electrical potential difference across the membrane is generated upon peptide/lipid association. The peptides will be transported to intracellular space through electorporation at the threshold concentration where the potential difference exceeds 0.2 V.[33,37,38] The sinking raft model (Fig 1.2 E) emphasizes that the formation of transient pores is caused by changes in the membrane curvature and peptide self association; subsequently, peptides are transported by sinking into the membrane.[33,39]

Although the majority of proposed models demonstrate that the mechanisms of action of AMPs are the disruption and permeabilization of the plasma membrane, studies have shown that some AMPs translocate through the membrane and act on specific intracellular targets.[13,34,40,41] The complexity of AMP action is one of the limitations due to which these peptide antibiotics are not yet widely available.

1.3 THE CHALLENGES AND LIMITATIONS OF PEPTIDE DRUG DEVELOPMENT

As mentioned earlier, 1200 different AMPs have been identified but only about 15 peptides have entered or completed clinical trials as antimicrobial or immunomodulatory agents — the cationic lipopeptide polymyxin is the last resouce to treat infection caused by multiresistant *Pseudomonas* species and *Acinetobacter* species; the cyclic peptide

gramicidin S has been used in eye drops and topical ointments to treat infection; the cationic lantibiotic nasin has been aprroved as food additive in Europe.[1]

The unknown toxicity and unknown mechanisms of action are the major limitations of commercial development of AMPs. Low bioavailability and high manufacturing costs of peptides are the other disadvantages of peptide drug development. Studies have shown that peptide sequences composed or substituted with unnatural D-amino acid enantiomers or N-alkylglycine polymers (peptoid) improve AMPs' half-life *in vivo* by preventing proteolysis by proteases while retaining the antimicrobial activity, which demonstrate the importance of peptides' amphipathicity and their non specific action.[11,34,42]

To compensate for the high cost in manufacturing peptides, few approaches have been used: further investigation and development of shorter AMPs, recombination with other biomolecules such as DNA, or incorporation into other therapeutic agents.[11,43] Haine et al. demonstrated in insects that AMPs are induced and act as the last line of defense after the immune cells and the activated enzyme cascade in the rapid constitutive defense have removed 99.5% of bacteria.[43] Therefore, in the development to combat antibiotic resistant pathogens, AMPs may also be used in the future as the last line of defense following the treatment with other therapeutic agents.

Moreover, alongside of the databases mentioned previously, innovative computer assisted design systems such as the database filtering technology recently suggested by Mishra and Wang will aid faciliating the clinical efficacy of these peptide therapeutic agents.[44]

1.4 MODEL MEMBRANES

The biological membrane is a complex system. The mammalian membrane (Fig 1.3 A) is composed of diverse phospholipids, sphingolipids, proteins, sterol, and sugars. The bacterial membrane (Fig 1.3 B) also consists of various forms of sugars, phospholipids, and proteins. It was discussed previously that AMPs disrupt the membrane mostly through non-specific interaction and the action depends on parameters such as charge, hydrophobicity, amphipathicity, conformation, and polar angles. Therefore model membranes are often used to isolate the effect of different variables on peptide activity. Phospholipids are the major components in a biological membrane; as a consequence, they are generally used for model composition. Although the biological activity of a peptide cannot be fully represented by its interaction with a model membrane, the specific role of each examined component can provide further insight into AMPs' mechanisms of actions.[45, 46]

Three forms of commonly used model membranes are the lipid monolayer, supported lipid bilayers, and unilamellar vesicles. A pressure/area isotherm of a monolayer provides information about the monolayer's stability at the air/water interface, the conformational and phase transition changes in a controlled two-dimensional system.[48-50] Interactions between peptides and the lipid monolayer provide information about first phase association. Supported lipid bilayers include parameters such as interleaflet coupling, lipid molecular shape, and packing density within a membrane that may affect peptide/lipid interaction.[46,51] They are often combined with microscopic techniques such as atomic force microscopy (AFM) to observe the peptide/membrane interaction. Unilamellar vesicles are composed of a single lipid bilayer enclosing an aqueous

environment. The separation between the interior and exterior of vesicles by a relatively impermeable lipid bilayer resembles the biological system therefore making unilamellar vesicles attractive models.[52,53]

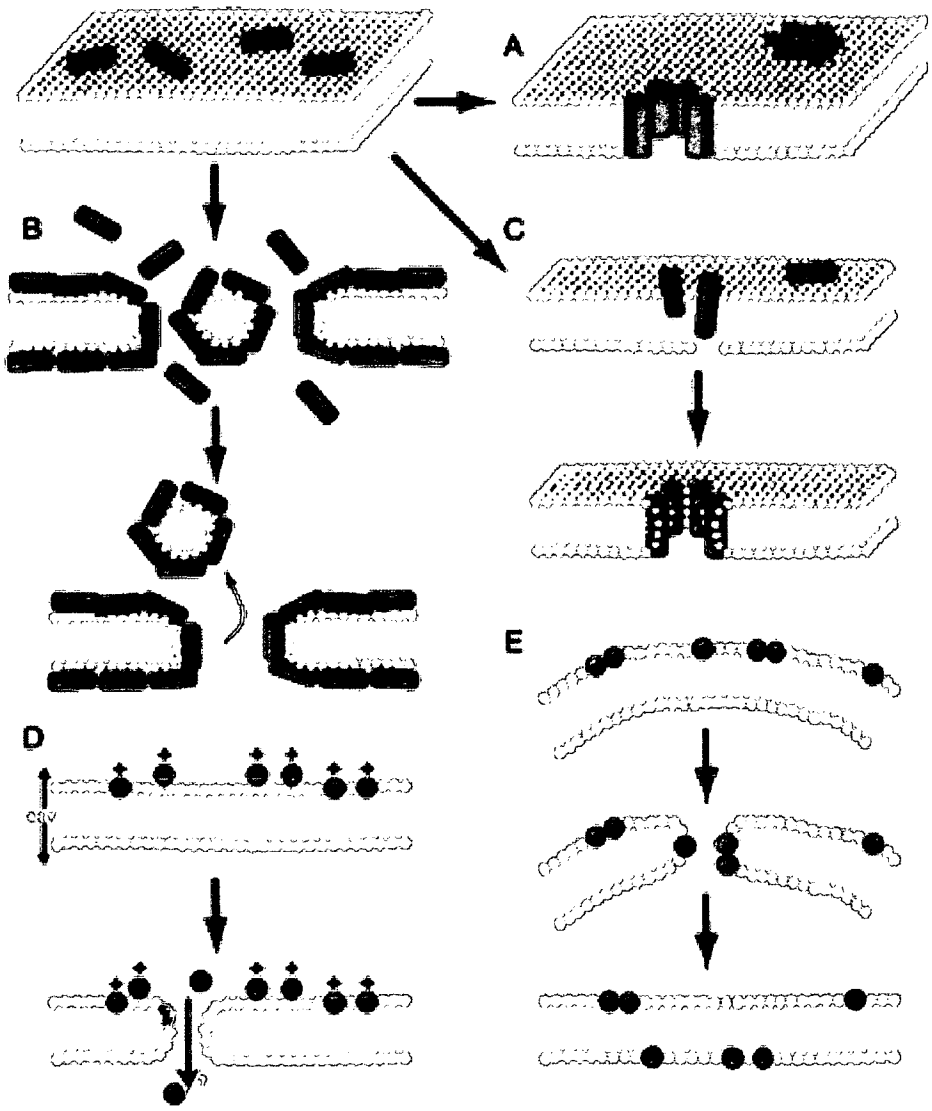

Figure 1.2: Proposed mechanisms of actions of antimicrobial peptides: (A) barrel-Stave model, (B) carpet model, (C) toroidal model, (D) molecular electroporation model, and (E) sinking raft model.[33] Reproduced with permission from Elsevier.

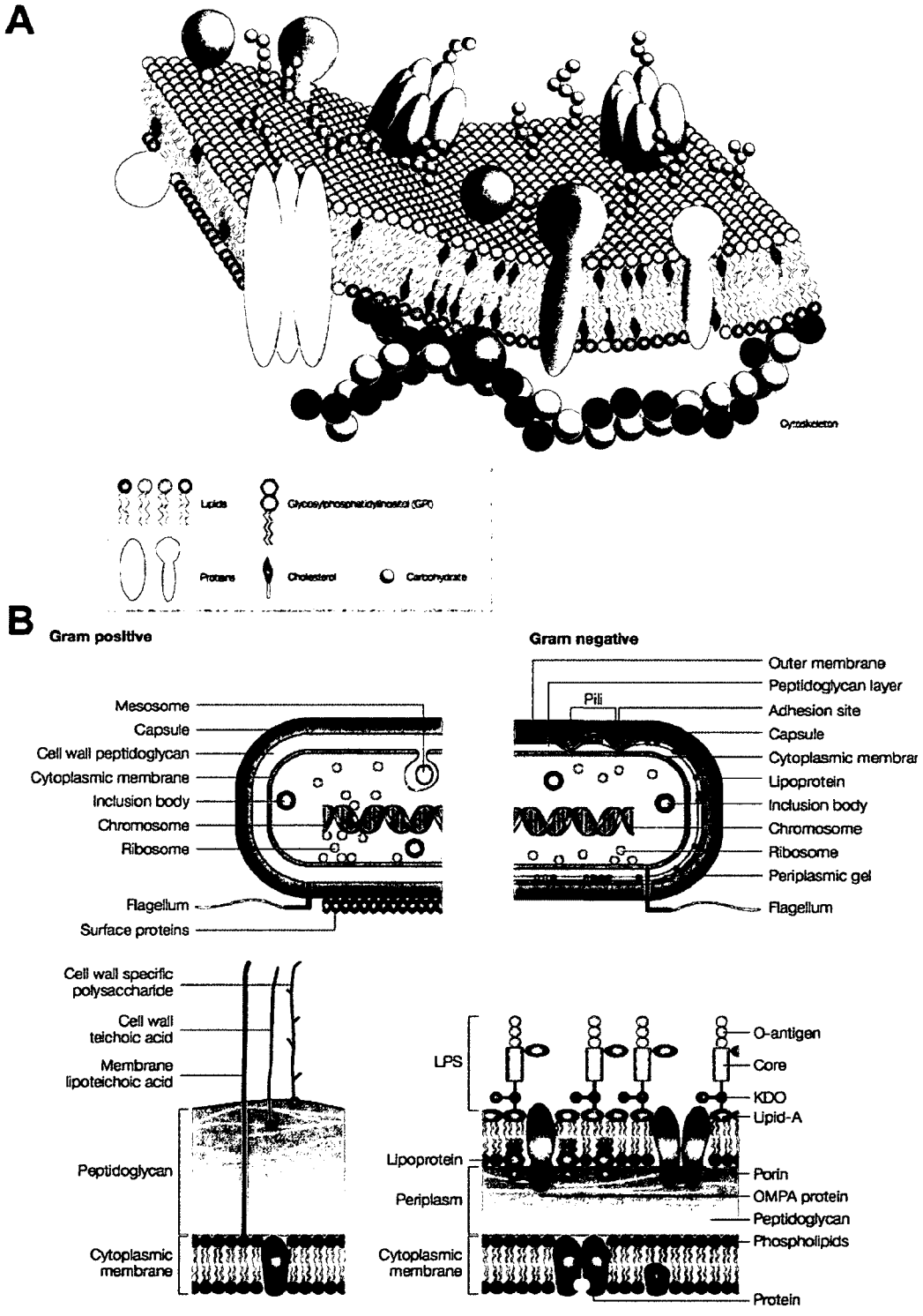

Figure 1.3: The composition of (A) mammalian membrane and (B) bacterial membrane.[19, 47] Reproduced with permission from Nature Publishing Group.

1.5 THESIS OBJECTIVE

The objective of this thesis was to investigate the fundamental mechanisms of AMP action to aid the development of alternatives to synthetic antibiotics. Small modifications of the AMP's sequence such as amidation of the C-terminus and introduction of tryptophan can improve the antimicrobial activity, while substitution of unnatural D-amino acid enantiomers may enhance the peptide stability. Moreover, various studies showed that the effect of single or multiple substitutions in primary sequence on AMP's activity and demonstrated that it is the physicochemical properties and the interfacial activity of a peptide rather than the specific amino acid sequence that determine the membrane lytic activity.[54-57]

In this thesis, interactions of three AMPs (and derivatives, Table 1.1) with model cell membranes and bacteria were investigated using various biophysical and biochemical techniques.

Table 1.1: The sequences and properties of the studied AMPs.

Peptide	Sequence	Q*	<H>$
pEM-2	KKWRWWLKALAKK	6	-0.353
anoplin	NH_2-GLLKRIKTLL-$CONH_2$	4	-0.113
anoplin-OH	NH_2-GLLKRIKTLL-CO**OH**	3	-0.113
D-anoplin#	NH_2-**d**G**d**L**d**L**d**K**d**R**d**I**d**K**d**T**d**L**d**L-$CONH_2$	4	-0.113
anoplin-8K	NH_2-GLLKRIK**K**LL-$CONH_2$	5	-0.205
anoplin-1K5V8K	NH_2-**K**LLK**V**IK**K**LL-$CONH_2$	5	-0.101
latarcin 2a	NH_2-GLFGKLIKKF**G**RKAISYAVKKARGKH-COOH	9	-0.238
latarcin 2a G11A	NH_2-GLFGKLIKKF**A**RKAISYAVKKARGKH-COOH	9	-0.235

*Q: peptide charge at physiological condition
$<H>: peptide mean hydrophobicity according to Eisenberg scale.[21]
peptide substituted with D-enantiomer amino acid residues

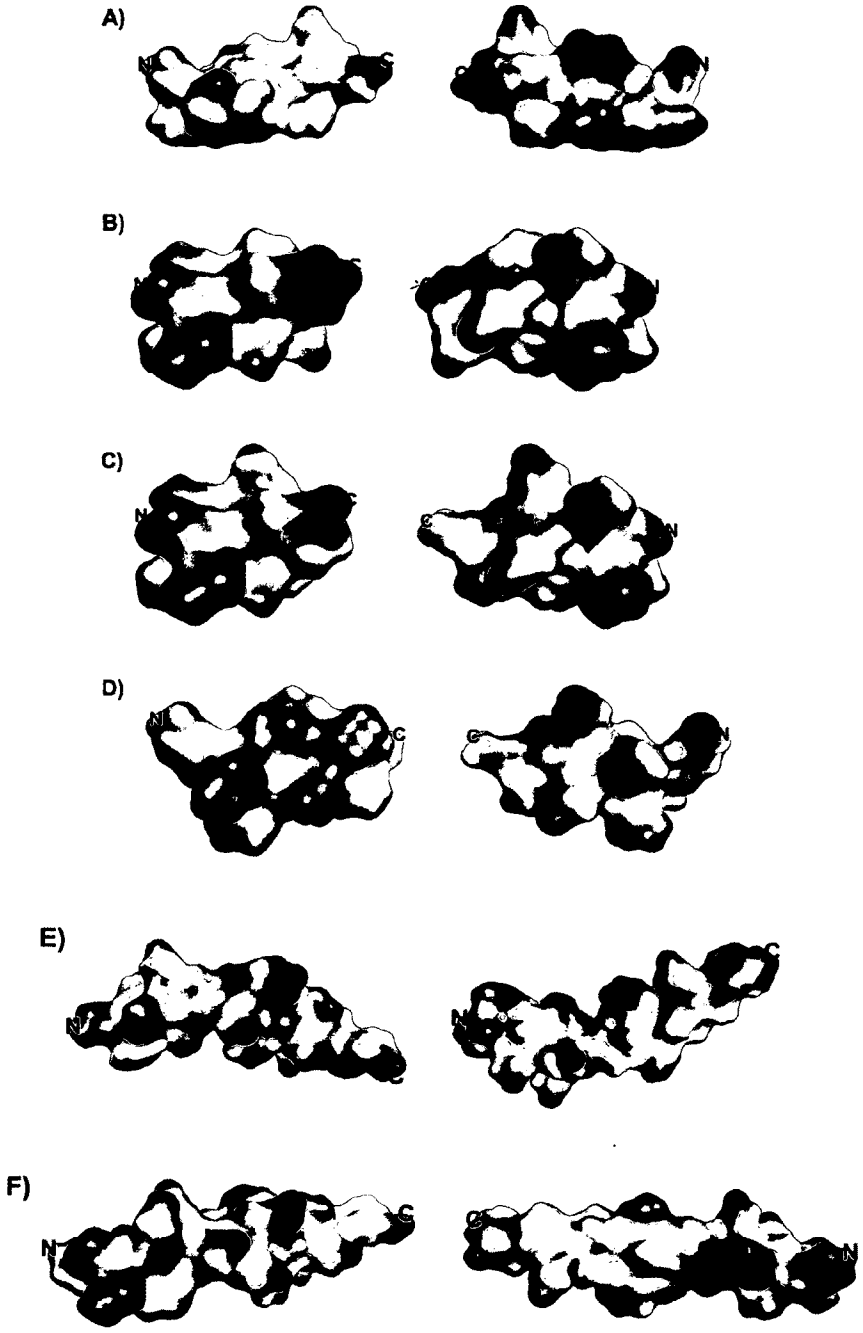

Figure 1.4: Structures of (A) pEM-2, (B) Ano-NH_2, (C) Ano-8K, (D) Ano-1K5V8K, (E) ltc2a, and (F) ltc2aG11A built in Molecular Operating Environment. Red, white, and blue represents hydrophobic, neutral, and hydrophilic surface, respectively.

Derived from the C-terminus of myotoxin II of the snake *Bothrops asper*, pEM-2 (Fig 1.4 A) is one of ten analogs that was previously found to maintain high bactericidal, fungicidal, and antitumor activities while having lower hemolytic activity.[55] Moreover, it is the only peptide studied in this thesis that contains **tryptophan**, an amino acid residue known to have a distinct preference towards the interfacial region of the membrane.[33] The interaction between pEM-2 and the lipid monolayer and vesicles provided further insight into the action of tryptophan containing peptides. Comparison to peptides with no tryptophan will be made.

Isolated from the venom of the solitary wasp *Anoplius samariensis*, anoplin (Fig 1.4 B) is the **smallest linear alpha-helical AMP**.[58] Anoplin studies would further assist the understanding of the action of short peptides that may reduce the development and production cost. The C-terminus of anoplin is naturally amidated; thus to observe the effect of amidation and further investigate its action and specificity, Ano-OH with deamidated C-terminus and D-Ano-NH_2 composed of all D-amino acid residues were synthesized and studied. Ano-OH was expected to have decreased activity with one less positive charge and a less defined helical structure. On the other hand, D-Ano-NH_2 was expected to have an action identical to the wild type anoplin since amphipathicity and structure of the peptide are retained in all L- to all D-enantiomer conversions. This study will confirm the idea that the mechanism of action of anoplin is nonspecific as with other antimicrobial peptides.

Previous structural and activity correlation study of anoplin showed that derivatives anoplin-8K (Fig 1.4 C) and anoplin-1K5V8K (Fig 1.4 D) exhibit strong antimicrobial activities while having relatively low hemolytic activities.[54] The significance of charge,

hydrophobicity, amphipathicity, and helicity on the action of anoplin was examined. The two mutants were expected to exhibit stronger actions with the additional positive charge and higher hydrophobic moment. It is known that peptides with **greater helicity** and thus amphipathicity would be expected to display higher activity. UVRR spectroscopy was used in this study to correlate helicity with other parameters and properties of the three peptides.

Purified from the venom of spider *Lachesana tarabaevi*, latarcin 2a (Fig 1.4 E) demonstrates the strongest antimicrobial activity and relatively low hemolytic activity out of the family of seven latarcin peptides.[59] Moreover, latarcin 2a has a unique **helix-hinge-helix structure**.[60] Thus to further understand function of the hinge in latarcin 2a, a derivative was made by substituting helix-breaking glycine at position 11 with helix-favouring alanine and the two peptides were compared. With a more rigid structure, the mutant latarcin 2aG11A (Fig 1.4 F) was expected to demonstrate stronger lytic activity than latarcin 2a. The anticipated activity enhancement is reached either by requiring variational dosage or through different mechanism of action was investigated.

1.6 REFERENCES

1. Fjell, C.D.; Hiss, J.A.; Hancock, R.E.W.; Schneider, G. *Nat. Rev. Drug Discovery* **2012**, *11*, 37-51.
2. Payne, D.J. *Science* **2008**, *321*, 1644-1645.
3. Mulvey, M.R.; Simor A.E. *Can. Med. Assoc. J.* **2009**, *180*, 408-415.
4. Taube, G. *Science* **2008**, *321*, 356- 361.
5. Conly J. *Can. Med. Assoc. J.* **2002**, *167*, 885-891.

6. World Health Organization. 2012. The evolving threat of antimicrobial resistance.
7. Spellberg, B.; Guidos, R.; Gilbert, D.; Bradley, J.; Boucher, H.W.; Scheld, W.M.; Bartlett, J.G.; Edwards Jr. *Clin. Infec. Dis.* **2008**, *46*, 155-164.
8. Hayes, J.D.; Wolf, C.R. *Biochem. J.* **1990**, *272*, 281-295.
9. Davies, J. *Science* **1994**, *264*, 375-382.
10. Dantas G.; Sommer M.O.A.; Oluwasegun R.D.; Church G.M. *Science* **2008**, *320*, 100-103.
11. Hancock, R.E.W.; Sahl, H.-G. *Nat. Biotechnol.* **2006**, *24*, 1551-1557.
12. Zasloff, M. *Nature* **2002**, *24*, 389-395.
13. Brogden, K.A. *Nat. Microbiology* **2005**, *3*, 238-250.
14. Yeaman, M.; Yount, N.Y. *Pharmacol. Rev.* **2003**, *55*, 27-55.
15. Lai Y. and R. L. Gallo. *Trend Immunol.* **2009**, *30*: 131-141.
16. Dathe, M.; Wieprecht, T. *Biochim. Biophys. Acta* **1999**, *1462*, 71-87.
17. Epand, R.F.; Savage, P.B.; Epand, R.M. *Biochim. Biophys. Acta* **2007**, *1768*, 2500–2509.
18. Glukhov, E.; Stark, M.; Burrows, L.L.; Deber, C.M. *J. Biol. Chem.* **2005**, *280*, 33960-33967.
19. Lolis, E.; Bucala, R. *Nat. Rev. Drug Discovery*, **2003**, *2*: 635-645.
20. Tossi, A., Sandri, L., Giangaspero, A. *Peptides*, **2002**
21. Eisenberg, D., Weiss, R.M., Terwilliger, T.C. and Wilcox, W. *Faraday Symp. Chem. Soc.* **1982**, *17*, 109-120.
22. Kyte, J.; Doolittle, R.F. *J. Mol. Biol* **1982**, *157*, 105-132.
23. Wimley, W.; White, S.H. *Nat. Struct. Biol.* **1996**, *3*, 842-848.

24. Eisenberg D.; Weiss, R.M.; Terwilliger T.C. *Nature* **1982**, *299*, 371-374.

25. Schiffer, M.; Edmundson, A.B. *Biophys. J.*, **1967**, *7*, 121-135.

26. Hancock, R.E. Peptide antibiotics. Lacet 1997, 349: 418-422.

27. M.L. Sforca, S. Oyama, F. Canduri, C.C.B. Lorenzi, T.A. Pertinhez, K. Konno, B.M.;Souza, M.S. Palma, J.R. Neto, W.F. Azevedo Jr., A. Spisni, *Biochemistry* **2004**, *43*, 5608–5617.

28. Oren, Z.; Shai, Y. *Euro. J. Biochem.* **1996**, *237*, 303-310.

29. Oh, D.; Shin, S.Y.; Lee, S.; Kang, J.H.; Kim, S.D.; Ryu, P.D.; Hahm, K.; Kim, Y. *Biochemistry* **2000** *39*:11855–11864.

30. Pukala, T.L.; Brinkworth, C.S.; Carver. J.A.; Bowie, J.H. *Biochemistry* **2004,** 43, 937-944.

31. Antiinfective Peptide Laboratory – Prof. Alessandro Tossi. http://www.bbcm.units.it/~tossi/amsdb.html

32. Deprtment of Pathology and Microbiology, UNMC. The Antimicrobial Peptide Database and Analysis System. http://aps.unmc.edu/AP/main.php

33. Chan, D.I.; Prenner, E.J.; Vogel, H.J. *Biochim. Biophys. Acta - Biomembranes* **2006**, *1758*, 1184-1202.

34. Shai, Y. *Biopolymer – Pept. Sci.* **2002**, *66*, 236-248.

35. Hale, J.D.F.; Hancock, R.E.W. *Expert Review of Anti-infective Therapy* **2007**, *5.6*, 951-.

36. Huang, H.W. *Biochim. Biophys. Acta* **2006**, *1758*,1292-1302.

37. Miteva, M.; Andersson, M.; Karshikoff, A.; Otting, G. *FEBS Letter* **1999**, *462*, 155-158.

38. Tieleman, D.P. *BMC Biochemistry* **2004**, 5, 10-.

39. Pokorny A.; Almeida, P.F.F. *Biochemistry* **2005**, *44*, 9538-9544.

40. Haydon, D.J.; Stokes, N.R.; Ure, R.; Galbraith, G.; Bennett, J.M.; Brown, D.R.; Baker, P.J.; Barynin, V.V.; Rice, D.W.; Sedelnikova S.E.; Heal, J.R.; Sheridan, J.M.; Aiwale, S.T.; Chauhan, P.K.; Srivastava, A.; Taneja, A.; Errington, J.; Czaplewski, L.G. *Science* **2008**, *321*, 1673 -1675.

41. Jean-Francois, F.; Castano, S.; Desbat, B.; Odaert, B.; Roux, M.; Metz-Boutigue, M.-H.; Dufourc, E.J. *Biochemistry* **2008**, *47*, 6394-6402.

42. Chongsiriwatana, N.P.; Patch, J.A.; Czyzewski, A.M.; Dohm, M.T.; Ivankin, A.; Gidalevitz, D.; Zuckermann, R.N.; Barron, A.E. *PNAS* **2008**, *105*, 2794-2799.

43. Haine, E.R.; Moret, Y.; Siva-Jothy M.T.; Rolff, J. *Science* **2008**, *322*, 1257-1259.

44. Papo, N.; Shai, Y. *Peptide* **2003**, *24*, 1693-1703.

45. Mishra, B.; Wang, G. *J. Am. Chem. Soc.* **2012**, *134*, 12426-12429.

46. Sevcsik, E.; Pabst, G.; Richter, W.; Danner S.; Amenitsch, H.; Lohner, K. *Biophys. J.* **2008**, *94*, 4688-4699.

47. Pietzsch, J. Mind the membrane. *Horizon Symposia: Living Frontier, 2004,* 1-4. URL: http://www.nature.com/scitable/topicpage/protein-function-14123348

48. Brockman, H. *Current Opinion in Structural Biology* **1999**, *9*, 438-443.

49. Birdi, K.S. 2002. Self-assembly Monolayer Structures of Lipids and Marcomolecules at Interfaces. Kluwer Academic Publishers. New York, Boston, Dordrecht, London, Moscow.

50. Ulman, A. 1991. An Introduction to Ultrathin Organic Films From Langmuir-Blogett to Self-Assembly. Academic Press Inc. San Diego.

51. Seeger, H.M.; Marino, G.; Alessandrini, A.; Facci, P. *Biophysical Journal* **2009**, *97*, 1067-1076.

52. Szoka Jr., F; Papahadjopoulos, D. *Annual Review of Biophysics and Bioengineering* **1980**, *9*, 467-508.

53. Hope, M.J.; Bally, M.B.; Webb, G.; Cullis, P.R. *Biochimica et Biophysica Acta* **1985**, *812*, 55-65.

54. Ifrah, D.; Doisy, X.; Ryge, T.S.; Hansen, P.R. *Journal of Peptide Science* **2005**, *11*, 113-121.

55. Santamaria, C.; Larios, S.; Angulo, Y.;Pizarro-Cerda, J.; Gorvel, J.-P.; Moreno, E.; Lomonte, B. *Toxicon* **2005**, *45*, 807-815.

56. Polyansky, AA; Vassilevski, A.A.; Volynsky, P.E.; Vorontsova, O.V.; Samsonova, O.V.; Egorova, N.S.; Krylov, N.A.; Feofanov, A.V.; Arseniev, A.S.; Grishin, E.V.; Efremov, R.G. N-terminal amphipathic helix as a trigger of hemolytic acitivy in antimicrobial peptides: a case study in latarcins. *FEBS Letter* **2009**, *583*, 2425-2428.

57. Zelezetsky, I.;Tossi, A. *Biochimica et Biophysica Acta*, **2006**, *1758*, 1436-1449.

58. Konno K.; Hisada M.; Fontana R.; Lorenzi C.; Naoki H.; Itagaki Y.; Miwa A.; Kawai N.; Nakata Y.; Yasuhara T.; Neto J.R.; Azevedo W.F.; Palma M.S.; Nakajima T. *Biochim. Biophys. Acta*, **2001**, *1550*, 70-80.

59. Kozlov, S.A.; Vassilevski, A.A.; Feofanov, A.B.; Surovoy, A.Y.; Karpunin ,D.V.; Grishin, E.V. *J. Biol. Chem.* **2006**, *281*, 20983-20992.

60. Dubovskii, P.V.; Volynsky, P.E.; Polyansky, A.A; Chupin, V.V.; Efremov, R.G.; Arseniev, A.S. *Biochemistry* **2006**, *45*, 10759-10767.

CHAPTER 2 EXPERIMENTAL

2.1 CHEMICALS

1,2-dipalmitoyl-*sn*-glycero-3-phosphocholine (DPPC), 1,2-dipalmitoyl-*sn*-glycero-3-phospho-(1'-*rac*-glycerol) (sodium salt) (DPPG), 1,2-dioleoyl-*sn*-glycero-3-phosphocholine (DOPC), 1,2-dioleoyl-*sn*-glycero-3-phospho-(1'-*rac*-glycerol) (sodium salt) (DOPG), 1,2-dioleoyl-*sn*-glycero-3-phosphoethanolamine (DOPE), cardiolipin (CL), egg sphingomyelin (SM), cholesterol (Chol, bovine wool, >98%), and *E. coli* total lipid extract were purchased from Avanti Polar Lipids Inc. pEM-2 (98.7%, purity with unmodified amino and carboxyl ends), Ano-NH_2 (>95.5% purity), D-Ano-NH_2 (98.6% purity), Ano-OH (>95% purity), Ano8K (98.9% purity), Ano1K5V8K (98.9% purity), ltc2a (95.4% purity), and ltc2aG11A (95.1% purity) were synthesized by Gen Script Corporation. Phosphate buffered saline (PBS, 0.01 M, 138 mM NaCl, 2.7 mM KCl, pH 7.4), $NaClO_4$ (98%), 2,2,2-trifluoroethanol (TFE, >99.0%), $HClO_4$, calcein, sephadex G-50, and ascorbic acid (>99.0%) were purchased from Sigma-Aldrich. Carboxyfluorescein (CF) and sodium bisulfate were purchased from ACROS Organic. 1-amino-4-naphtholsulfonic acid was purchased from Ricca Chemical Company. Mueller hinton broth (MHB) was purchased from BBL (Becton Dickinson, Sparks, MD). Ammonium molybdate, sodium sulfite, ethylenediaminetetraacetic acid (EDTA), tris(hydroxymethyl)aminomethane (Tris), agar and Triton X-100 were purchased from Bioshop.

2.2 LANGMUIR BLODGETTRY

2.2.1 Pressure-area isotherm

Lipid monolayers were prepared on a LB trough using ~200 mL of PBS as the subphase by spreading 30 μL (DPPC and DPPG) or 20 μl (*E. coli* extract) of 1 mg/mL lipid solution in chloroform at the air/water interface. Peptide monolayer of pEM-2 was done by first dissolution in PBS followed by adding it to the subphase to obstaina final peptide trough concentration between 100 to 842 nM. This method of peptide introduction is more representative of the natural association phenomena of a peptide with a biological membrae. However, it was rather difficult to associate the peptide trough concentration to its molecular surface area. Thus peptide monolayers of anoplin, ltc2a, and derivatives were prepared by spreading 10 μl of 1 mg/mL peptide solutions (in chloroform or chloroform/methanol 3:1 to 1:1) at the air/water interface.

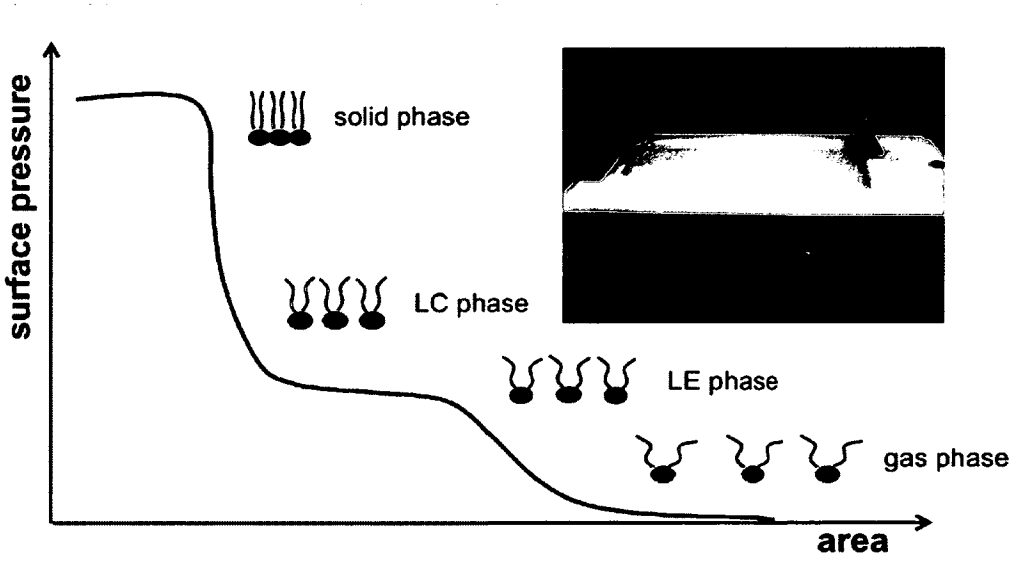

Figure 2.1: Schematic diagram of pressure-area isotherm and various phases of a phospholipid.[1,2] Insert: LB NIMA 311-D trough (Coventry, U.K.).

Lipid/peptide mixture monolayers (for anoplin, ltc2a, and derivatives) were prepared by spreading the mixtures (lipid/peptide in 50:50 mol ratio, or 20 μl of 1 mg/mL *E. coli* with 10 μl of 1 mg/mL peptide) at the air/water interface drop by drop and 15 to 25 min were allowed for solvent evaporation. High lipid to peptide ratio was to mimic excess peptides quantity at the site of interest and also to enable the accessment of the nature of peptide-lipid interaction at one to one ratio. In the case of pEM-2, it was injected into the subphase under the lipid monolayer at 0 mN/m and 20 to 30 min were allowed to establish equilibrium for a uniform pEM-2 distribution. At least two compression-expansion isotherm cycles were performed for the annealing process with a barrier speed of 5, 10, or 20 cm^2/min. The monolayer was then compressed to the desired pressure and transferred onto freshly cleaved mica (1 × 1'' Hi-Grade Mica, Ted Pella, Inc. Redding, CA) at 1 mm/min with the transfer ratios between 60 - 100%.

The magnitude and nature of miscibility between peptide and lipid molecules of the monolayer were assessed using excess free energy: excess Gibbs free energy (ΔG_{ex}, Eq. 1) or excess Helmholtz free energy (ΔF_{ex}, Eq. 2).[3,4] Negative values indicate a stronger interaction between the two components than between the pure components themselves, and positive values signify otherwise. If the mixing is ideal, a value of zero will be obtained. The excess free energy could not be successfully determined in this thesis because peptides and/or the peptide/lipid complex were squeezed into the subphase during the annealing process.

$$\Delta G_{ex} = \int_0^{\pi} [A_{12} - (X_1 A_1 + X_2 A_2)] d\pi \qquad \text{(Eq. 1)}$$

$$\Delta F_{ex} = -\int_{A_0}^{A} [\pi_{12} - (X_1 \pi_1 + X_2 \pi_2)] dA \qquad \text{(Eq. 2)}$$

where A_1 = area occupied by component 1 at pressure π

A_2 = area occupied by component 2 at pressure π

$A_{1,2}$ = area occupied by the mixture at pressure π

X_i = molar fraction of component i

π_1 = surface pressure of component 1 at area A

π_2 = surface pressure of component 2 at area A

2.2.2 Critical micelle concentration

Stock solutions of the peptides were prepared in PBS. PBS (20 mL) was added to a round PTFE dish along with a magnetic stirring bar. A small amount of peptide solution was incrementally injected into the subphase through a small opening in the dish and the surface pressure was monitored until equilibrium was attained.

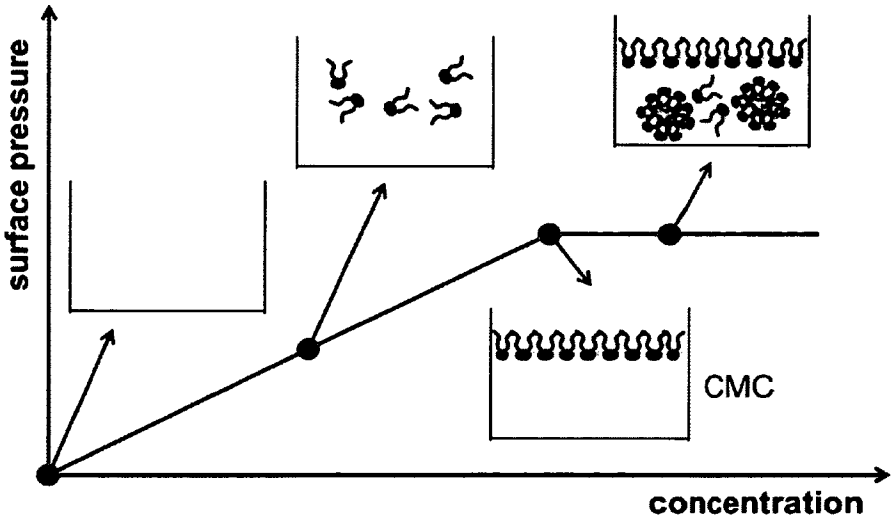

Figure 2.2: Schematic diagram of pressure increases as the number of phospholipid molecules saturates the air-water interface. The final concentration at which the surface pressure ceases increasing is the CMC of the molecule.[5]

2.2.3 Kinetic adsorption and critical pressure of insertion

The kinetics of peptide binding to the lipid monolayer were also studied in a LB trough or a round PTFE dish with PBS (200 mL and 20 mL, respectively) as the subphase. The change from using a LB trough to a round PTFE dish was to limit the amount of peptide used. Lipid solutions in chloroform were spread drop-wise at the interface until the desired surface pressure was reached. Peptide solutions were injected from beneath the barrier of the LB trough or through a small opening in the PTFE dish under the lipid monolayer. Slow stirring using a magnetic stirring bar for about 10 seconds was done in PTFE dish — to minimize pressure measurement error. The surface area or pressure increase with time was recorded in the LB trough or PTFE dishes, respectively, until no further changes occurred.

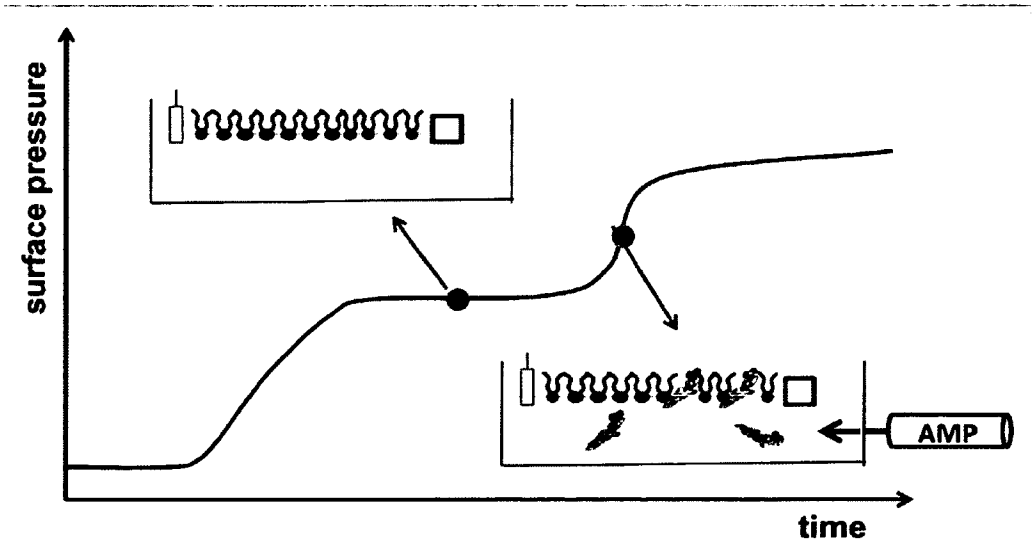

Figure 2.3: Schematic diagram of surface pressure change with time as injected peptide adsorbs to a lipid monolayer.

To determine the CPI for a peptide into a lipid monolayer, a lipid monolayer was prepared at the air-water interface of the PTFE dish until a constant surface pressure was obtained. A small amount of peptide solution (slightly below the CMC of a peptide to prevent formation of peptide micelles) was injected beneath the monolayer and the surface pressure was monitored until equilibrium. The process was repeated with different initial surface pressures using 1 or 0.1 mg/mL solutions of DPPC and DPPG in chloroform or chloroform/methanol (3:1, v/v) mixtures. Pressure increase upon peptide addition, $\Delta\pi$, was then plotted as a function of initial surface pressure, π_0. The data points were further fitted using a linear function. Extrapolation at zero change in pressure ($\Delta\pi$=0) gives the CPI.[5]

2.3 LIPOSOME PREPARATION

The liposomes were prepared by first dissolving an appropriate amount of DPPC, DPPG, and the lipid mixtures (Table 2.1) in chloroform, evaporating the solvent under a gentle stream of nitrogen, followed by placing the sample in vacuum for at least 24 hours to ensure complete removal of chloroform.

The lipid films were hydrated for 30 min in a medium of interest — 18.2 MΩ cm Milli-Q water, PBS, or leakage buffer (10 mM Tris-HCl, 150 mM NaCl, 1 mM EDTA pH 7.45 in 18.2 MΩ MilliQ water) containing 70 mM CF/calcein — for each experiment to obtain a final lipid concentration of 1 mg/mL. The hydration temperature was between 30 to 50 °C — above the lipids' transition temperatures.

For the leakage assay, subsequent to hydration the lipid suspension was mixed vigorously and sonicated in an Elma S10H Elmasonic between 30 to 50 °C for 5 min. The

liposomes were sized by extruding through a polycarbonate membrane (100 or 200 nm) 10 to 31 times between 30 to 50 °C. Five freeze/thaw cycles — between liquid nitrogen and a water bath (60 °C) — were performed before or after extrusion to maximize CF/calcein encapsulation. Free CF/calcein was separated from the encapsulated CF/calcein by a size exclusion column with sephadex G-50 as a gel filtration medium. Leakage buffer was used for column equilibriation (1 to 3 hrs) and elution. Fresh dye encapsulating liposomes were used for each fluorescence measurement. To clean the sephadex G-50, the column was rinsed with deionized water followed by 0.2 M NaOH until it became clear. Sephadex G-50 was stored in 10% ethanol solution at 4 °C.

For AFM imaging, the lipid suspension was first vigorously vortexted and then sonicated with the Elma S10H Elmasonic between 40 °C to 50 °C until clear.

For UVRR spectroscopy, 10 mg/mL liposome solution was made by sonicating the suspension with a Branson 1510 sonicator at 60 °C until clear, followed by extruding 30 times through a 100 nm polycarbonate membrane. The liposomes were stored at 4 °C and were used for Raman measurements within 2 to 3 days.

Table 2.1: Model membrane composition in mole percentage.[6-8]

Model membrane	**SM**	**Chol**	**DOPC**	**DOPG**	**DOPE**	**CL**
Mammalian	-	33.4	44.4	-	22.2	-
Raft	40	20	40	-	-	-
E. coli	-	-	-	20	80	-
S. aureus	-	-	-	55		45
B. subtilis	-	-	-	84	12	4

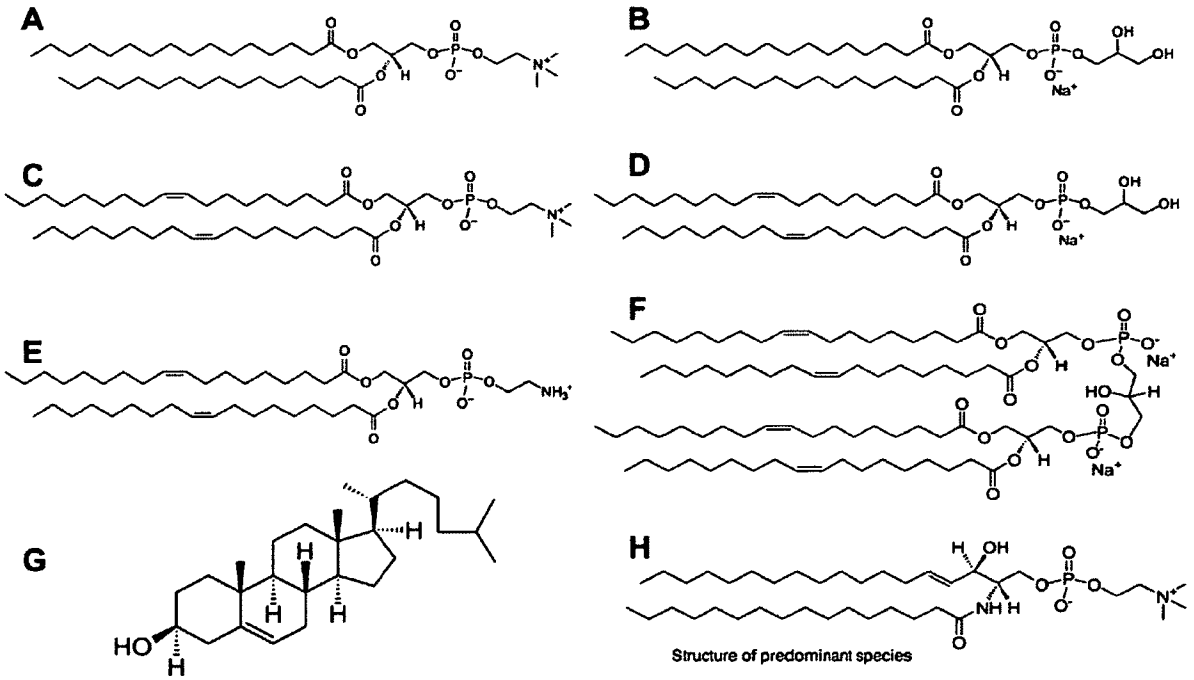

Figure 2.4: Structure of (A) DPPC, (B) DPPG, (C) DOPC, (D) DOPG, (E) DOPE, (F) 18:1 CL, (G) Chol, ovine wool, and (H) egg SM.[9]

2.4 LEAKAGE ASSAY

Leakage experiments were performed using 2 mL of dye-encapsulating vesicles diluted 10 to 20 times with the leakage buffer on a Varian Cary Eclipse spectrofluorometer. The change from calcein to CF was due to CF has lesser negatively charged (-1) and smaller in size than calcein (-3). Excitation and emission wavelengths were between 475 nm to 490 nm and 510 nm to 525 nm, respectively. Excitation and emission slits were 2.5 nm, the voltage of the photomultiplier tube was 540V and the integration time was at 1.0 to 1.5 seconds. The baseline fluorescence (F_0) was monitored until a steady signal intensity was reached before the addition of peptide. After the peptide was added, the fluorescence signal intensity was monitored for 15 minutes or until no further changes were observed. The final fluorescence signal intensity (F) was

then measured. The maximum fluorescence signal that corresponds to complete disruption of the vesicles (F_M) was measured and monitored for 5 minutes after adding 20 μL of 10% triton X-100 to the mixture at the end of the experiment. The following formula was used to measure the leakage fraction:

$$\% \ leakage = \frac{[(F - F_0) \times 100\%]}{(F_M - F_0)} \qquad \text{(Eq. 3)}$$

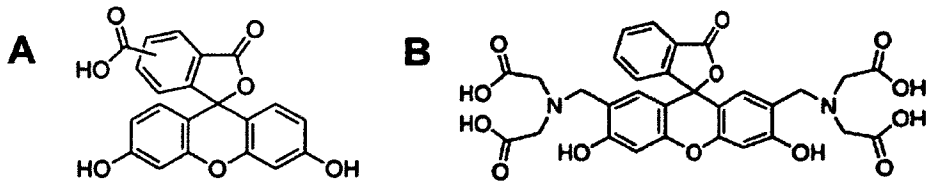

Figure 2.5: Structures of (A) CF and (B) calcein.[10]

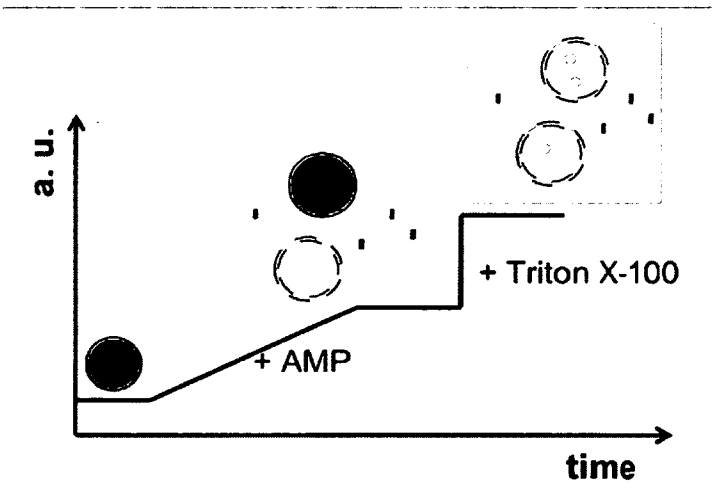

Figure 2.6: Schematic diagram of fluorescence signal increases as encapsulated dye that self-quenches at high concentration leaks out from the liposomes subsequent to the addition of AMP or Triton X-100.

2.5 PHOSPHATE ASSAY

Three protocols were used to evaluate phosphorus content of liposomes of leakage assay – to correlate peptide/lipid ratio to percent leakage. All assays were based on the colour formation of the reduced phosphomolybdate complex. The phosphorus standard solutions were prepared up to 1 mM using monobasic sodium phosphate in 18.2 MΩ cm Milli-Q water.

2.5.1 Ashed by KNO_3 and reduced by Fiske & Subbarow reagent[11,13]

Dye encapsulating vesicles (500 uL) were mixed with 0.1 mL of KNO_3 and heated with a Bunsen burner to form potassium pyrophosphate on flame. Each sample was mixed with 0.3 mL of 1 M HCl and incubated in a 100 °C water bath for 15 min. Next, 4.6 mL of 0.22 % ammonium molybdate and 0.2 mL Fiske-Subbarow reducing agent were added followed by vigorous mixing. The samples were subsequently incubated in a 40 °C water bath for 15 min. Absorption of the signal at 835 nm was measured.

Fiske-Subbarow reagent was prepared by mixing 40 mL of 15% (w /v) sodium bisulfate, 0.2 g sodium sulfite and 0.1 g of 1-amino-4-naphtholsulfonic acid. The solution was filtered and stored in the dark at 4 °C for up to 1 week.

2.5.2 Ashed by $HClO_4$ and reduced by Fiske & Subbarow reagent[13,14]

Dye-encapsulating vesicles (300 μL) were mixed with 1 mL of $HClO_4$ and heated at 200 °C on a block heater for an hour. Upon cooling, 4.6 ml of 0.22% ammonium molybdate and 0.2 mL of Fiske-Subbarow agent were added to each sample followed by

vigorous mixing. The solution was incubating in a water bath at 100 °C for 15 min. Absorption of the signal at 817 nm was measured.

2.5.3 Ashed by H_2SO_4 and reduced by ascorbic acid[11,15]

Dye-encapsulating vesicles (200 μL) were mixed with 0.45 mL of H_2SO_4 and heated with a block heater on a hot plate for 25 min at 200-220 °C that was monitor using mineral oil. Upon cooling, 150 μL of H_2O_2 was added to each sample and heated further for 30 min. Next, 3.90 mL of deionized water, 0.50 mL of 2.5% ammonium molybdate and 0.50 of 10% ascorbic acid, in this order, were added to each sample. The solution was incubated in a water bath at 100°C for 7 min. Signal absorption was measured at 817 nm. Ammonium molybdate and ascorbic acid were stored in the dark at 4 °C for up to a month.

2.6 ATOMIC FORCE MICROSCOPY

All topography images were obtained using an Ntegra (NT-MDT, Russia) atomic force microscope by a 100 × 100 μm^2 scanner (Ntegra) with 512 × 512 points per image.

2.6.1 Imaging monolayers of peptide, lipid, and peptide/lipid mixtures in air

Cantilevers with rotated monolithic silicon tips ContAl (450 μm-long, force constant 0.2 N/m ContAl, resonant frequency 13 kHz; Budget Sensor) and Tap 300 Al (125 μm-long, 40 N/m spring constant, resonance frequency 315 kHz; Budget Sensors) were used for all topographic measurements. The typical scan rate was 0.5 Hz. At least three areas of the same sample were imaged for several independent sample preparations.

2.6.2 Imaging supported lipid bilayers in solution

Cantilevers with rotated monolithic silicon tips (450 μm-long, force constant 0.2 N/m ContAl, resonant frequency 13 kHz; Budget Sensor) and silicon nitride V-shaped cantilevers (100 μm-long, force constant 0.27 N/m, 30 kHz; Budget Sensor) were used for topography measurements in MilliQ deionized water and 150 mM NaCl solution, respectively. The fluid cells and the cantilevers were cleaned with ethanol and irradiated with UV light prior to every experiment for the removal of organic contaminants.

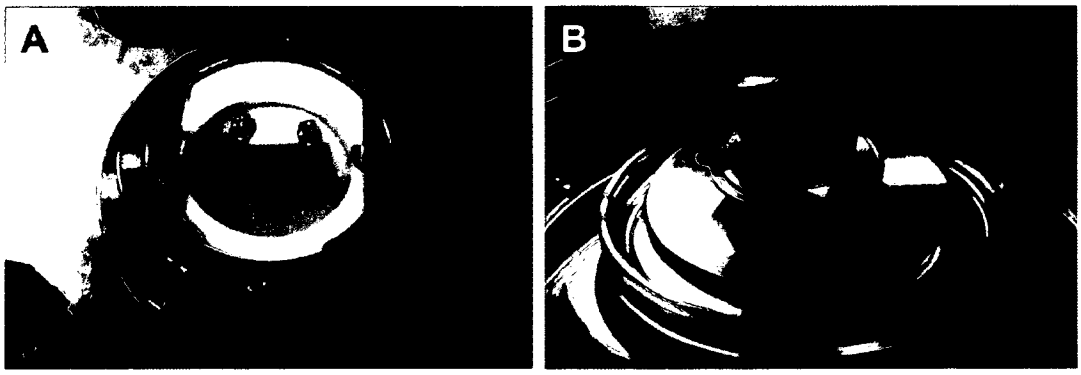

Figure 2.7: (A) Sealed liquid cell with sample holder (MP4LCNTF, NT-MDT, Russia) (B) cantilever on the glass pedestal for liquid imaging (NT-MDT, Russia).

The SLBs were formed on freshly cleaved mica sheet substrates sealed with a silicon O-ring in a fluid cell (NT-MDT, Russia) through vesicle fusion method by adding 1 mL of PBS, 40 μL of 1M $CaCl_2$ and 1 mL of 1 mg/mL lipid vesicles. After incubating at room temperature for 50 minutes, the fluid cell was rinsed with PBS followed by imaging medium to remove excess vesicles. To observe the effect of salt on the interaction between the peptide and raft SLBs, 150 mM NaCl solution and 18.2 MΩ cm MilliQ

deionized water were used separately as imaging media. The importance of Chol was investigated by preparing SLBs without cholesterol (DOPC/SM 1:1 mol%)

Imaging the SLBs prior to and after the 30 min peptide incubation provided a preliminary study of the effect of peptide on the morphology of raft SLBs. Subsequently; peptides were directly injected into the fluid cell for *in situ* observation of peptide/SLBs interaction in real time. Peptides were first added sequentially from 15 μL 0.29 mg/ml in PBS (approximately 0.3 μM) and up to 0.9 μM to investigate peptides/SLBs interaction as a function of time and concentration. To observe the potential outcome of peptide oligomerization, 30 μL of 0.29 mg/mL peptides in PBS (approximately 0.6 μM) were directly added to SLBs and imaged *in situ* in real time. The scanning rate was 0.71 Hz (equivalent to 12 minutes per image) and the scan was carried out from top left to bottom right.

2.7 UVRR SPECTROSCOPY

2.7.1 Sample preparations for Chapter 4

Each peptide stock solution (5 mg/mL Ano-NH_2 and Ano-OH and 6 mg/mL D-Ano-NH_2.) was dissolved in PBS and frozen at −14 °C until used. For PBS examination, peptide samples were diluted to 2 mg/mL with PBS having 0.1 M $NaClO_4$ as an internal standard. For D_2O analysis, peptide samples were diluted to 2 mg/ml with 50% (v/v) D_2O for Ano-NH_2 and Ano-OH and 57% (v/v) D_2O for D-Ano-NH_2; the volume difference was made up with pH 7.4 aqueous 0.01 M PBS and 0.1 M $NaClO_4$. For TFE investigation, peptide samples were diluted to 2 mg/ml in 30% (v/v) TFE for Ano-NH_2 and D-Ano-NH_2 and 40% (v/v) TFE for Ano-OH; the volume difference was made up

with PBS and 0.1 M $NaClO_4$. UVRR spectra were obtained immediately after sample preparation.

SUVs were combined with peptide in a lipid/peptide ratio of 6: 1 for DPPG and DPPC with a final peptide concentration of 1.5 mg/ml. The volume difference was made up with deionised water and 0.1 M $NaClO_4$. UVRR spectra were obtained immediately after sample preparation.

2.7.2 Sample preparation for Chapter 5

Each peptide stock solution was dissolved to 5mg/mL in PBS with 0.1 M $NaClO_4$ as an internal standard and frozen at -20°C until used. Prior to immediate UVRR spectra collection, peptide samples were diluted to 2 mg/mL in PBS in 0.1 M $NaClO_4$ as an internal standard or diluted to 2 mg/ml in 50% (v/v) TFE. The volume difference was made up with PBS in 0.1 M $NaClO_4$.

2.7.3 UVRR spectra collection[16,17]

All experiments were carried out using a Coherent 90C FreD argon ion laser with β barium borate intra-cavity second harmonic generation, producing continuous wave light at 229 nm with a nominal power of 8 mW. The laser was focused on a 3mm × 3mm quartz cuvette with the temperature controlled by a Neslab RTE-7 circulating water bath with magnetic stirring (Starna). The Raman signal was collected in a 135° backscattering geometry using a JobinYvon 1000 mm single optical spectrometer and Spec-10 1340×400 B/LN CCD camera with UV coating (Roper Scientific). Multiple spectra were collected in order to assess sample integrity and the sum was used for the spectra in the

figures; for Chapter 4, the experimental error for intensity measurements was found to be ~5%. In Chapter 4, total accumulation times were 15 and 30 min for Ano-NH_2, D-Ano-NH_2, and Ano-OH samples in PBS and TFE and 7.5 min for all peptide in lipid solution, In Chapter 5, total accumulation time was 45 min for each sample (Ano, Ano8K, Ano1K5V8K) in PBS and TFE. Solvent contributions to sample spectra were minimized by subtraction of pure solvent with internal standard spectra after correcting all spectra to the same standard intensity value for accuracy. Cyclohexane was used for Raman shift calibration. All spectra were processed and peak fitting was performed using GRAMS/AI software (Galactic Industries, Inc.).

In Chapter 4, spectral resolution was estimated using the full width at half maximum for the 1157 cm^{-1} band of cyclohexane and was found to be ~5 cm^{-1}.

In Chapter 5, four peaks were chosen in the amide II[18] and five- in the amide I regions[19] to achieve the best fit to the original trace while minimizing χ^2 values. Using an alternative number of peaks did not provide as successful of a fit or increased the χ^2 undesirably. A Gaussian-Lorentzian mix was employed for the peak characteristic shape with a linear baseline and a maximum band width at half height (BWHH) restriction of 25 cm^{-1}.

2.8 X-RAY SPECTROMICROSCOPY[20-22]

Lipid/peptide monolayers were deposited on 1 × 1 cm^2 silicon wafer (for X-ray photoemission electron microscopy, X-PEEM) or a 0.5 × 0.5 cm^2 Si_3N_4 window with underside covered by foil (for scanning transmission X-ray microscopy, STXM) with LB technique mentioned previously. STXM results were very nosiy thus are not presented.

All X-PEEM measurements were performed at the Advanced Light Source on bend magnet beamline 7.3.1 or the polymer STXM on beamline 5.3.2.2. Data analysis in short: images were taken at various photon energies followed by their stacking. A unique near edge X-Ray absorption fine structure spectrum was provided by each pixel of a stacked image. The component maps were obtained by fitting reference spectra of lipid and peptide to each pixel. The bright area corresponds to pixels of the component whereas the dark area corresponds to the absence of the component — unlike the height representation in AFM images. Detailed accounts for experimental apparatus, beamline setup, and data analysis of XPEEM and STXM can be found in the *European Biophysical Journal* **2011**, *40*: 805-810.

2.9 ANTIMICROBIAL ASSAY

The antimicrobial activities of Anoplin derivatives were determined for Gram-negative bacteria *E. coli* (DH5-α) and Gram-positive bacteria *B. subtilis* (ATCC23857). Fresh bacteria were diluted with MHB to a final concentration of ~10^7 CFU/mL. In each well of a 96-well sterile microtiterplate (Corning), 10 μL of bacteria liquid culture were inoculated in 80 μL of MHB. Ten μL of each peptide were added at final concentrations of 0, 0.1, 1, 10, 50, 100 and 200 μg/mL. Following incubation at 30°C and 200 rpm for 24 to 48 hours, 10 μL of each mixture were spread on MHA plate in duplicates. The experiment was repeated three times. MIC determination was defined as the lowest concentration, which did not cause bacterial growth.

In order to determine the dose of each peptide that killed 50% of each bacterium, LD_{50}, Probit analysis was performed with the PROC Probit procedure in the SAS System

(SAS Institute, Cary, NC). Analysis of variance was performed and when significant, mean comparisons were performed with Fisher's protected least significant difference (LSD) test at P=0.05.

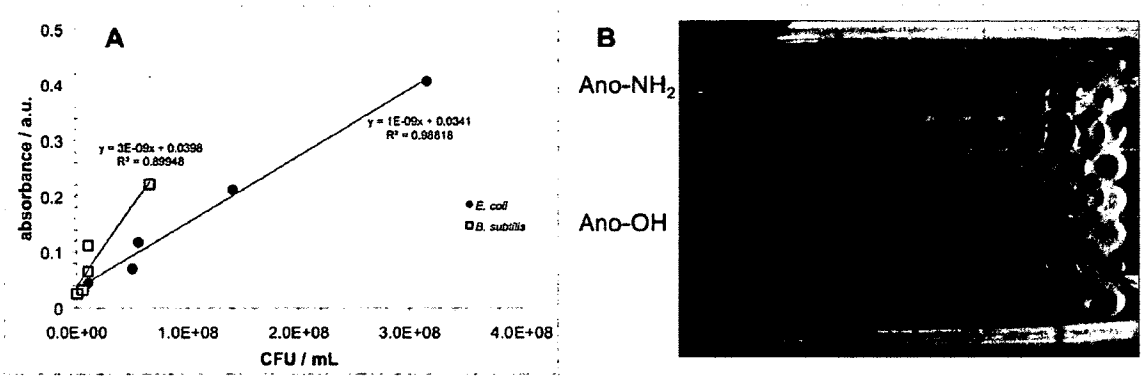

Figure 2.8: (A) Standard curve of *E. coli* and *B. subtilis* culture in MHB and (B) MIC determination of Ano-NH_2 and Ano-OH on *B. subtilis* in a 96 well microtiterplate.

2.9 REFERENCES

1. Birdi, K.S. 2002. Self-assembly Monolayer Structures of Lipids and Marcomolecules at Interfaces. Kluwer Academic Publishers.
2. Jones, M.N.; Chapman, D. Micelles, Monolayers, and Biomembranes. 1995.Wiley-Liss, Inc.
3. Maget-Dana, R. *Biochim. Biophys. Acta - Biomembranes.* **1999**, *1462*, 109-140.
4. Feng, S.-S.; Gong, K.; Chew, J. *Langmuir* **2002**, *18*, 4061-4070.
5. Eiriksdottir, E.; Konate, K.; Langel, U.; Divita, G.; Deshayes, S. *Biochim. Biophys. Acta—Biomembranes* **2010**, *1798*, 1119–1128.
6. Smirnov, A. I. *J. Magn. Reson.* **2008**, *190*, 154–159.

7. Epand, R. F.; Savage, P. B.; Epand, R. M. *Biochim. Biophys. Acta - Biomembranes* **2007**, *1768*, 2500–2509.

8. Ira.; Johnston, L.J. *Langmuir*, **2006**, *22*, 11284-11289.

9. Avanti Polar Lipids, http://www.avantilipids.com

10. Sigma Aldrich, http://www.sigmaaldrich.com/canada-english.html

11. Fiske, C.H.; Subbarow, Y. *J. Biol. Chem.* **1925**, *LXVI*, 375- 400.

12. Edwards, K.A.; March, J.C. *Anal. Biochem.* **2007**, *368*, 39 - 48.

13. Pokorny, A.; Birkbeck, T.H.; Almeida, P.F.F. *Biochemistry* **2002**, *41*, 11044 -11056.

14. Bartlett, G.R. *J. Biol. Chem.* **1959**, *234*, 466- 468.

15. Chen, P.S.; Toribara, Jr., T.Y.; Warner, H. *Anal. Chem.*, **1956**, *28*, 1756-1758.

16. Pripotnv, S.; Won, A.; Ianoul, A. *J. Raman Spectrosc.* **2010**, *41*, 1645-1649.

17. Won, A.; Pripotnev, S., Ruscito, A.; Ianoul, A. *J. Phys. Chem. B.* **2010**, *41*, 1355-1359.

18. JiJi, R.D.; Balakrishnan, G.; Hu, Y.; Spiro, T.G. *Biochemistry*, 2006, 45, 34- 41.

19. Guiffo-Soh, G.; Hernandex, B.; Coic, Y.; Boukhalfa-Heniche, F.; Fadda, G.; Ghomi, M. *J. Phys. Chem. B* **2008**, *112*, 1282- 1289.

20. Anders, S.; Padmore, H.A.; Duarte, R.M.; Renner, T.; Stammler, T.; Scholl, A.; Scheinfein, M.R.; Stohr, J.; Seve, L.; Sinkovic, B. *Rev. Sci Instrum.* **1999**, *70*, 3973-3982.

21. Kilcoyne, A.L.D.; Tylisczak, T.; Steele, W.F.; Fakra, S.; Hitchcock, P.; Franck, K.; Anderson, E.; Harteneck, B.; Rightor, E.G.; Mitchell, G.E.; Hitchcock, A.P.; Yang, L.; Warwick, T.; Ade, H. *J. Synchrotron Rad* **2003**, *10*, 125–136

22. Leung, B.O.; Hitchcock, A.P.; Won, A.; Ianoul, A.; Scholl, A. *Eur. Biophys. J.* **2011**, *40*: 805-810.

CHAPTER 3

THE EFFECT OF ANTIMICROBIAL PEPTIDE PEM-2 ON THE INTERACTIONS WITH PHOSPHOLIPID MONO- AND BILAYERS

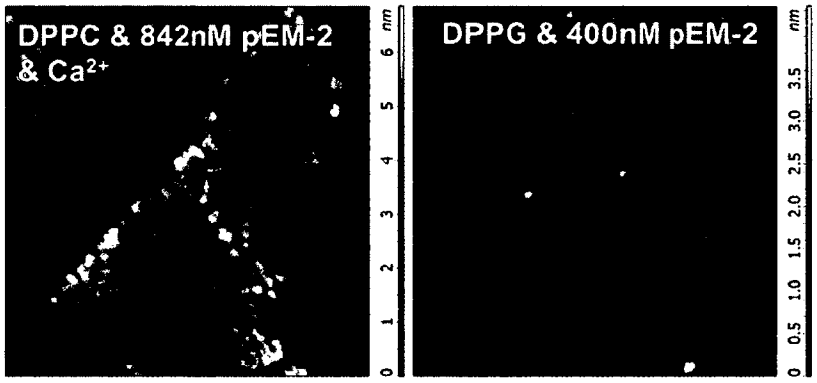

3.1 INTRODUCTION

A series of 10 synthetic peptides was derived from the C-terminus of myotoxin II of *Bothrops asper* (KKYRYYLKPLCKK) which is homologous to catalytically inactive Lys 49 phospholipase A_2.[1,2] In the series, peptides were obtained by substituting one or several tyrosine residues with tryptophan. A general correlation between the number of tryptophan substitutions and microbicidal potency was observed. However, together with high bactericidal activity most of these newly derived peptides were more cytolytic towards skeletal muscle cells, thus limiting their potential *in vivo* application.[2] One of the derivatives called pEM-2 was obtained through substituting 117, 119 and 120 Tyr with Trp, and 123 Pro and 125 Cys with Ala giving the sequence KKWRWWLKALAKK. This derivative was found to maintain high bactericidal[1,2], fungicidal[3] and also antitumor activity[4] while having reduced toxicity toward eukaryotic cells. The all D-enantiomer of pEM-2 retains the same bactericidal potency as the L-enantiomer but is also less susceptible to degradation by proteases, suggesting a non specific nature of interactions between the peptide and the target.[1] In this work, the role of hydrophobic and ionic components in these non specific interactions was explored by LB technique, AFM as well as leakage assay.

3.2 RESULTS AND DISCUSSION

3.2.1 Monolayers of pEM-2

Monolayers of pEM-2 at the air-water interface were obtained through injecting the peptide into the subphase and allowing the system to equilibrate. At equilibrium, a fraction of the peptide adsorbs at the interface and forms a monolayer following the

annealing process. Fig 3.1A shows LB isotherms obtained for pEM-2 at the peptide concentrations up to 842 nM, which is comparable to its minimum microbicidal concentration against a number of bacteria, including *E. coli* and *S. aureus*.[1] The surface pressure increases almost linearly to about 15 mN/m with decreasing surface area. Around 15 mN/m the slope of the isotherm changes indicating peptide loss into the subphase during compression.[5] The expansion isotherms do not overlap with the compression isotherms also signaling the loss of pEM-2 into the subphase above a certain pressure. After the complete expansion of the monolayer, the peptide re-adsorbed back onto the interface. At higher peptide concentration in the trough, higher surface pressure could be achieved and led to increase in the hysteresis. Such behavior has been observed for other antimicrobial peptides.[5]

In this monolayer experiment, pEM-2 was added directly into the subphase rather than deposited at the interface. This method of peptide introduction is more representative of the natural association phenomena of a peptide with a biological membrane.[5-7] At the same time, since the amount of the peptide at the interface was not known it was impossible to calculate the molecular area for pEM-2 in the monolayer. Instead, the increase in the monolayer surface area was related to the total peptide concentration in the trough. Figure 3.1B shows the surface area occupied by pEM-2 relative to the peptide concentration as a function of the surface pressure. In the 4-18 mN/m surface pressure range the area slowly decreases from 0.16 to 0.08 cm^2/nM. These values were calculated from compression isotherms (Fig 3.1A) and obviously represent the upper area limit, as the expansion isotherms would give significantly lower values

due to the loss of the peptide into the subphase. However, the numbers provide some quantitative measure of the peptide surface activity.

The monolayers were transferred onto mica at 15 mN/m surface pressures for further AFM analysis. AFM measurements however did not reveal any aggregation of the peptide at the substrate (Fig 3.2).

3.2.2 Kinetics of pEM-2 binding to lipid monolayers

Since most AMPs exhibit their activity at the level of the bacterial cell membrane, model cell membranes such as phospholipid monolayers at the air/water interface are often used in studies of AMPs.[6-13] The effect of membrane lipid composition on binding properties of pEM-2 was studied by conducting insertion experiments with the peptide injected into the subphase under the monolayer of zwitterionic DPPC, anionic DPPG phospholipids or *E. coli* total lipid extract maintained at a constant surface pressure (7.5 or 30 mN/m). The peptide final concentration in the trough was 400 nM and the time dependence of the area increase at constant surface pressure was measured (Fig 3.3).

At 7.5 mN/m, the peptide readily inserted into monolayers of all three lipid types with insertion half times around 1000 s (Fig 3.3A). However the degree of the area change is different. For DPPC monolayer, the relative area increase was 20 %, whereas for DPPG and for *E. coli* extract it was almost 35%, giving relative molar area change $\Delta A/(A \times c)$ 4.8×10^{-4} nM^{-1} for pEM-2 insertion into DPPC and 8×10^{-4} nM^{-1} for pEM-2 insertion into DPPG, where A is surface area, ΔA is the area change and c is the peptide trough concentration.

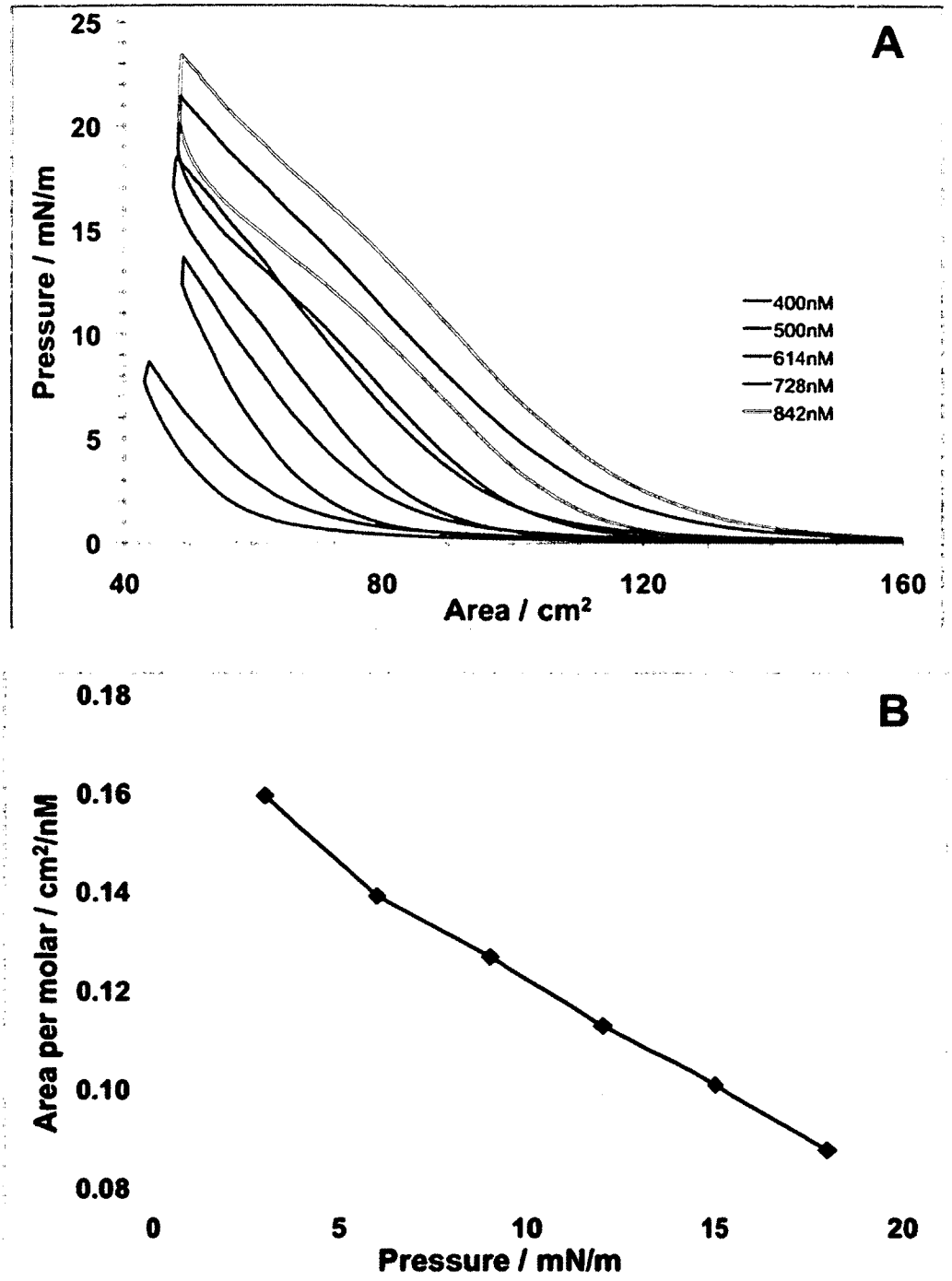

Figure 3.1: (A) LB compression-expansion isotherm cycles of pEM-2 monolayers of different peptide concentrations. (B) Area per nanomolar of peptide as a function of surface pressure. Average data calculated for different pEM-2 concentrations as presented.

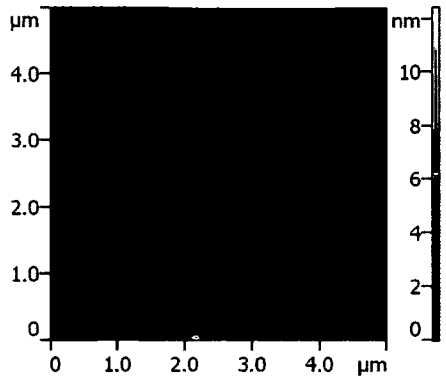

Figure 3.2: Selected AFM topography image of 420 nM pEM-2 monolayer transferred at 15 mN/m.

The insertion experiment was also performed with the monolayers pre-compressed to 30 mN/m (Fig 3.3B). After the peptide injection, the relative area change was found to be 2.5 % for DPPG, about 1% for *E-coli* extract and barely any change was observed for DPPC. Relative molar area change $\Delta A/(A \times c)$ was found to be 5.4×10^{-5} nM^{-1} for pEM-2 insertion into DPPG, 2.5×10^{-5} nM^{-1} for insertion into *E-coli* extract and essentially zero (9.4×10^{-8} nM^{-1}) for insertion into DPPC. The insertion half time was ~500 s which is shorter than for the 7.5 mN/m experiment.

From this experiment it is clear that the nature of the head group plays an essential role in the initial pEM-2/membrane recognition and binding. At low surface pressure of 7.5 mN/m, the peptide was capable of incorporating into both anionic and zwitterionic membranes due to the intrinsic surface activity of the peptide. However, at the biologically relevant pressure of 30 mN/m, pEM-2 had a much higher affinity for anionic DPPG membranes and a modest but detectable affinity to the *E-coli* membrane, which also carries some negative charge. This suggests the importance of electrostatic attraction between the peptide and the anionic model cell membrane.

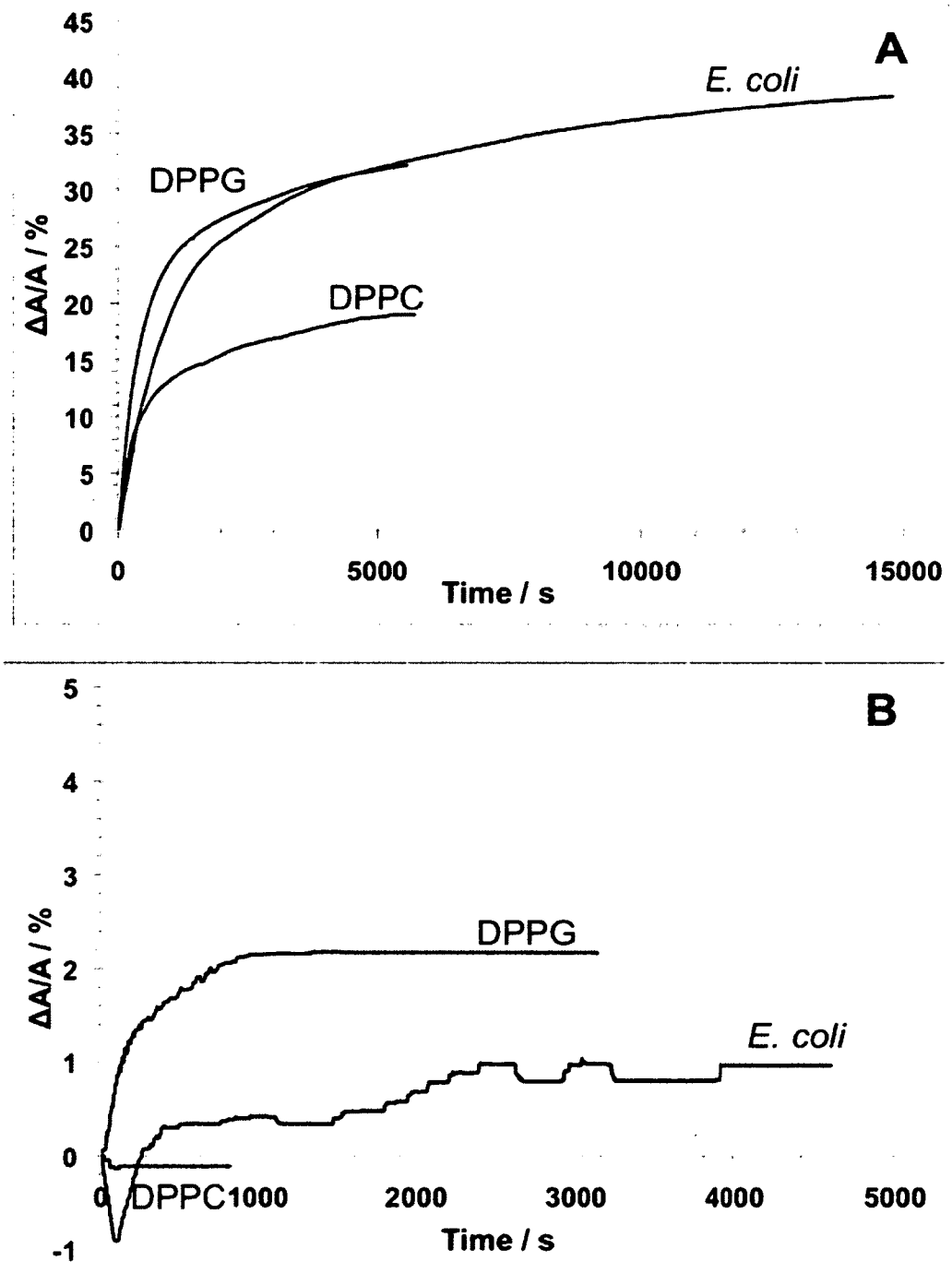

Figure 3.3: Relative increase of the area of DPPG, DPPC, or *E. coli* monolayer compressed to (A) 7.5 mN/m and (B) 30 mN/m as a function of time after pEM-2 was injected into the subphase. Final pEM-2 concentration was 400 nM.

3.2.3 Interaction of pEM-2 with monolayer of zwitterionic phospholipid DPPC

LB isotherms for monolayers of zwitterionic phospholipid DPPC in the presence of pEM-2 were further obtained (Figure 3.4A). In this set of experiments phospholipid monolayers were first prepared and the peptide was injected into the subphase with the monolayer fully expanded, at 0 mN/m surface pressure.

The compression isotherm for a monolayer of pure DPPC shows a characteristic LE-LC phase transition at 7.5 mN/m (Fig 3.4A).[14] When pEM-2 was added to the trough with the DPPC monolayer fully expanded, the peptides tended to adsorb at the air/water interface. Upon further compression, the resulting mixed pEM-2/DPPC monolayer occupied a greater area than the pure DPPC monolayer. With increasing concentration of pEM-2 this total area increased as well (Fig 3.4A). The phase transition around 7.5 mN/m was still present when the concentration of the peptide was as high as 842 nM. At higher surface pressure (25 - 30 mN/m), surface areas occupied by the monolayer of DPPC alone and pEM-2/DPPC mixtures were very similar; suggesting that at this pressure most of the peptide was lost into the subphase.

The changes in the surface area with respect to the peptide concentration were further calculated (Fig 3.4B). Each curve represents a relative increase in the area of the monolayer for different final pEM-2 concentrations (calculated as the area of the pEM-2/DPPC mixture minus the area of pure DPPC and divided by the total concentration of the peptide in the trough). As can be seen from Fig 3.4B, up to 100 nM, the increase of surface area upon the peptide addition varies from 0.2 to 0.02 cm^2/nM and is greater or comparable to the area occupied by the peptide alone. Therefore, the peptide has slightly

higher affinity for the monolayer of DPPC rather than for the air/water interface, especially at the lower surface pressure.

Figure 3.5 shows AFM topography images of a pEM-2/DPPC monolayer deposited onto a mica substrate at 30 mN/m for two pEM-2 concentrations: 100 nM and 842 nM. Some small aggregates were observed in both cases. There were two kinds of aggregates observed at 100 nM with corresponding heights of 2 nm and 4-6 nm respectively and lateral dimensions of 30-50 nm. At 842 nM, we could only detect aggregates with the average height of 3-4 nm and lateral size of 30-50 nm. In both cases, the small clusters were organized into larger irregularly shaped micro-domains. The surface area occupied by the clusters is similar at both concentrations, which is consistent with LB data showing very similar monolayer surface area at 30 mN/m for 100 nM and 842 nM. Since no aggregation was observed for the monolayers of the peptide alone, it is reasonable to assume that the observed clusters resulted from the peptide interaction with the lipid and the formation of some lipid/peptide aggregates. Similar behavior was recently observed for other AMPs.[11] The effect of calcium ions will be discussed in section 3.2.5.

3.2.4 Interaction of pEM-2 with monolayer of anionic phospholipid DPPG

LB isotherms for monolayers of anionic phospholipid DPPG in the presence of pEM-2 were further obtained (Fig 3.6A). Similar to the previous experiment, phospholipid monolayers were first prepared and the peptide was injected into the subphase with the monolayer fully expanded (0 mN/m surface pressure). A characteristic LE-LC phase transition was observed at around 10 mN/m.[15-17]

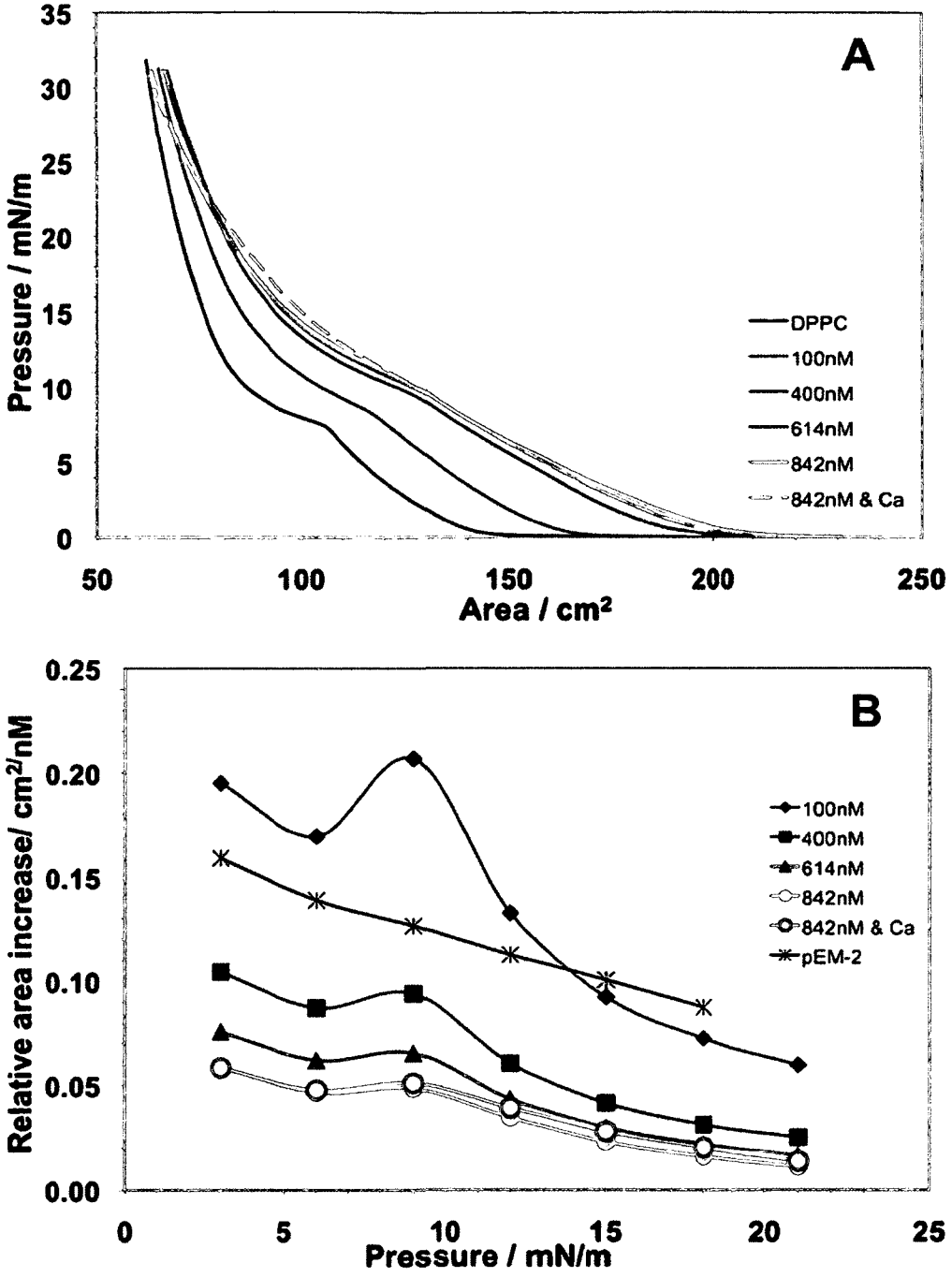

Figure 3.4: (A) Effect of different pEM-2 concentrations on the compression isotherms of a DPPC/pEM-2 monolayer. (B) Relative area increase at different pressures calculated from the isotherms shown in Fig 3.4A.

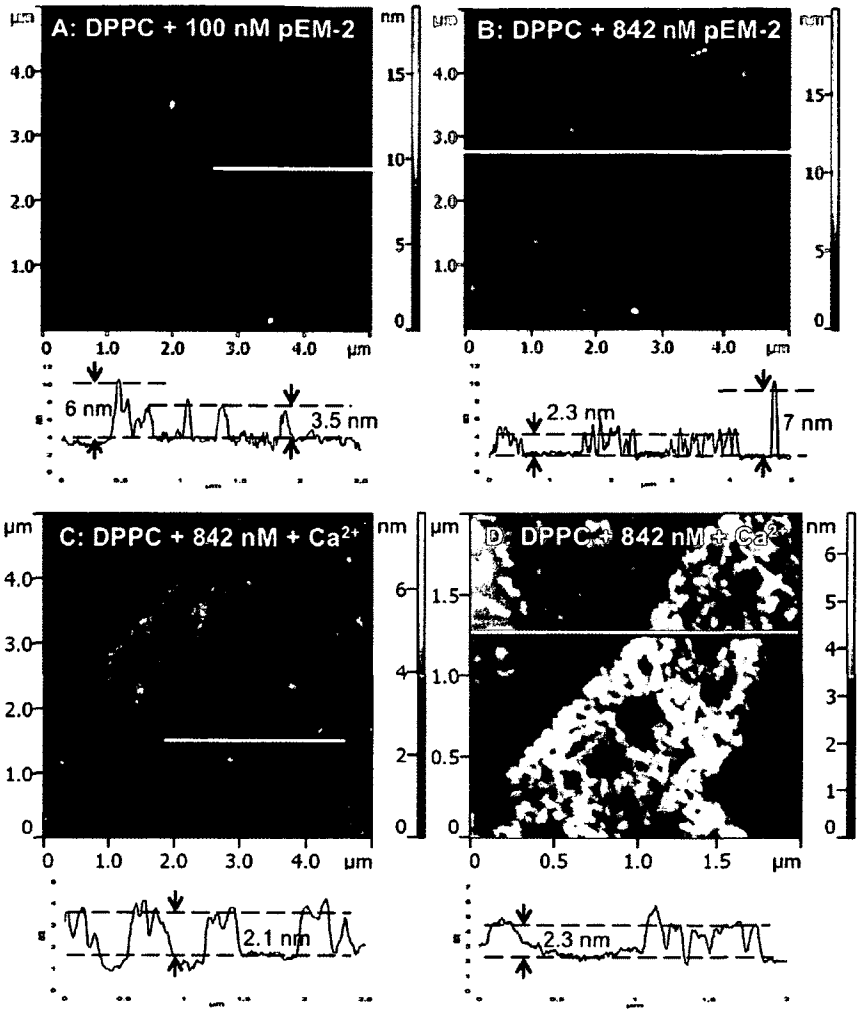

Figure 3.5: Selected AFM topography images of DPPC/pEM-2 monolayers transferred at 30 mN/m in the absence or presence of calcium chloride.

With increasing pEM-2 concentration, the phase transition around 10 mN/m disappeared, and as the monolayer surface area increased, a second transition at 20-25 mN/m appeared. In the 100-400 nM concentration range, the relative increase in the surface area of the monolayer (Fig 3.6 B) is found to be between 0.1 and 0.3 cm^2/nM which is greater than DPPC containing monolayer (Fig 3.4 B); and in most cases is greater than the area occupied by pEM-2 alone (Fig 3.6B). At the same time, at higher surface pressure of 30 mN/m, the pEM-2/DPPG monolayer surface area is almost

independent of the peptide trough concentration but is considerably greater than for DPPG alone (Fig 3.6A). This indicates that unlike DPPC monolayer, a small fraction of the peptide remained in DPPG monolayer even at high surface pressure. Given the strong positive charge of the peptide (+6), it is reasonable to assume that the surface concentration of pEM-2 in DPPG monolayer is larger than in DPPC due to electrostatic attraction, that also limited pEM-2 being squeezed out at high surface pressure.

AFM topography measurements revealed small nanoscale aggregates (Fig 3.7) in the pEM-2/DPPG monolayers. At lower peptide concentration (100 nM) these aggregates are 1-4 nm in height and 20-60 nm in diameter and are organized into large microscale domains. However, unlike pEM-2/DPPC monolayers, the boundaries of these domains are smooth and well defined. At this peptide concentration, the LE-LC transition was still clearly visible in the LB isotherm (Fig 3.6 A).

At higher peptide concentration (400 nM), the plateau corresponding to the phase transition in DPPG monolayer disappeared (Fig 3.6 A) and the topography of the monolayer changed (Fig 3.7 C, D). The size of the small nanoscale aggregates decreases to 1.5-2 nm in height and 10 nm laterally. The micro scale domains become more circular with well defined edges. Finally, there are some small holes 0.5 nm deep observed in the area between the micro scale domains. Similar to DPPC/pEM-2 monolayer the nanoscale aggregates appear most likely as a result of the peptide/lipid interactions and contain molecules of both types. However, unlike DPPC, the nano aggregates in DPPG monolayer are well separated from each other.

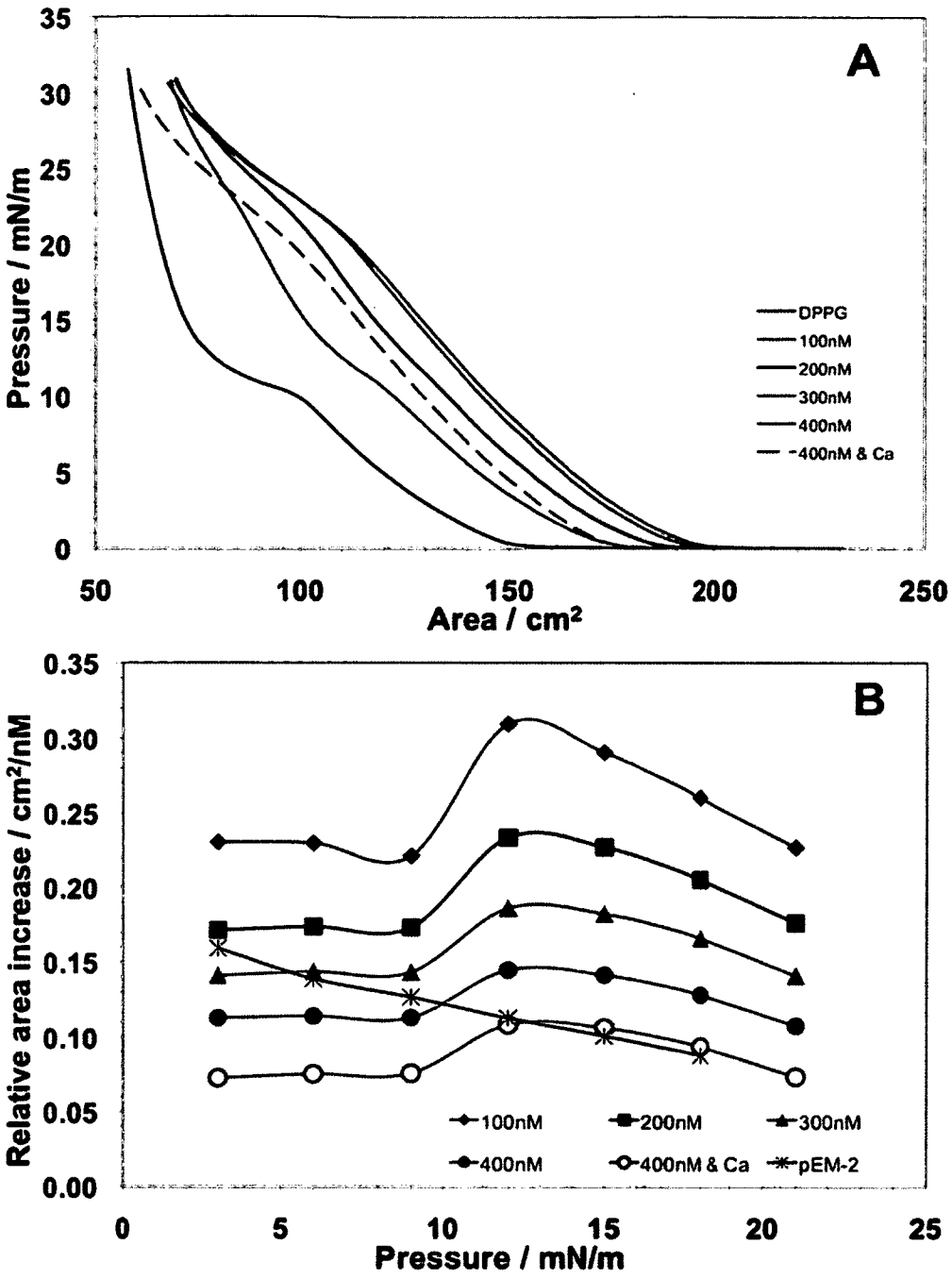

Figure 3.6: (A) Effect of increasing pEM-2 concentration on the compression-expansion isotherm cycles of the DPPG/pEM-2 monolayer. (B) Relative area increase at different pressure calculated from Fig 3.6 A isotherms.

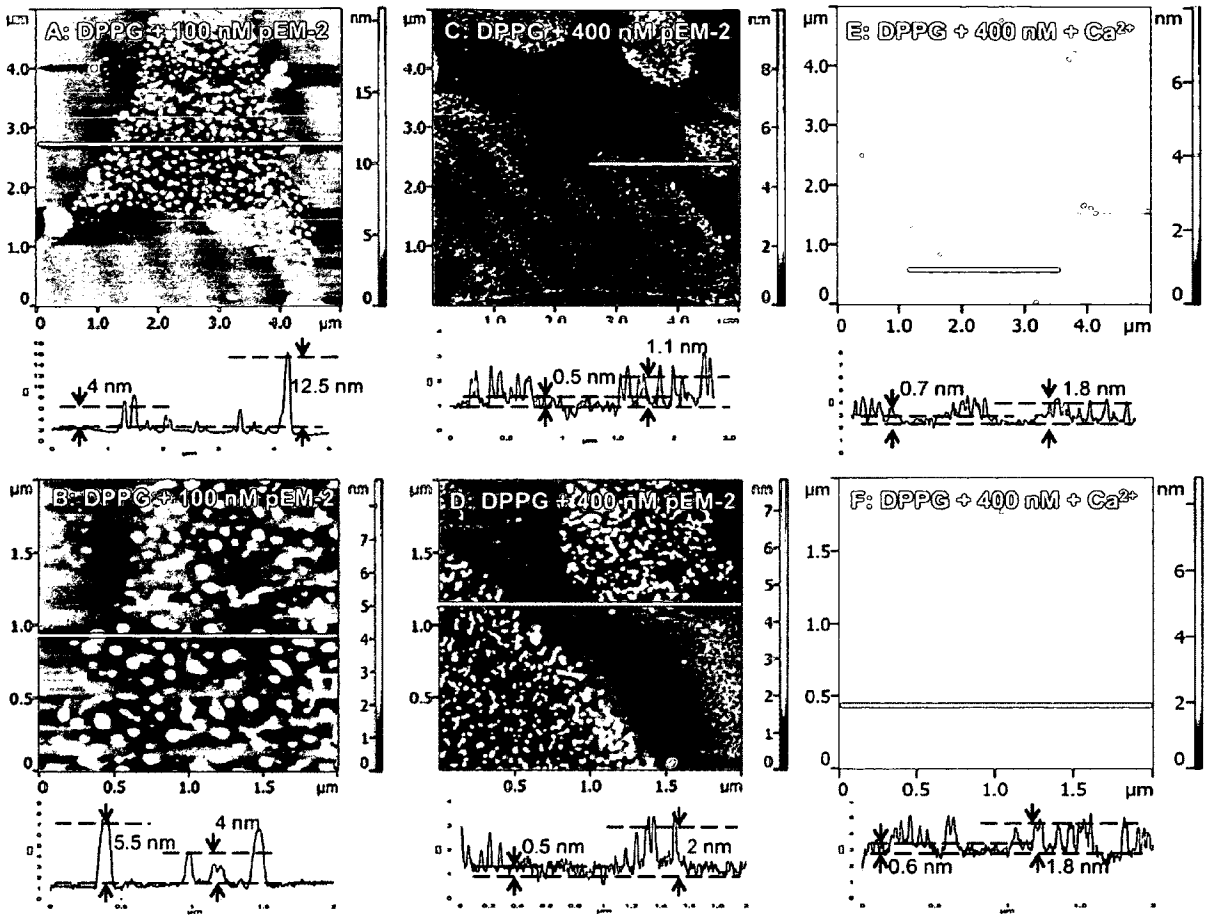

Figure 3.7: Selected AFM topography images of DPPG/pEM-2 monolayers transferred at 30 mN/m in the absence or presence of calcium chloride.

Since the presence of the peptide significantly affects the phase behavior of the lipid monolayer it is possible that the large circular domains are in fact areas of DPPG in LC phase whereas the areas with small holes correspond to the LE phase. A similar effect of other peptides on the behavior of the lipid monolayer has been observed before.[10] The different pattern of the peptide distribution as well as higher surface concentration of the peptide in anionic DPPG as compared to zwitterionic DPPC lipid monolayers indicate a different nature of interactions between the peptide and the two phospholipid model cell membranes.

3.2.5 The effect of calcium ions on pEM-2/lipid interaction

The properties of membrane lipids are known to be strongly affected by the pH and ionic strength of the subphase. Upon binding of cations to lipid headgroups, lipid conformation can be altered and this may increase the order of lipid acyl chains.[18-20] Therefore it was of interest to investigate the effect of calcium ions on the interaction between lipid monolayers and pEM-2.

Calcium ions dramatically decreased the surface area of pEM-2/DPPG (Fig 3.6) but only slightly changed that of pEM-2/DPPC (Fig 3.4). Negatively charged headgroups of DPPG ionize and repel each other in aqueous solution. The presence of positively charged ions neutralized the electrostatic repulsion and thus condensed the surface area. This effect of condensation was reported to depend on lipid net charge ion, and pressure.[21,22] At low surface pressure divalent ions condense the anionic lipid monolayer whereas monovalent ions preferentially condense the zwitterionic lipid monolayer.[22] Calcium ions, however, have a more pronounced effect on both zwitterionic and anionic lipid monolayers since sodium ions are squeezed out from the surface into the subphase at high surface pressure.[21] This may contribute to the minor area changes between the two monolayers (with and without calcium ions) before and after the phase transition of DPPC (Fig 3.4 B).

AFM topography measurements show calcium ions affected pEM-2/DPPC monolayers where the LC domains changed from irregular-shaped to circular shaped (Fig 3.5 B, C). On the other hand, calcium ion did not change the morphology of pEM-2/DPPG monolayer (Fig 3.7 C-F). It is known that large circular domains are favoured by line tension at the domain boundary whereas small extended or irregular shaped domains

are favored by dipole-dipole and electrostatic interactions.[23] Line tension may not play a major role in the reorganization of domain shape but rather the intermolecular interactions. At high surface pressure, 30 mN/m, increasing strength of the interaction between phosphate of DPPC and calcium ions decreased the dielectric permittivity of the surroundings and may order the acyl chains. As a result, extended or irregular shaped domains are not favourable and circular domains were observed. In the case of DPPG, calcium ions might as suggested order its acyl chains but the dielectric permittivity of the surrounding may have already been decreased by cationic peptides; thus no changes occur in the circular domains.

3.2.6 Leakage assay

Lastly, to assess the ability of pEM-2 to rupture the bacterial cell membrane, calcein leakage assay was further performed (Fig 3.8). Five different model cell membranes were used: two single lipid membranes (DPPC and DPPG) and three model mixtures mimicking Gram-positive (*B. subtilis, S. aureus*) and Gram-negative (*E. coli*) bacteria. The amount of calcein release from the vesicles at different peptide concentrations with time was determined. Results show similar lytic activity of pEM-2 to DPPC, *E-coli, B. subtilis*, and *S. aureus* model vesicles. The calcein leakage experiment indicates that the fluorescence signal increases rapidly after peptide addition and was observed at a relatively high peptide to lipid ratio. The fluorescence intensity increased by around 20% for those model cell membranes at the peptide/lipid ratio of 1/10 (Fig 3.8). At the same time, the effect of peptide on anionic DPPG vesicles is considerably weaker: only about 5% of calcein release was observed at the pEM-2/DPPG ratio of 1/10. This observation is

quite different from the monolayer experiments where the peptide showed much higher affinity for anionic DPPG. At pH 7.4, DPPG lipids are completely ionized, which increases repulsion and distance between lipid head groups that allow binding of counterions and results in decreased hydrophobic interaction.[18-20,24] Therefore, the interactions other than electrostatic play the main role in pEM-2 lytic activity.

Interactions of antimicrobial peptides with the bacterial cell membrane represent a multi step process, which includes initial recognition and binding, accompanied by peptide conformational transformation, peptide aggregation, insertion into, and finally disruption of the cell membrane.[25-32] LB monolayer surface tension measurements allowed us to monitor the initial step in the peptide binding. Even though the kinetics of the reaction were limited by the peptide diffusion in the trough, the degree of the peptide binding to the monolayer depended on the initial peptide/membrane interactions. It was conceivable that for this initial recognition and binding step the nature of the lipid headgroup rather than other membrane properties (such as thickness and lateral mobility) plays a determining role. Therefore in this context, LB measurements represent a fairly good model of this initial step and indicate that electrostatic interactions contribute considerably to this process.[13]

On the other hand, the calcein leakage assay monitors the final step of the AMP/membrane interactions: formation of pores and/or membrane rupture. In the experiment the degree of membrane disruption is estimated from the relative amount of calcein released outside the vesicles. It appears that the membrane rupturing ability of pEM-2 does not correlate with the membrane charge, at least for the model membranes

used in the present study, suggesting that electrostatic interactions might not play such a critical role in pEM-2's ability to rupture the membrane.[2]

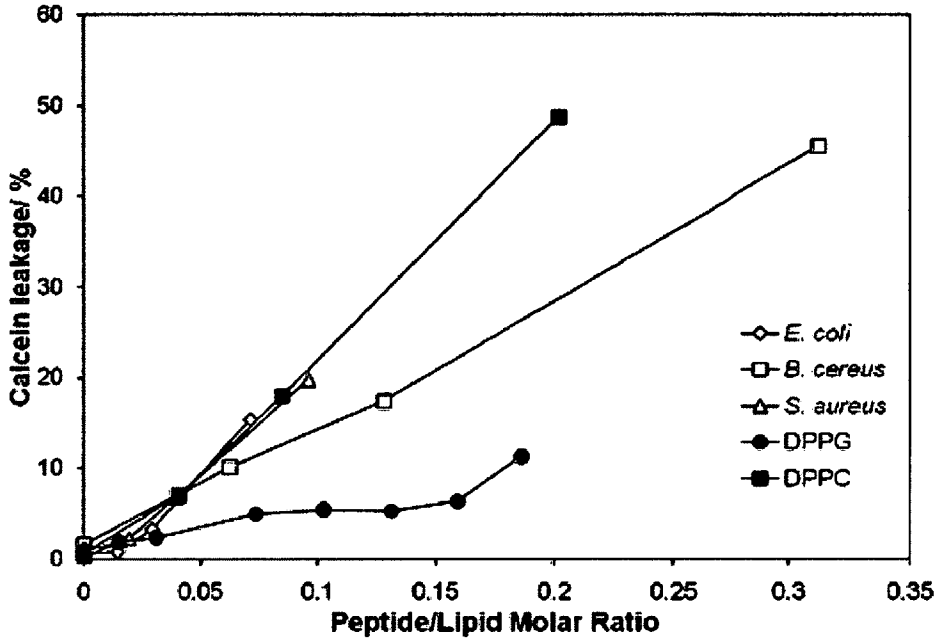

Figure 3.8: Calcein fluorescence signal increase measured about 15 min after the addition of pEM-2 into DPPC, DPPG, *E. coli* model, *S. aureus* model, and *B. subtilis* model vesicles.

Therefore, although the initial recognition and binding of pEM-2 was driven by electrostatic interactions, the membrane lytic activity of the peptide was governed by other interactions such as hydrophobic and depends strongly on the bacterial membrane composition and physicochemical properties. This conclusion is supported by the correlation between the number of Trp residues and the bactericidal activity of other derivatives similar to pEM-2.[2] With an increasing number of Trp residues from 1 to 3, bactericidal potency of the peptides was found to increase, suggesting that hydrophobic interactions are critical for membrane damage.[2] This is also consistent with previous

studies of other antimicrobial peptides.[33] For example, although the membrane charge was found to play a significant role in the rates of the cell-penetrating peptide transportan binding to the cell membrane, dye efflux occurred at about the same rate from charged and uncharged vesicles.[31,34]

Recent studies of pEM-2 by UVRR spectroscopy demonstrated that in a membrane mimicking environment, the peptide changes its conformation and likely folds into a helical amphipatic structure on the membrane surface.[35] Since pEM-2 is a relatively short peptide, it is unlikely that the peptide forms permanent pores in the membrane. Besides, calcein leakage was observed at relatively large peptide/lipid ratios. For these reasons the carpet mechanism or a recently proposed mechanism based on interfacial activity of the peptide are the most likely mechanisms of pEM-2 action in DPPC, *E. coli, B. subtilis*, and *S. aureus* models, but not in DPPG.[32,36] More support for this hypothesis comes from the peptide's ability to induce the formation of nanoscale aggregates in phospholipid monolayers. Lateral organization of these aggregates strongly depends on the membrane composition and is different for DPPC and DPPG models. It is not clear at the moment if similar aggregates occur at the bacterial cell membrane. Further microscopic investigations of pEM-2 interactions with phospholipid bilayers will help establish the mechanisms in more detail.

3.3 REFERENCES

1. Santamaria, C.; Larios, S.; Quiros, S.; Pizazzro-Cerda,J.; Gorvel, J.; Lomonte, B.; Moreno, E. *Antimicrob. Agents Chemoth.* **2005**, *49*, 1340-1345.

2. Santamaria, C.; Larios, S.; Angulo, Y.; Pizarro-Cerda, J.; Gorvel, J.-P.; Moreno, E.; Lomonte, B. *Toxicon,* **2005**, *45*, 807-815.
3. Murillo, L.A.; Lan, C.-Y.; Agabian, N.M.; Larios, S.; Lonomte, B. *Re. Esp. Quimioterap*, **2007**, *20*, 330-333.
4. Araya, C.; Lomonte, B. *Cell. Biol. Int.* **2007**, *31*, 263-268.
5. Edwards, K.A.; March, J.C. *Anal. Biochem,* **2007**, *368*, 39-48.
6. Signor, G.; Mammi, S.; Peggion, E.; Ringdorf, H.; Wagenknecht, A. *Biochemistry*, **1994**, *33*, 6659-6670.
7. Maget-Dana, R. *Biochim. Biophys. Acta - Biomembrane*, **1999**, *1462*, 109-140.
8. Devine, D.A.; Hancock, R.E.W. Cambridge University Press, 2004.
9. Majerowicz, M.; Waring, A.J.; Wen, S.; Bringezu, F. *J. Phys. Chem. B*, **2007**, *111*, 3813-3821.
10. Plenat, T.; Deshayes, S.; Boichot, S.; Milhiet, P.E.; Cole, R.B.; Heitz, F.; Le Grimellec, C. *Langmuir*, **2004**, *20*, 9255-9261.
11. Vie, V.; Van Mau, N.; Chaloin, L.; Lesniewska, E.; Le Grimellec, C.; Heitz, F. *Biophys. J.*, **2000**, *78*, 846-856.
12. Wagner, K.; Van Mau, N.; Boichot, S.; Kajava, A.V.; Krauss, U.; Le Grimellec, C.; Beck-Sickinger, A.; Heitz, F. *Biophys. J.*, **2004**, *87*, 386-395.
13. Gidalevitz, D.; Ishitsuka, Y.; Muresan, A. S.; Konovalov, O.; Waring, A.J.; Lehrer, R.I.; Lee, K.Y.C. *Proc. Natl. Acad. Sci.*, **2003**, *100*, 6302-6307.
14. Yang, X.-M.; Xiao, D.; Xiao, S.J.; Wei, Y. *Applied Phys. A*, **1994**, *59*, 139-143.
15. Takamoto, D.Y.; Lipp, M.M.; von Nahmen, A.; Lee, K.Y.C.; Waring, A.J.; Zasadzinski, J.A. *Biophys. J.*, **2001**, *81*, 153-169.

16. Dubreil, L.; Vié, V.; Beaufils, S.; Marion, D.; Renault, A. *Biophys. J.*, **2003**, *85*, 2650-2660.

17. Minones Jr., J.; Dynarowicz-Latka, P.; Minones, J.; Rodrigez Patino, J.M.; Iribarnegaray, E. *J. Colloid Interface Sci.*, **2003**, *265*, 380-385.

18. Pandit, S.A.; Bostick, D.; Berkowitz, M.L. *Biophys. J.* **2003**, *84*, 3743-370.

19. Bockman, R.A.; Hac, A.; Heimburg, T. *Biophys. J.* **2003**, *85*, 1647-1655.

20. Pedersen, U.R.; Leidy, C.; Westh P.; Peters, G.H. *Biochim. Biophys. Acta* **2006**, *1758*, 573-582.

21. Sovago, M.; Wurpel, G.W.H.; Smits, M.; Muller, M.; Bonn, M. *J. Am. Chem. Soc.* **2007**, *129*, 11079-11084.

22. Grigoriev, D; Miller, R.; Wiistneck, N.; Pison, U.; Mohwald, H. *J. Phys. Chem. B* **2003**, *107*, 14283 -14288.

23. Benvegnu, D.J. & McConnell, H.M. *J. Phys. Chem.* **1993**, *97*: 6686-6691.

24. Taneva, S.G.; Keough K.M.W. *Biochim. Biophys. Acta - Biomembrane* **1995**, *1236*, 185-195.

25. Yeaman, M.R.; Yount, N.Y. *Pharm. Rev.*, **2003**, *5*, 28-56.

26. Mookherjee, N.; Hancock, R.E.W. *Cell. Mol. Life Sci.*, **2007**, *64*, 922-933.

27. Hancock, R.E.W.; Sahl, H.-G. *Nature Biotech.* **2006**, *24*, 1551-1557.

28. Brogden, K.A. *Nature Rev. Microbiology* **2005**, *3*, 238-250.

29. Marshall, S.H.; Arenas, G. *Electr. J. Biotech.* **2003**, *6*, 1-12.

30. Zasloff, M. *Nature* **2002**, *415*, 389-395.

31. Yandek, L.E.; Pokomy, A.; Floren, A.; Knoelke, K.; Langel, U.; Almeida, P.F. *Biophys. J.* **2007**, *92*, 2434-2444.

32. Rathinakumar, R.; Wimley W.C. *J. Am. Chem. Soc.* **2008**, *130*, 9849-9858.

33. Toke, O. *Biopolymers* **2005**, *80*, 717-735.

34. Yandek, L.E.; Pokorny, A.; Almeida, P.F. *Biochemistry* **2008**, *41*, 3051-3060.

35. Quan, B.; Ianoul, A. *J. Raman Spectrosc.* **2009**, *40*, *260-263.*

36. Rathinakumar, R.; Walkenhorst, W.F.; Wimley, W.C. *J. Am. Chem. Soc.* **2009**, *131*, 7609-7617.

CHAPTER 4

THE EFFECTS OF DEAMIDATION AND L- TO D- AMINO ACID SUBSTITUTION ON THE ACTIVITY AND MEMBRANE INTERACTIONS OF ANTIMICROBIAL PEPTIDE ANOPLIN

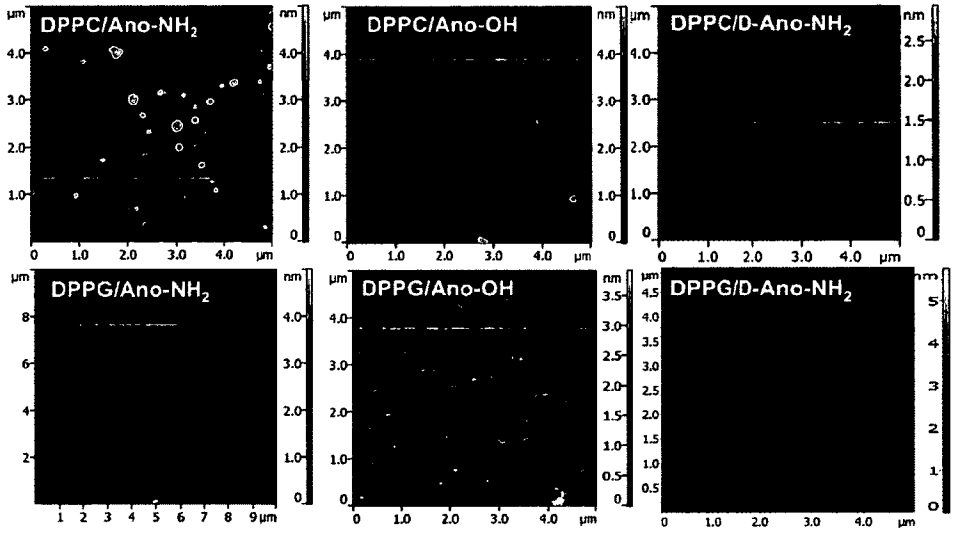

Reproduced with permission from

1. Pripotnev, S.; Won, A.; Ianoul, A. The effects of L- to D- isomerisation and C-terminus deamination on the secondary structure of antimicrobial peptide anoplin in aqueous and membrane mimicking environment. *Journal of Raman Spectroscopy* **2010**, *41*, 1355-1359. Copyright 2010 John Wiley & Sons, Ltd.

2. Won, A.; Khan, S.; Gustin, S.; Akpawu, A.; Seebun, D.; Avis, T.J.; Leung, B.O.; Hitchcok, A.O.; Ianoul, A. Investigating the effects of L- to D- amino acid substitution and deamidation on the activity and membrane interactions of antimicrobial peptide anoplin. *Biochimica et Biophysica Acta – Biomembrane* **2011**, *1808*, 1592-1600. Copyright 2011 Elesvier.

3. Leung, B.O.; Hitchcock, A.P.; Won, A.; Ianoul, A.; Scholl, A. Imaging interactions of cationic antimicrobial peptides with model lipid monolayers using X-ray spectromicroscopy. *European Biophysical Journal* **2011**, *40*, 805-810. Copyright 2011 Springer.

4.1 INTRODUCTION

Anoplin (NH_2-GLLKRIKTLL-$CONH_2$) is one of the major peptide components of the venom of *Anoplius samariensis* and has significant homology with the amphipathic α-helical wasp AMPs crabrolin and mastoparan-X.[1,2] It is a potent mast cell degranulator that shows a broad spectrum of activity in low-salt media against both Gram-positive and Gram-negative bacteria.[1] In addition, anoplin exhibits low hemolytic activity towards human erythrocytes and thus has a great potential for further development.[1,2]

Detailed investigations of anoplin's antimicrobial activity revealed a strong dependence of antibacterial and hemolytic properties of anoplin on physico-chemical properties.[2,3] For example, an increase in the Eisenberg mean hydrophobicity with the introduction of alanine at positions 5, 7, and 8 led to an improved antimicrobial activity, which is however accompanied by an increased hemolytic activity.[4] Replacement of residues at position 5 and 8 by phenylalanine or tryptophan resulted in increased antibacterial as well as hemolytic activities due to the role of these aromatic residues in anchoring the peptide in the membrane. Introduction of lysine at position 8 increased peptide selectivity for prokaryotic cells due to the increased overall charge, while truncation of the peptide at both C- and N- termini gave analogues with lower antibacterial activity. Moreover, deamidation of the anoplin C-terminus dramatically decreased the antimicrobial activity of the peptide due to introduction of a negative charge in a positively charged peptide causing a loss of amphiphathicity.[2,3] In a study of a cell penetrating peptide, transportan, deamidation was found to dramatically decrease the binding of peptide zwitterionic lipid vesicles.[5] At the same time, the effect of

deamidation on binding to anionic vesicles was negligible, suggesting non-additivity of electrostatic and hydrophobic interactions.

Previous studies suggested that partial or complete D-amino acid substitution aids in improving the *in vivo* activity of AMPs without affecting the secondary structure and stability.[7] In order to further investigate structure/function relationships of anoplin, in the present work, the effects of deamidation and L- to D-amino acid conversion on membrane binding and lytic properties of the peptide were investigated using various biophysical techniques. We used antimicrobial assay to show that the interaction of anoplin with bacterial cell membranes is non-specific, since the all D-form shows the same antibacterial activity as the all L-form of the peptide. We further applied LB monolayer techniques, AFM and X-PEEM to observe a strong dependence of anoplin membrane binding properties on the peptide and lipid charge. Dye leakage assay showed the importance of lipid composition on membrane lytic activity. Finally UVRR spectra demonstrated that small modifications in the primary structure of anoplin do not considerably affect its solution structure suggesting a rather complex nature of physicochemical properties that determine the peptide's activity.

4.2 RESULTS AND DISCUSSION

4.2.1 Antimicrobial activity

Antimicrobial activities of all three anoplin derivatives were measured against the Gram-negative *E. coli* and the Gram-positive *B. subtilis*. Table 4.1 shows that both amidated anoplin derivatives exhibited MIC values of 50 mg/mL for *B. subtilis* and 100 mg/mL for *E. coli* while having similar LD_{50} values. Thus replacement of all amino acids

with their D stereoisomers does not change the peptide bacterial activity, providing strong evidence that the mechanism by which the peptide induces bacterial death is through a non-specific interaction with cells such as membrane disruption and is consistent with previous observations.[1,2] The deamidated form of the peptide, on the other hand, showed much lower bactericidal activity with MIC values for both types of bacteria exceeding 200 mg/mL and with a 10- to 30-fold lower LD_{50} value (Table 4.1).

Table 4.1: Antimicrobial activities of anoplin and derivatives toward *E. coli* and *B. subtilis*.

	E. coli		*B. subtilis*	
	MIC (μg/mL)	LD_{50} (μg/mL)	MIC (μg/mL)	LD_{50} (μg/mL)
Ano-NH_2	100	5.8 ± 2.9	50	3.9 ± 1.2
Ano-OH	>200	78.9 ± 4.7	>200	69.4 ± 5.1
D-Ano-NH_2	100	3.0 ± 0.9	50	2.2 ± 0.6

LD_{50} values are means ± standard deviations.

4.2.2 Raman spectra of anoplin derivatives in aqueous PBS, D_2O and TFE

UVRR spectra of the three derivatives of anoplin in PBS at room temperature are presented in Fig 4.1. The bands observed can be clearly identified as amide III (1220-1325 cm^{-1} range), $C_\alpha H$ (~1380 cm^{-1}), CH_3 (1430-1480 cm^{-1}), amide II (1550 -1560 cm^{-1}) and amide I (1600-1700 cm^{-1}).[6,7] There were no major visible differences in the number and position of the bands for all three anoplin derivatives, indicating no change in conformation between those derivatives in aqueous buffer solution. The conformation of the peptides in aqueous solution does not appear to be α-helical. The amide III band for an α-helical conformation has a maximum at ~1300 cm^{-1} whereas the $C_\alpha H$ band at ~1380

cm^{-1} is absent.[6-10] In the UVRR spectra of all three anoplin derivatives, the Amide III band was found at ~1260 cm^{-1} and a relatively strong $C_\alpha H$ band at ~1380 cm^{-1} was also observed (Fig 4.1). Previous studies of anoplin derivatives by CD showed that the peptides adopt a random-coil like conformation in aqueous environment.[1,3] At the same time UVRR data indicate that it is unlikely that the peptides adopt an "unordered" structure in solution. "Unordered" structures are characterized by the amide II position at ~1550 cm^{-1}, and the amide I at ~ 1660 cm^{-1}.[6,7] In the anoplin UVRR spectra we observe the amide II band centered at 1550-1560 cm^{-1}, and the amide I at ~ 1687 cm^{-1}. These band positions (particularly that of amide I) are indicative of a β-structure like conformation, most likely a β-turn.[6,7]

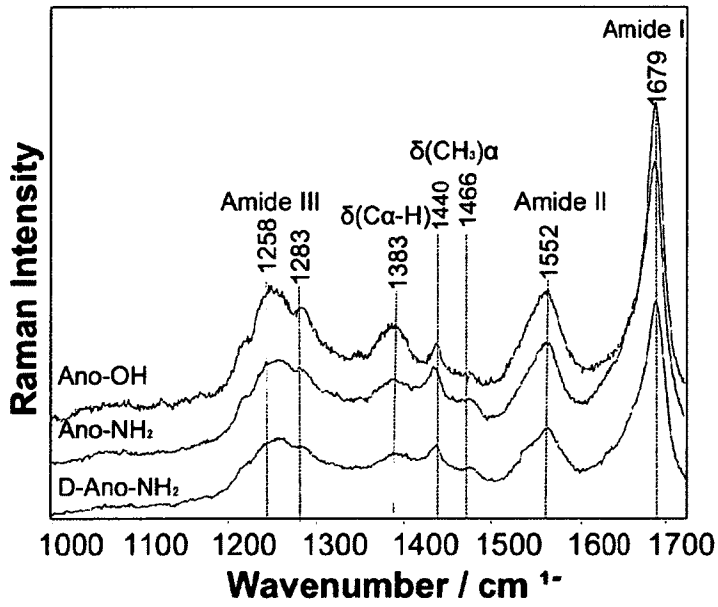

Figure 4.1: UVRR spectra of Ano-OH, Ano-NH_2, and D-Ano-NH_2 in PBS.

The temperature dependence of both amidated peptides presented in Fig 4.2 shows no shift in positions of the amide I and amide III bands, indicating no change in the

secondary structure with temperature. The positions of all bands remained fairly constant in the 1-55 °C temperature range while the intensity of some bands decreased with increasing temperature. This is most likely due to the temperature dependence of the Raman cross sections for these bands.[10]

Since the amide III band results from the coupled vibration of the C-N stretching and N-H bending modes of the amino acids, deuteration can be used to help identify it because it causes the band to decrease in intensity and appear at a lower (~1000 cm^{-1}) range.[7,11] The spectra of all three anoplin derivatives display this very trend and support the identification of the amide III bands (Fig 4.3). In the presence of 50-60 % D_2O, the intensities of the amide III and amide II bands decreased, amide I's band down-shifted by ~6 cm^{-1} and amide II's appeared at 1470 cm^{-1}, which is consistent with previously reported behavior of the bands.[11]

TFE was then used to stabilize the peptide's secondary structure and to mimic a membrane environment.[12] The mechanism by which TFE acts is by disrupting water-peptide hydrogen bonds, thereby favouring intra-peptide hydrogen bonds and compact secondary structure such as the α-helix.[12,13] While this does not fully mimic the heterogeneous environment of lipid membranes, TFE presents a simple model for membrane stabilization of secondary structure, and does result in local heterogeneity in that it does not significantly affect intra-peptide hydrophobic interactions.[12]

Intensity and position of the amide I and amide II bands were considerably affected by TFE (Fig 4.3). For example, in the amide I spectral region, the intensity of the band at ~1685 cm^{-1} decreased while the intensity of the band at ~1660 cm^{-1} increased for all three anoplin derivatives. The change was slightly more prominent for Ano-OH where a higher

TFE concentration was used. A ~5 cm^{-1} down-shift of the amide II band was observed as well. It was difficult to draw conclusion on the effect of TFE on the amide III band position due to interference from the TFE bands. However, the intensity of the $C_\alpha H$ band at ~1380 cm^{-1} slightly decreased. All of these changes are indicative of an α-helical conformation for all three derivatives in the membrane mimetic environment.[6,7] This is in agreement with CD analysis of anoplin which indicates a 6% α-helical content in aqueous solution but 44% and 55% α-helical contents in 30% TFE and 160 μM SDS respectively.[1,3]

Overall, UVRR data indicated that all three anoplin derivatives adopt similar conformations in aqueous buffer solutions and tend to adopt an α- helical conformation in a membrane mimicking environment.

4.2.3 Interactions of anoplin derivatives with lipid vesicles

To further model interactions of Ano-NH_2 and its two derivatives with cell membranes, UVRR spectra of the peptide complex at 1:6 peptide/lipid ratios with large unilamellar vesicles composed of zwitterionic DPPC or anionic DPPG were measured (Fig 4.4). Although there was a minor interference from the lipid vesicles at approximately 1620 cm^{-1}, the amide I and amide III bands as well as $C_\alpha H$ and CH_3 bands were clearly identified in the spectra. The spectra of all three derivatives in complex with DPPC vesicles were very similar to those in aqueous buffer solution with the amide I and amide III bands observed at ~1686 and 1260 cm^{-1} respectively. In complex with DPPG however, the intensity of the amide I band at 1686 cm^{-1} decreased and a small shoulder at ~1650 cm^{-1} appeared, most noticeably for Ano-OH. This spectral change was very

similar to the change observed for the peptides in TFE, suggesting the formation of an α-helical conformation.

The data indicated that all three derivatives experienced conformational transformations when bound to anionic phospholipid vesicles and thus suggested preferential interactions with these model cell membranes. These results are consistent with previous reports for other AMPs obtained using Raman spectroscopy.[14] The cationic nature of the peptides was most likely responsible for this preferential interaction of AMPs with the negatively charged membranes. The two lysine and one arginine residues give the peptide its positive charge of +3. The amidated form of the peptide had an extra charge due to the absence of a COO^- group at the C terminus.

It is unlikely however, that the electrostatic interactions alone determine the peptide's antimicrobial activity. It has been shown that membrane permeabilization activities are not dependent on specific amino acid sequences or specific three- dimensional peptide structure.[15] Therefore, even though all three derivatives preferentially bound to anionic membranes and experienced similar conformational transformations, their membrane rupturing properties were not similar, as shown in the leakage assay (section 4.2.5).

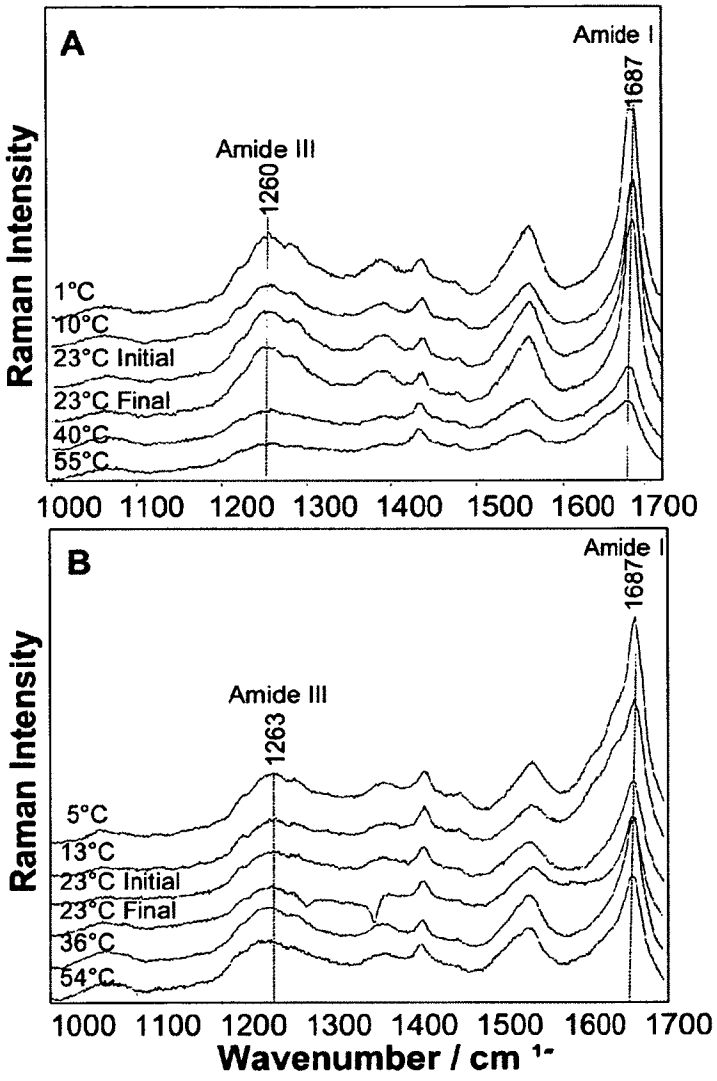

Figure 4.2: The effect of temperature on the UVRR spectra of (A) Ano-NH_2 and (B) Ano-OH.

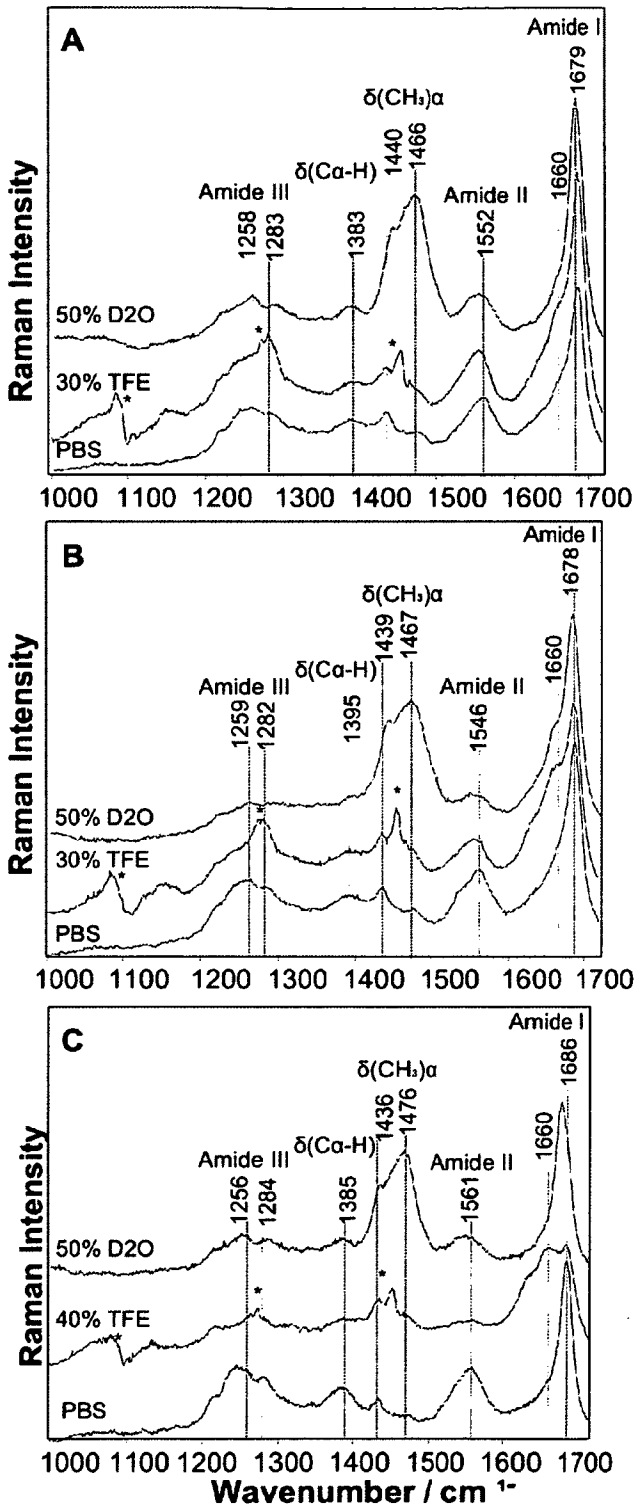

Figure 4.3: UVRR specta of Ano-NH_2, (B) D-Ano-NH_2, and (C) Ano-OH in 30% TFE for both amidated derivatives or 40% TFE for Ano-OH and PBS. Contribution from TFE subtraction are marked by asterisks.

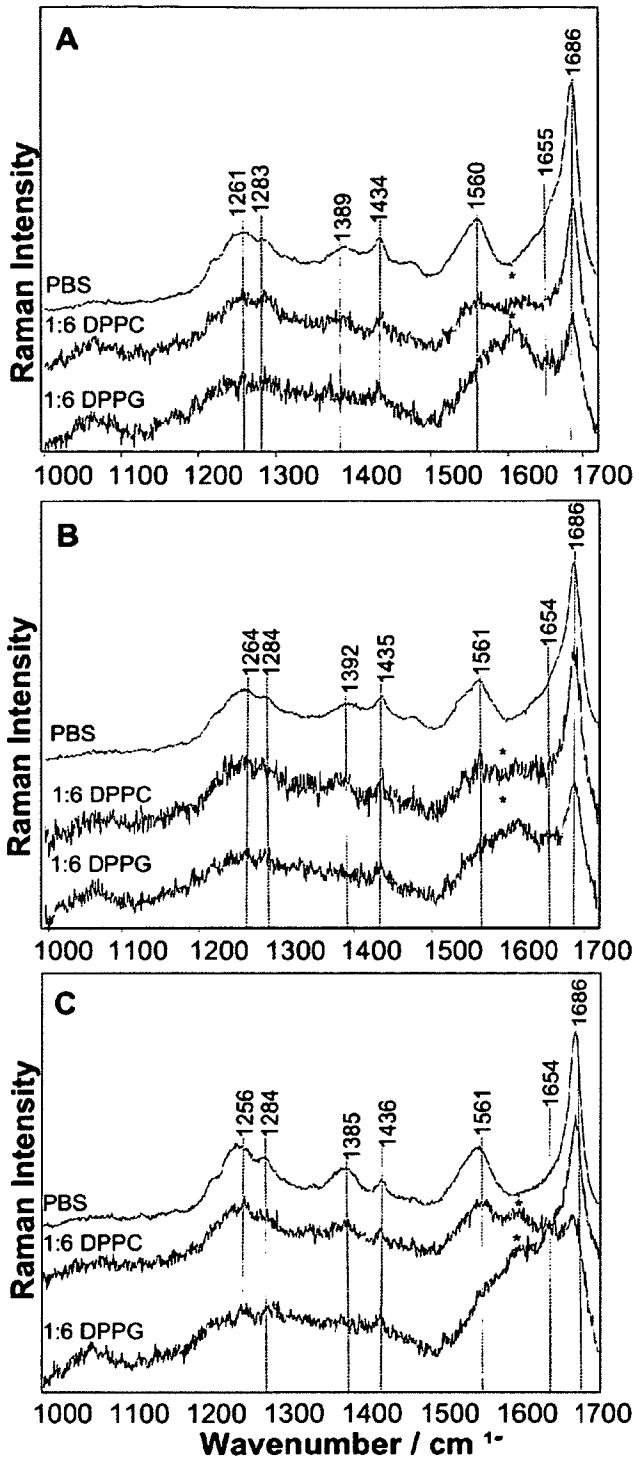

Figure 4.4: UVRR spectra of (A) Ano-NH_2, (B) D-Ano-NH_2, and (C) Ano-OH in PBS, 1:6 DPPG, and 1:6 DPPC. Contribution from the lipids are marked by asterisks.

4.2.4 Monolayers of anoplin derivatives with DPPC, DPPG and *E. coli* total lipid extract

The helical wheel analysis indicates that anoplin adopts an amphipathic structure when it folds into an α-helical conformation.[1,2] Peptides should form a stable monolayer at the air/water interface as shown in Fig 4.5. Deamidation of anoplin decreases the total peptide positive charge and therefore decreases the electrostatic repulsion between molecules. As a result of deamidation, a 25% drop in area per single peptide molecule in a monolayer from 195 $Å^2$ to 140 $Å^2$ (Fig 4.5B), which is characteristic of an area occupied by a single anoplin molecule in the α-helical conformation.[16] In addition, the contribution to the greater molecular area arises from a less defined secondary structure of Ano-OH in comparison to Ano-NH_2 as was shown in molecular dynamics simulation.[3] After compressing the monolayer to a surface pressure above 20 mN/m a hysteresis between the compression and expansion isotherms is observed. If the peptide is injected in the subphase instead of being spread at the air/water interface, a considerable fraction of the peptide is transferred to the interface and a monolayer is formed at ~40 nM bulk concentration (demonstrated by previous lab member). Therefore, both peptides are surface active with a considerably greater area/molecule for the amidated form of anoplin. The peptide in the D form (D-Ano-NH_2) was also found to form a monolayer at the interface with the area per molecule slightly greater than for L-Ano-NH_2 (Fig 4.5 B).

Small domains were observed in peptide monolayers transferred at 15 mN/m (Ano-NH_2 and D-Ano-NH_2) and 20 mN/m (Ano-OH) under AFM (Fig 4.6). The height of these domains is ~2 nm and the lateral dimension varies from tens to several hundreds of nanometers. The number of domains is considerably greater for the deamidated peptide.

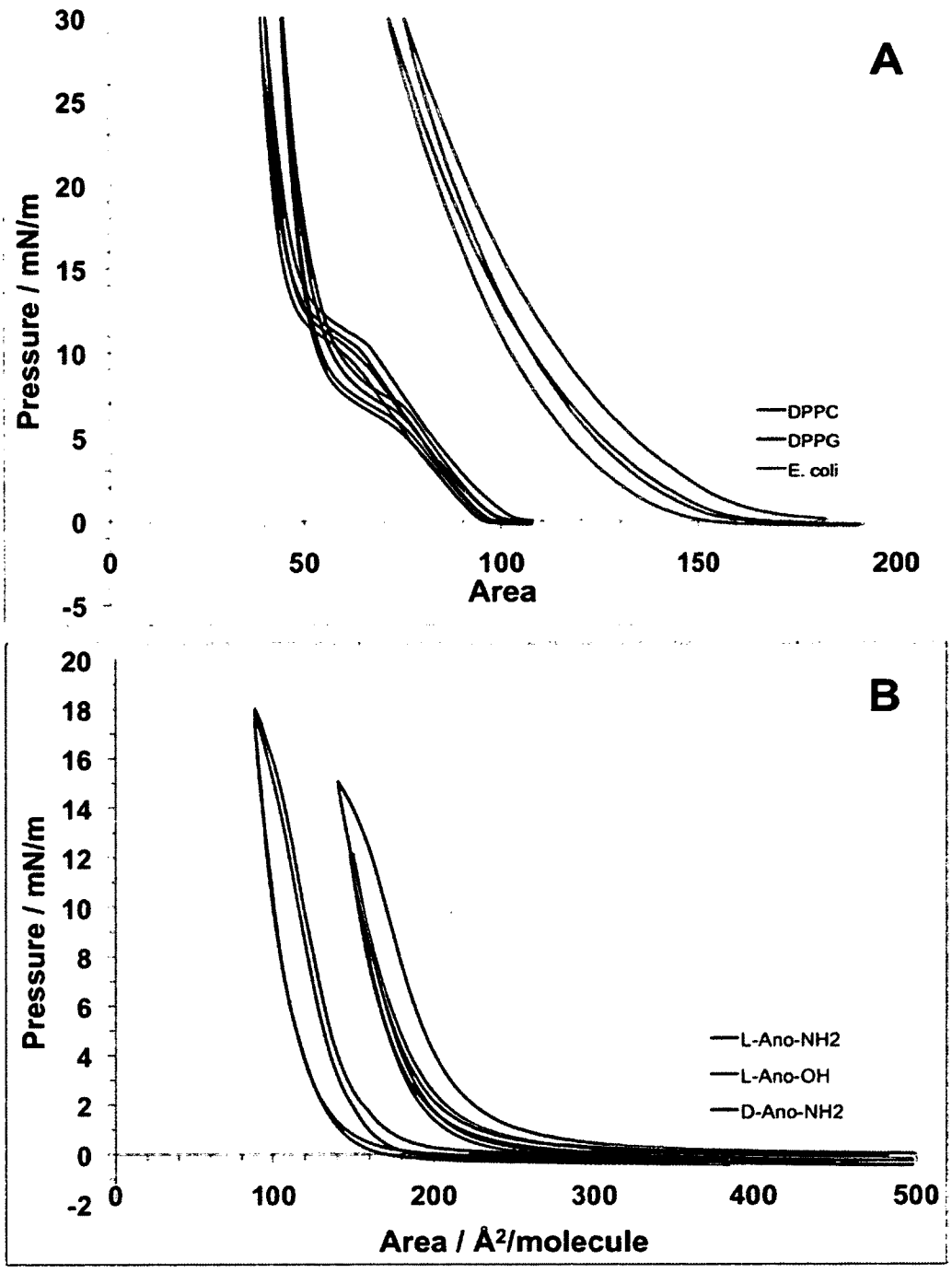

Figure 4.5: Langmuir isotherm cycles for monolayer of (A) DPPC (blue), DPPG (red) and *E. coli* total lipid extract (green), and (B) Ano-NH_2 (black), Ano-OH (grey) and D-Ano-NH_2 (beige) at air/water interface. Overlapping compression and expansion isotherms suggested lipid or peptide molecules recover to the air/water interface sufficiently.

The nanoscale clusters have somewhere between 5 and 10 molecules per cluster as follows from the AFM images (Fig 4.6). Formation of multimeric clusters for anoplin was previously suggested.[1] However, observed aggregates might also be a result of the monolayer transfer onto a solid support, as was observed in some cases for lipid mono- and bilayers.[17]

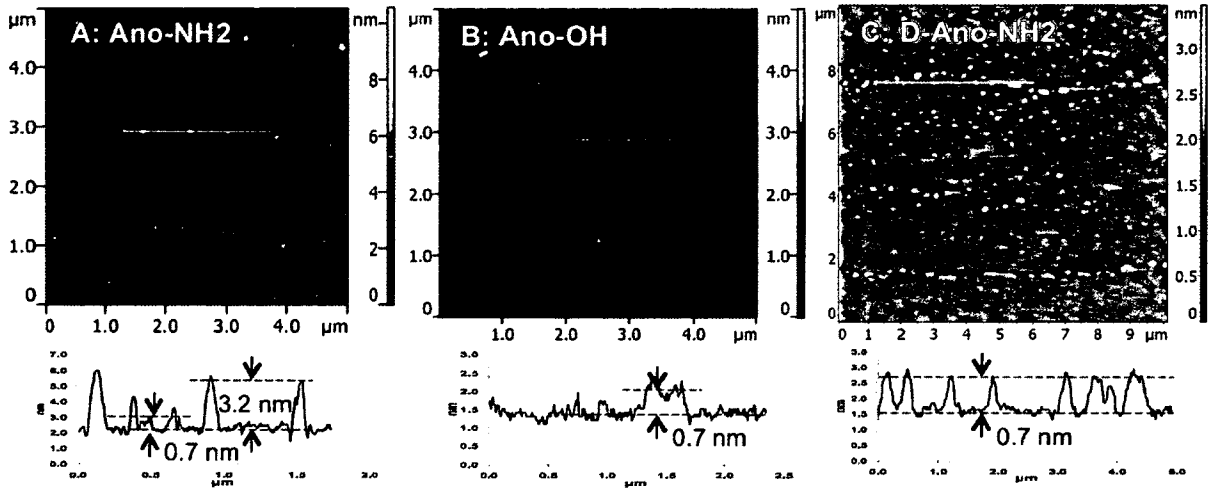

Figure 4.6: Selected AFM topography images and cross sections of (A) Ano-NH_2 at 15 mN/m, (B) Ano-OH at 20 mN/m, and (C) D-Ano-NH_2 at 15 mN/m.

Monolayers of mixtures composed of 50 mol% zwitterionic DPPC or anionic DPPG and 50 mol% Ano-OH or Ano-NH_2 were prepared in order to investigate the effect of deamidation on the interactions of anoplin with model cell membranes (Fig 4.7). The compression isotherms of pure DPPC showed a typical first-order transition from the LE phase to LC phase at ~8 mN/m (Fig 4.5 A and 4.7A).[19]

For DPPC/anoplin mixtures, initial compression isotherms were similar for monolayers containing L-Ano-NH_2 and L-Ano-OH and show two features at ~8 mN/m and ~18 mN/m. The first feature corresponds to the phase transition of the lipid fraction

of the monolayer. The second feature could either be the phase transition of the peptide fraction or caused by the loss of peptide molecules into the subphase. The latter was confirmed by a significant hysteresis between the compression and expansion isotherms for both mixtures and by a decreasing area per molecule with each isotherm cycle (Fig 4.8 A). With each cycle, the fraction of the peptide in the monolayer decreases and the subphase peptide concentration increases, leading to a smaller total number of molecules in the monolayer.[20,21]

The compression isotherm for the monolayer of anionic phospholipid DPPG alone (Fig 4.5 A and 4.7 B) showed a characteristic phase transition region at around 10 mN/m, corresponding to the LE - LC transition.[22] The DPPG/anoplin mixture isotherms behaved in a similar fashion as DPPC/anoplin isotherms: a hysteresis between the compression and expansion isotherms was observed for both amidated and deamidated forms indicating that the peptide is squeezed out from the monolayer into the subphase (Fig 4.8 B). Similar behavior of the lipid/peptide mixture monolayers was observed for the D-Ano-NH_2 derivative. This suggests that the lipid/anoplin interaction in a monolayer is not greatly affected by deamidation or chirality considerably. The only noticeable difference between DPPC and DPPG containing mixtures was the absence of the phase transition around ~10 mN/m for DPPG/anoplin, indicating a different nature of mixing in DPPG/anoplin as compared to DPPC/anoplin monolayers.

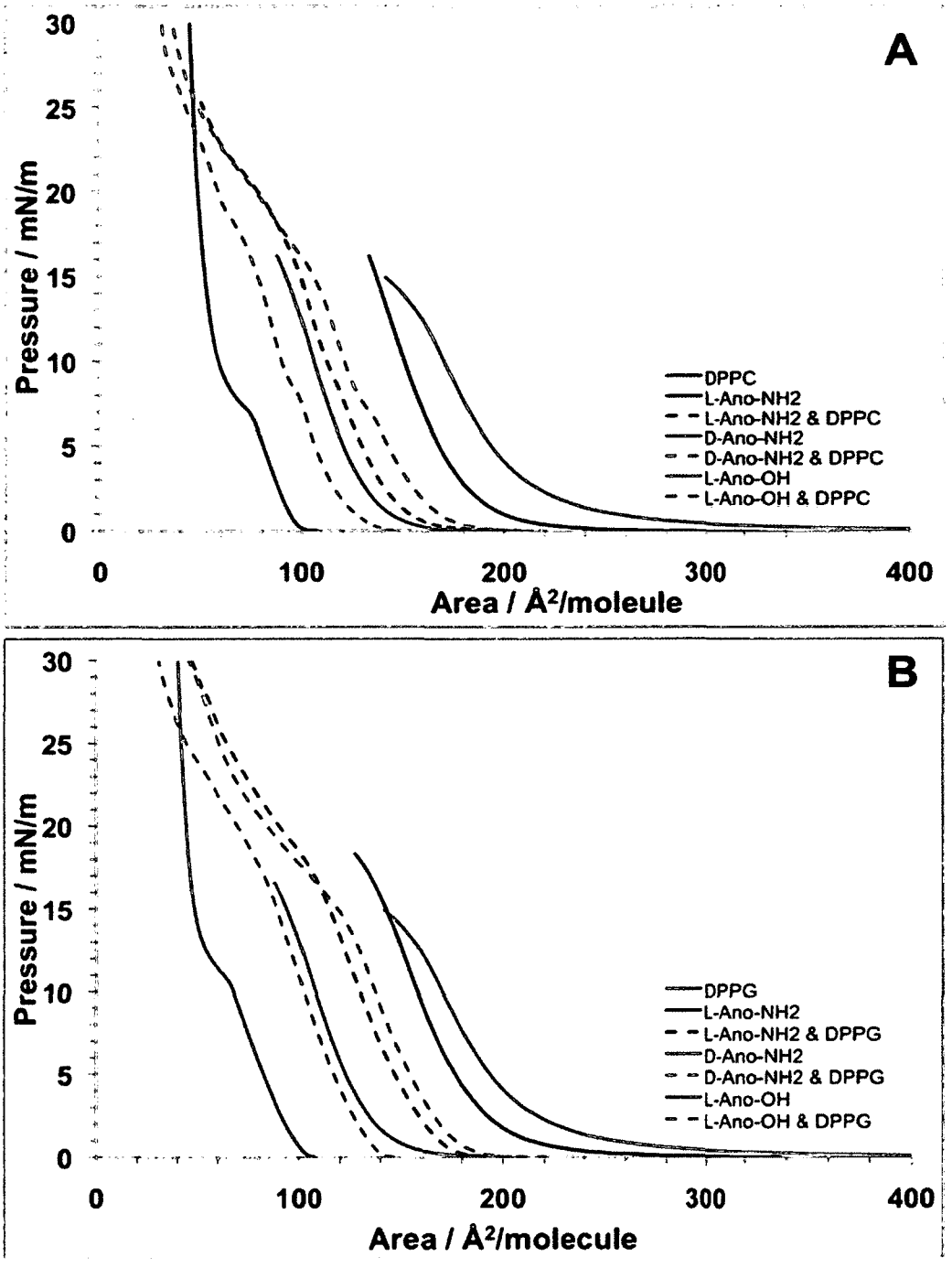

Figure 4.7: First compression of anoplin, (A) DPPC and DPPC/anoplin 50/50 mol% mixtures, and (B) DPPG and DPPG/anoplin 50/50 mol% mixtures monolayers.

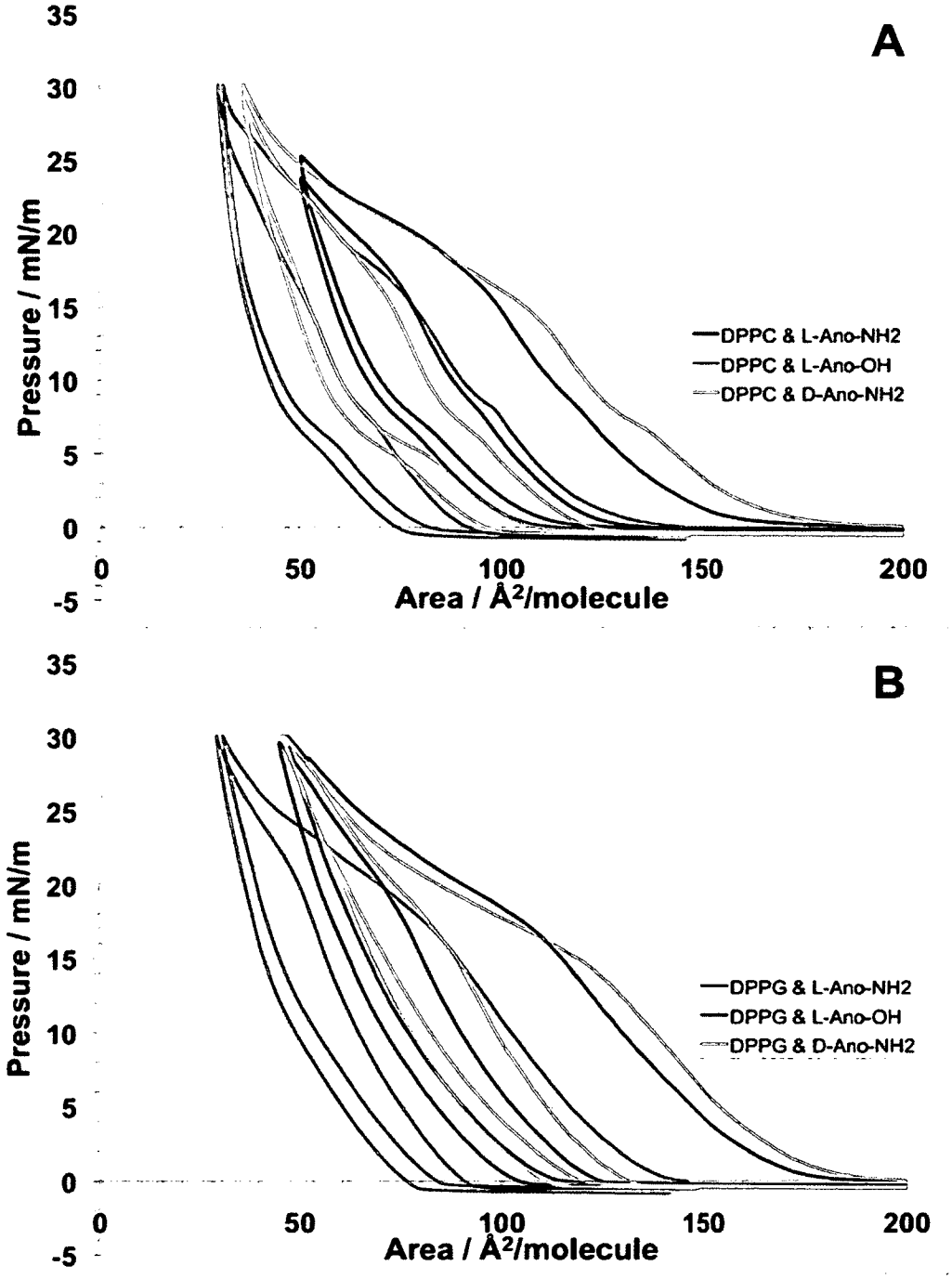

Figure 4.8: Isotherm cycles of (A) DPPC/anoplin 50/50 mol% mixtures and (B) DPPG/anoplin 50/50 mol% mixtures monolayers. Large hysteresis suggested lost of peptide/lipid molecules in the subphase.

Free energy is often used to assess the magnitude and nature of miscibility between two components of a monolayer mixture — negative excess Gibbs free energy is evidence of attractive forces between the two components.[23] It was rather impossible to calculate precisely the free energy of mixing from these experiments, as the peptide and perhaps the complex with lipids did not remain in the monolayer at higher surface pressure — indicated by the hysteresis between the compression and expansion isotherms (Fig 4.8). Such behavior has been observed for other surface active peptides.[20,21]

AFM topography (Fig 4.9) and X-PEEM (Fig 4.10 and 4.11) images of the mixture monolayers transferred onto mica substrate at 30 mN/m surface pressure further support this observation. At 30 mN/m the lipid monolayers essentially have no features since the lipid was in the LC phase with small areas of LE phase and some defects due to impurities in the monolayer can occasionally be observed (Fig 4.9 A,E). For DPPC/anoplin monolayers, both AFM and X-PEEM (Fig 4.9 B-D and Fig 4.10) demonstrated noticeable coexistence of two different phases: large continuous domains, which could be assigned as lipid-rich, and areas consisting of a large number of small clusters tens of nanometers in diameter and several nanometers in height (slightly taller than the lipid phase), which could be considered peptide-rich. The X-PEEM component maps along with NEXAFS spectra chemically assigned that the large domains consist mostly of lipid while the smaller domains are composed of peptide. The quantitative analysis revealed that the lipid-rich domains were consistently composed of ~91-97% DPPC while the Ano-NH_2-rich small domains varied in the composition of peptide (52-99%) depending on the area sampled (Fig 4.10 C). In the case of DPPC/Ano-OH, the monolayer predominately consisted of DPPC (81-98%) the high immiscibility between

the two components (Fig 4.10 F). DPPC/D-Ano-NH_2 exhibited similar topography with distinct breakdown of continuous LC domains (in DPPC only image) into coexistence of LC and LE phases (Fig 4.9 D). No X-PEEM image was obtained for the components assignment. There is little difference between the topography of monolayers containing Ano-NH_2 versus D-Ano-NH_2 as observed via AFM. This further supported that it is the amphiphilicity of a peptide that affects its interaction with the lipid membrane.

In DPPG/anoplin monolayers transferred at 30 mN/m, two phases could be distinguished with a height difference of about 1-2 nm (Fig 4.9 E-H and Fig 4.11). The domains were considerably smaller for the monolayer containing Ano-NH_2. In contrast to mixing with DPPC, raised peptide-rich clusters were not observed. The X-PEEM results showed in DPPG/Ano-NH_2 the circular domains to be composed dominantly of DPPG lipid (91-100%) while the matrix is composed mainly of Ano-NH_2 (63-98%), depending on the region sampled (Fig 4.11 C). Similar quantitative analysis was also obtained for DPPG/Ano-OH, where domains were composed of 98% DPPG and the matrix was composed of 53% Ano-OH (Fig 4.11 F). Clearly, the morphology of the lipid monolayer interaction with anoplin was different between DPPC and DPPG. For example, the areas occupied by DPPG/Ano-NH_2 were much more extensive compared to DPPC/Ano-NH_2 indicating that Ano-NH_2 mixes better with DPPG compared to DPPC — Ano-OH resembled similarly. Therefore, these results further support that the interactions and lateral organization of anoplin and lipid molecules in an anionic model cell membrane is different from that in a zwitterionic membrane.

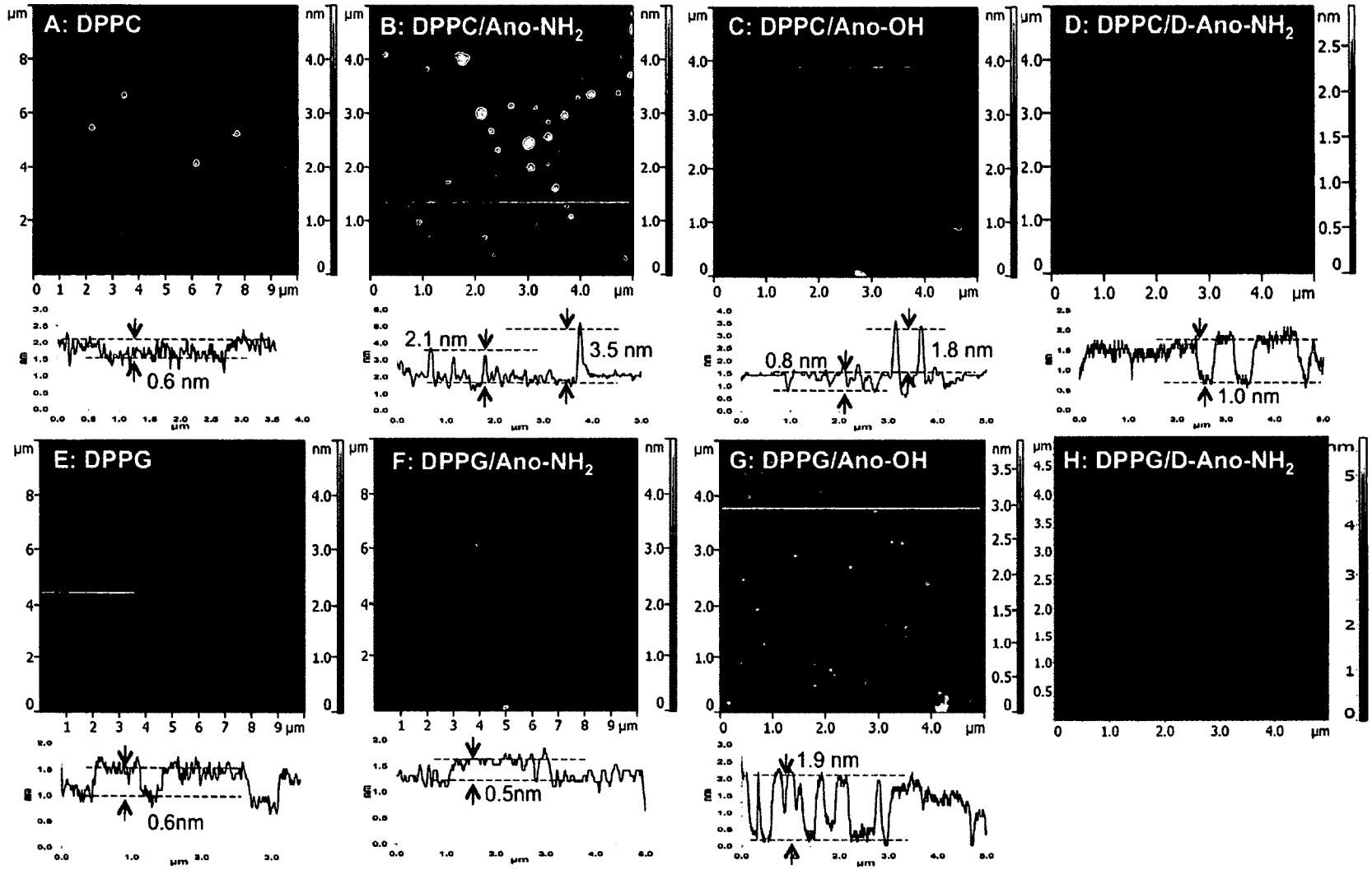

Figure 4.9: Selected AFM topography images and corresponding cross sections of single lipid monolayer and 50/50 mol% lipid/peptide mixtures deposited at 30 mN/m.

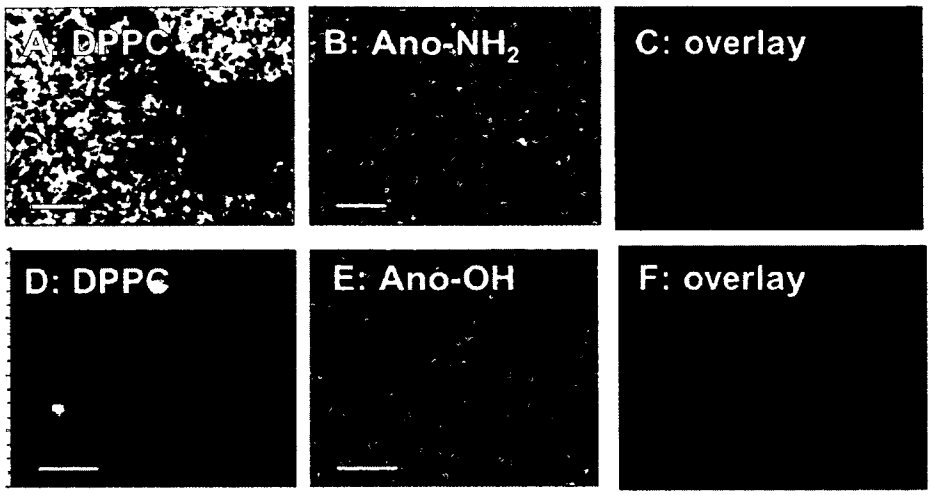

Figure 4.10: X-PEEM images of (A-C) DPPC/Ano-NH_2 and (D-F) DPPC/Ano-OH 50/50 mol% mixtures. Images C and F represent the overlay between the lipid (red) and peptide (green) signal. Scale bar is 5 μm.

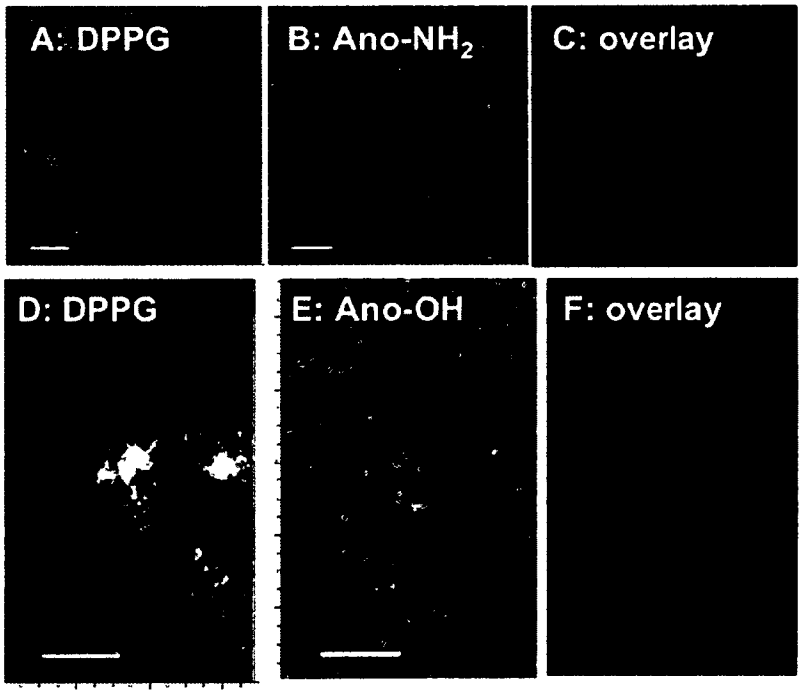

Figure 4.11: X-PEEM images of (A-C) DPPG/Ano-NH_2 and (D-F) DPPG/Ano-OH 50/50 mol% mixtures. Images C and F represent the overlay between the lipid (red) and peptide (green) signal. Scale bar is 5 μm.

Monolayers of Ano-OH and Ano-NH_2 mixtures with *E. coli* total lipid extract were also prepared. There was no obvious phase transition in the *E. coli* total lipid extract isotherm, suggesting that the monolayer exists in LE phase, confirmed by a featureless AFM image (Fig 4.12 A). The isotherms of the lipid/peptide mixtures shows a single feature at ~18 mN/m. Similarly to monolayers discussed earlier, this feature appears as a result of the peptide loss from the monolayer into the subphase. The AFM images for the monolayers reveal the appearance of large micro-scale domains after the addition of the peptide (Fig 4.12 B, C). Since small clusters are not observed, it is difficult to identify the location of the peptide. The monolayer mixtures were not examined under X-PEEM due to their complexity and 20% unknown component in the phospholipid profile (PE/PG/CL/unknown 57.5/15.1/9.8/17.6 wt/wt%). [24]

4.2.5 Kinetics of anoplin binding to a lipid monolayer

Initial steps in the action of AMPs involve membrane recognition and binding. To investigate how deamidation of anoplin influences these initial events, an experiment was performed with a phospholipid monolayer formed at the air-water interface at ~30 mN/m surface pressure and the peptide was injected into the subphase at MIC (21.5 μM). The area of the monolayer was kept constant. Activity of the peptides was further monitored as an increase in the surface pressure with time.

Fig 4.13 shows the results of these experiments for insertion of anoplin derivatives into DPPC, DPPG, and *E. coli* total lipid extract (only with Ano-NH_2 and Ano-OH) monolayers. After injection of the peptides, increasing surface pressure was observed indicating the adsorption of peptide molecules into the lipid monolayer. The surface

pressure increase ceased after several minutes and the pressure remained constant for as long as the observations were performed (usually 20-30 min) signaling saturation of the monolayer with the peptide.

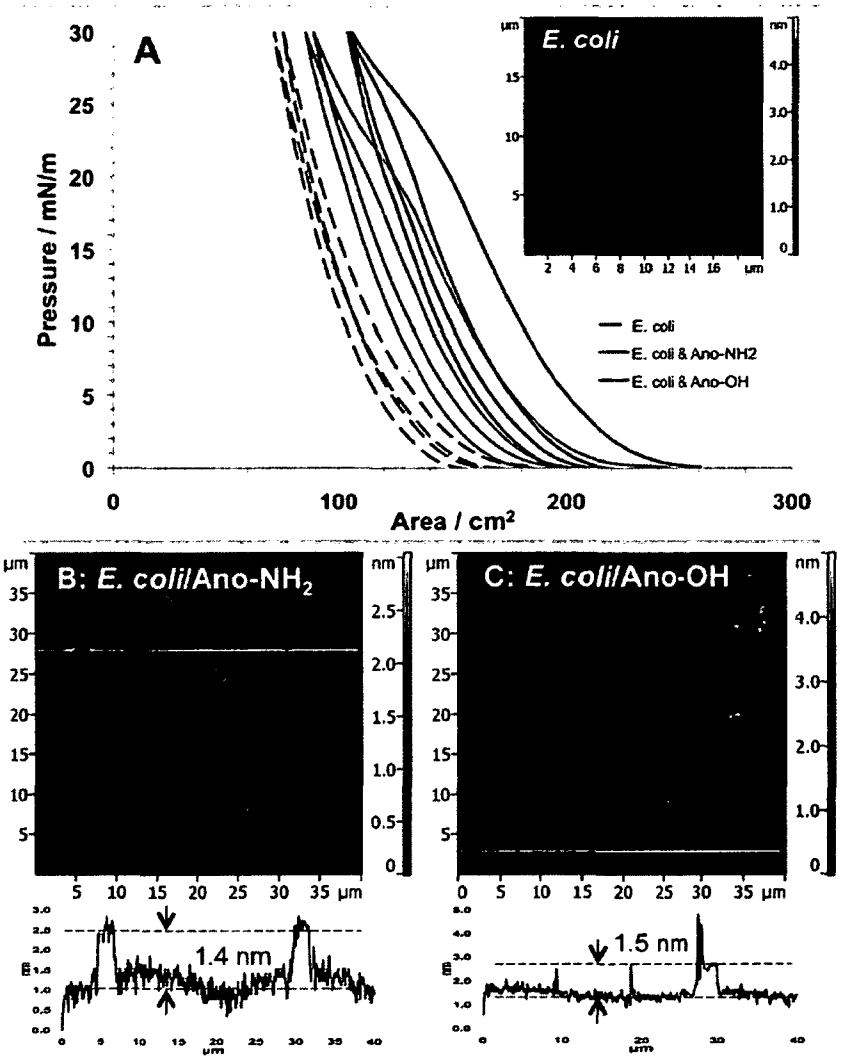

Figure 4.12: (A) Langmuir isotherm cycles of *E. coli* total lipid extract and *E. coli*/peptide (20 µL 1mg/mL/10uL 1mg/mL). Selected AFM topography images of (A inserted) *E.coli*, (B) *E.coli*/Ano-NH_2 and (C) *E. coli*/Ano-OH deposited at 30 mN/m.

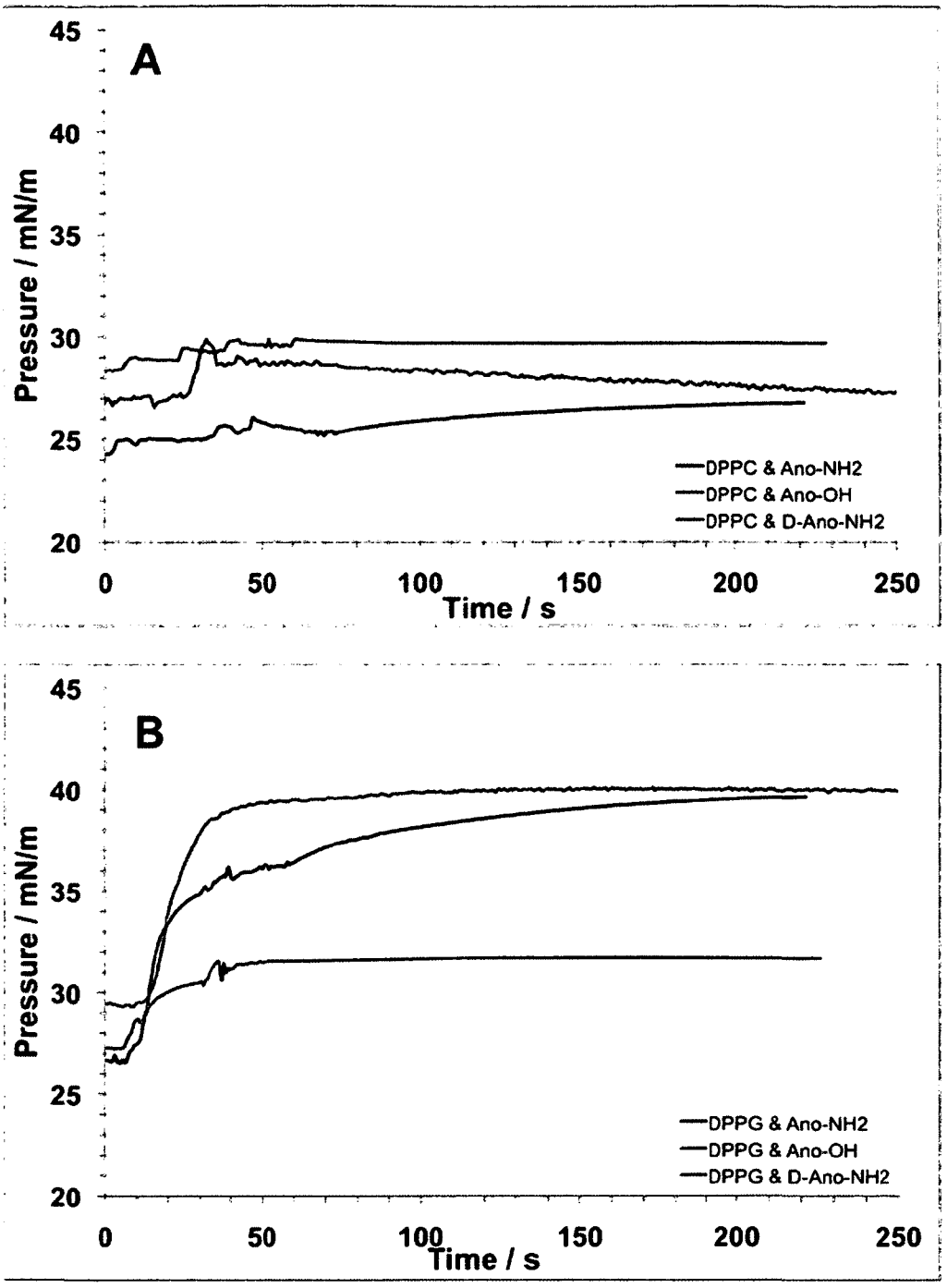

figure continued

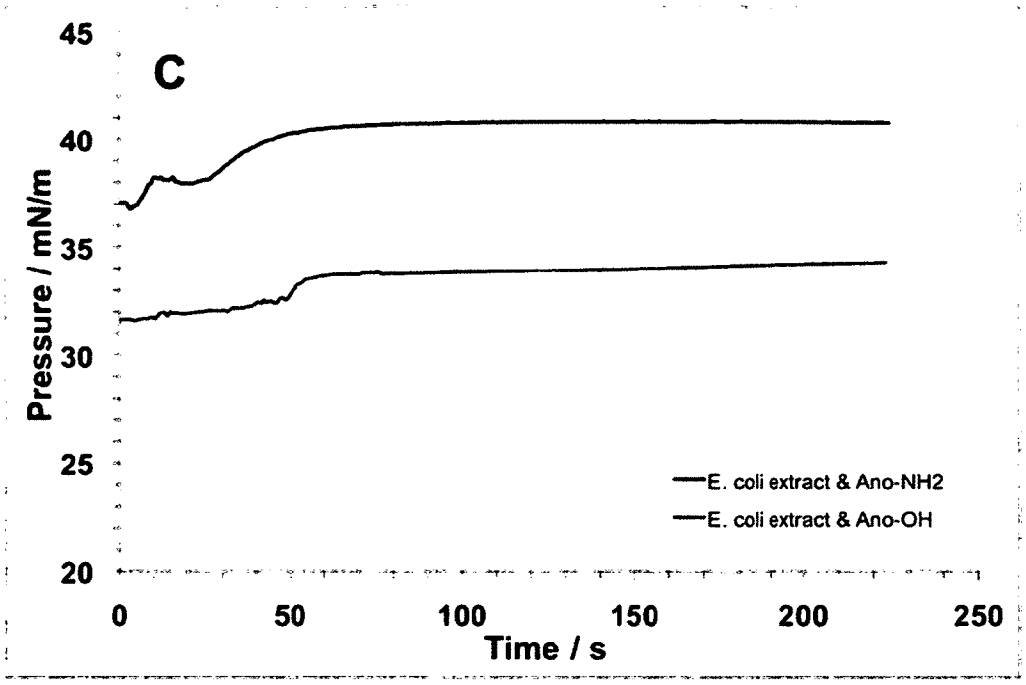

Figure 4.13: Increase of the surface pressure at constant area for monolayer of (A) DPPC, (B) DPPG and (C) *E. coli* total lipid extract after injecting 21.5 μM anoplin derivatives under lipid monolayer.

The degree of the pressure increase was found to be dependent on the lipid and peptide type. For all three model membranes Ano-NH_2 shows greater increase in the surface pressure of the monolayers as compared to Ano-OH. However, there was no significant difference in time of increase between the peptides. The surface pressure increase for Ano-NH_2 was the greatest for anionic lipid DPPG (~ 30%) followed by *E. coli* total lipid extract (~10%) and zwitterionic lipid DPPC (< 5%). This most likely results from a greater accumulation of the amidated peptides at the membrane surface due to the greater partition coefficient.[3,18] Overall, experiments with lipid monolayers indicate that electrostatic interactions play a crucial role in anoplin initial recognition and binding to a cell membrane. Deamidation weakens this interaction and therefore decreases the antimicrobial properties of anoplin. Similar effects exhibited by D-Ano-NH_2 on both

DPPG and DPPC monolayers to that of Ano-NH_2 were observed with the same relative pressure increase.

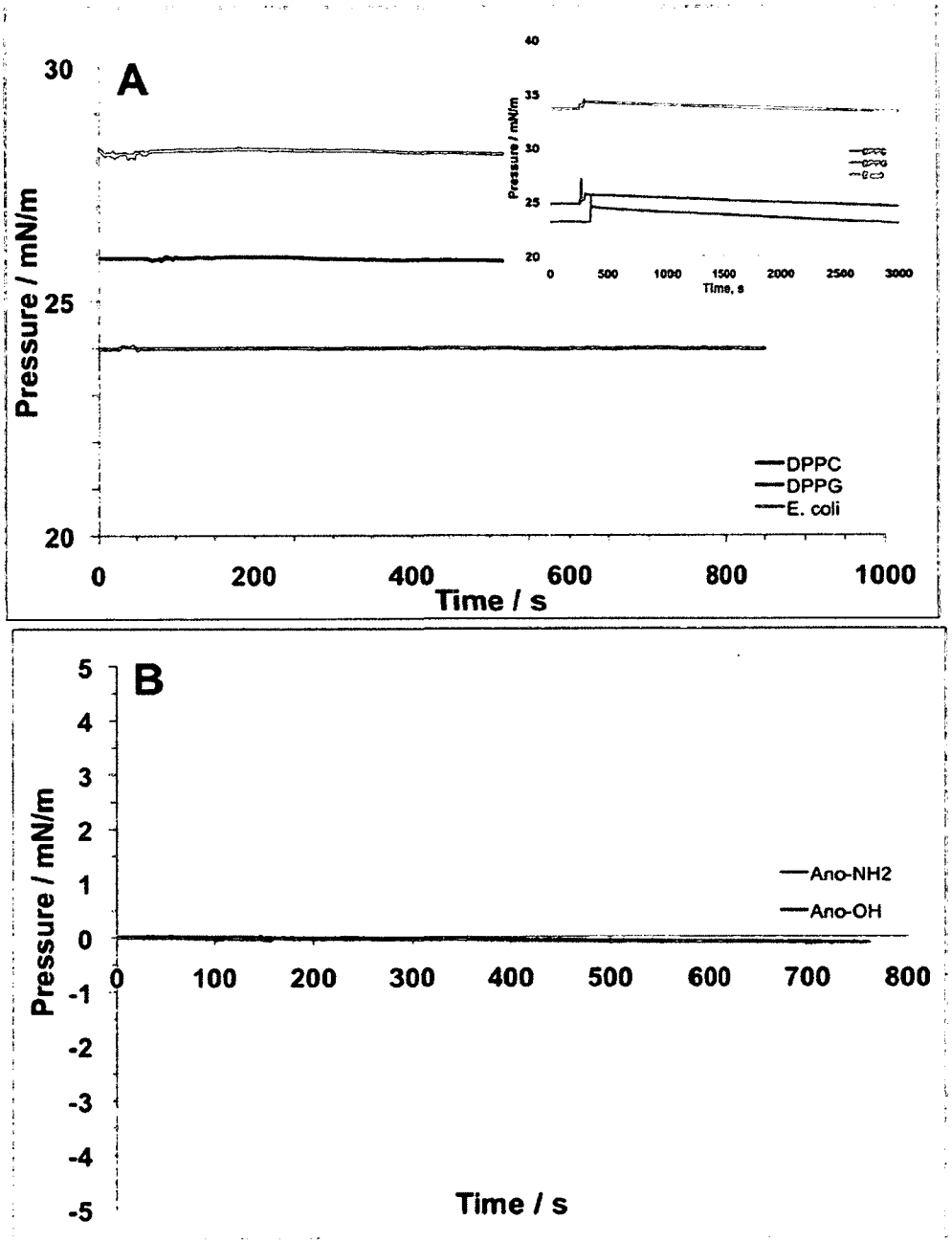

Figure 4.14: Increase of the surface pressure at constant area for (A) lipid monolayers after injecting 5 μL PBS (insert: 100 μL PBS) under lipid monolayer, and (B) PBS after injecting 80 nM of peptides under the interface.

4.2.6 Leakage assay

Leakage assay was performed to probe the effect of deamidation and L- to D-amino acid replacement on the membrane rupturing activity of anoplin (Fig 4.15). Five different model cell membranes were used: DPPC, DPPG, two mixtures modeling Gram-positive bacteria *S. aureus* and *B. subtilis*, and one model of Gram-negative bacteria *E. coli*.

In all cases Ano-NH_2 and D-Ano-NH_2 induced very similar (within experimental error) dye leakage, which was found however to be quite different from Ano-OH. The degree of dye leakage strongly depends on the lipid mixture used.

All three peptides showed modest activity against the DPPC vesicles (Fig 4.15 A). Even at a very high peptide to lipid ratio, the leakage did not exceed 5% to 10%. In contrast to Ano-OH, both amidated forms of the peptide induce significant leakage of the dye from anionic vesicles of saturated lipid DPPG (Fig 4.15 B). At low peptide/lipid ratio, the membrane disruption by both amidated peptides was insignificant but as the peptide/lipid ratio increased, up to 50% leakage was detected. Ano-OH, on the other hand remained inactive even at high peptide concentration. Thus, it is evident that interactions between the peptides and the model cell membrane composed of single saturated phospholipid are dominated by electrostatic attractions.

The interactions became much more complex when the membrane was composed of a mixture of unsaturated lipids — DOPE, DOPG and CL. At low peptide concentrations (peptide/lipid ratio below 0.1) Ano-NH_2 and D-Ano-NH_2 induced modest (5-10%) dye leakage from vesicles of all three types (Figure 8C-E). In comparison, Ano-OH was found to be less active against the *E. coli* and *B. subtilis* model membranes, which

correlated with MIC and LD_{50} values for the peptides. Conversely, Ano-OH was significantly more active against the *S. aureus* model membrane.

At high peptide concentrations however (peptide/lipid ratio greater than 0.1), deamidated Ano-OH induced dye leakage more efficiently than amidated peptides from vesicles modeling membranes of both Gram-positive bacteria *S. aureus* and *B. subtilis* (Fig 4.15 C, E). The same trend was observed for vesicles modeling Gram-negative *E. coli* (Fig 4.15 D) although the fluorescence increase was significantly smaller. Lytic acitivty of all anoplin derivatives was found to correlate with the relative amount of CL in the membrane: the higher the CL content — the more active the peptides were that is consistent with previous data.[3] As a dimeric form of PG lipid, CL is known to impose negative curvature to the bilayers and increase their compressibility modulii.[3,25] The ability of AMPs to induce model cell membrane leakage has previously been shown to depend dramatically on CL fraction in model membranes, since upon interaction with polycations, CL tends to destabilize the bilayer and forms a hexagonal phase.[26,27] Therefore, the difference in membrane lytic activity between Ano-OH and Ano-NH_2 at high concentration against *S. aureus* and *B. subtilis* model cell membranes was likely to arise from the difference in interactions of these derivatives with cardiolipin. In that respect, electrostatic interactions seem to be playing a less significant role than local membrane curvature, fluidity and ability to form hydrogen bonds.[27]

It has to be mentioned that experiments with the *E. coli* model vesicles performed at high concentrations of Ano-NH_2 and D-Ano-NH_2 gave surprising results: fluorescence intensity was found to decrease after the peptide addition, although reproducibility of these experiments was poor (the error bar in this experiment was very large). This

unusual behavior of the fluorescence signal could be attributed to the additional dye quenching as a result of vesicle or dye aggregation in the presence of a high concentration of peptides.[28,29]

Amidated forms of antimicrobial peptides are known to be generally more active.[33,34] It is unlikely, however, that this increase in activity can be solely explained by an increase in electrostatic attraction or change in peptide secondary structure. Cell membrane lipid composition appears to be playing a significant role, which could be due to the different susceptibility to undergo anoplin-induced lipid phase separation for the two peptide forms.[30]

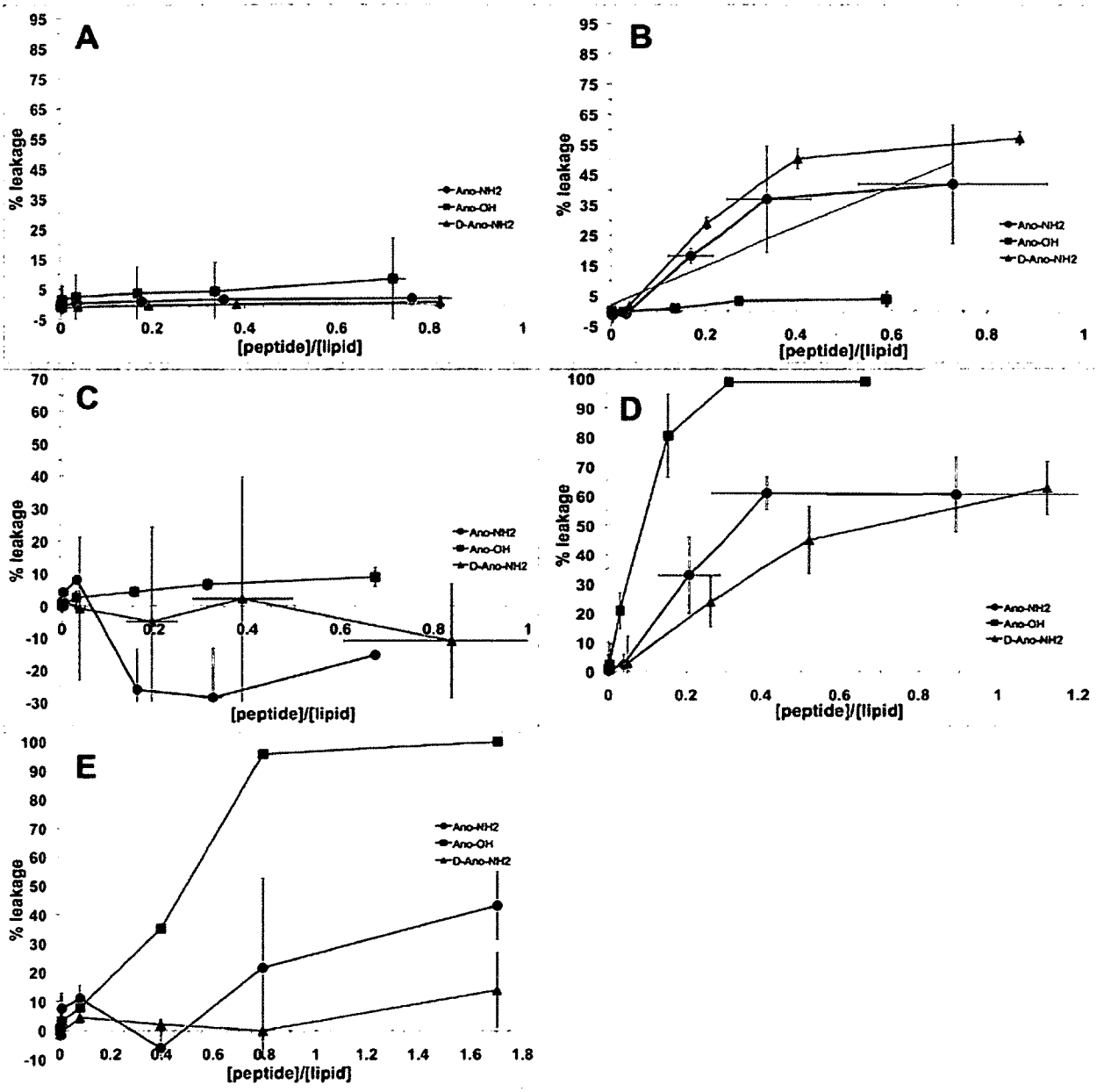

Figure 4.15: CF fluorescence signal increase after addition of anoplin into (A) DPPC, (B) DPPG, (C) *E. coli* model, (D) *S. aureus* model, and (E) *B. subtilis* model vesicles.

4.3 CONTRIBUTIONS

Special thanks to Stahs Pripotnev on his NSERC USRA work in UVRR measurements; Mourin Khan on her 4908 work in D-anoplin using LB and AFM; Dr. Tyler J. Avis's guidance and Sorin Gustin's assistance on antimicrobial assay; Akapawa Akuvi's assistance on leakage assay; Deeptee Seebun on her preliminary LB investigation in anoplin; Dr. Bonnie O. Leung, Dr. Adam O. Hitchcok, and Dr. Andreas Scholl on their work in X-ray spectromicroscopy measurements.

4.4 REFERENCES

1. Konno, K.; Hisada, M.; Fontana, R.; Lorenzi, C.; Naoki, H.; Itagaki, Y.; Miwa, A.; Kawai, N.; Nakata, Y.; Yasuhara, T.; Neto, J.R.; Azevedo, W.F.; Palma, M.S.; Nakajima, T. *Biochim. Biophys. Acta*, **2001**, *1550*, 70-80.
2. Ifrah, D.; Doisy, X.; Ryge, T.S.; Hansen, P.R. *J. Peptide Sci.*, **2005**, *11*, 113-121.
3. Dos Santos Cabrera, M.P.; Arcisio-Miranda, M.; Broggio Costa, S.T.; Konno, K.; Ruggiero, J.R.; Procopio, J; Ruggiero, Neto J. *J. Pept. Sci.*, **2008**, *14*, 661-669.
4. Eisenberg, D.; Weiss, R.M.; Terwilliger, T.C.; Wilcox, W. *Faraday Symp. Chem. Soc.*, **1982**, *17*, 109-120.
5. Yandek, L.E.; Pokorny, A.; Almeida, P.F.F. *Biochemistry*, 2008, 47, 3051-3060.
6. Huang, C.-Y.; Balakrishnan, G.; Spiro, T.G. *J. Raman. Spectrosc.* 2006, **37**, 277.
7. Bandekar, J. *Biochim. Biophys. Acta.* 1992, **1120,** 123.
8. Apetri, M.M.; Maiti, N.C.; Zagorski, M.G.; Carey, P.R.; Anderson, V.E. *J. Mol. Biol.* 2006, **355,** 63.
9. Tuma, R. *J. Raman Spectrosc.* 2005, **36,** 307.

10. Lednev, I.K.; Karnoup, A.S.; Sparrow, M.C.; Asher, S.A. *J. Am. Chem. Soc.* 1999, **121**, 8074.

11. Yu, N.T.; Lin, T.S.; Tu, A.T. *J. Biol. Chem.* 1975, **250**, 1782.

12. Buck, M. *Q. Rev. Biophys.* 1998, **31**, 297.

13. Holtz, J.S.W.; Holtz, J.H.; Chi, Z.; Asher, S.A. *Biophys J.* 1999, **76**, 3227.

14. Ianoul, A., Westwick, H., Nowacka, L.; Quan, B. *J. Raman Spectrosc.* 2007, **38**, 200.

15. Rarhinakumar, R., Wimley, W.C. *J. Am. Chem. Soc.* 2008, **130**, 9849.

16. Dennison, S.R.; Morton, L.H.G.; Brandenburg, K.; Harris, F.; Phoenix, D.A. *FEBS J.*, **2006**, *273*, 3792-3803.

17. Moraille, P.; Badia, A. *Langmuir* **2003**, *19*, 8041-8049.

18. Manuel, N.; Melo, M.N.; Ferre, R.; Castanho, M.A.R.B. *Nature Reviews Microbiology*, **2009**, *7*, 245-250.

19. Yang, X.-M.; Xiao, D.; Lu, Z.-H.; Yu, W. *Appl. Surf. Sci.*, **1995**, *90*, 175-183.

20. Won, A., Ianoul, A. *Biochim. Biophys. Acta –Biomembrane* **2009**, *1788*, 2277–2283.

21. Majerowicz, M.; Waring, A. J.; Wen, S., Bringezu, F. *J. Phys. Chem. B* **2007**, *111*, 3813-3821.

22. Minones, Jr., J.; Dynarowicz-Latka, P.; Minones, J.; Rodrigez Patino, J.M.; Iribarnegaray, E.J. *J. Colloid Interface Sci.* **2003**, *265*, 380-385.

23. Maget-Dana, R. *Biochim. Biophys. Acta - Biomembranes.* **1999**, *1462*, 109-140.

24. Avanti polar lipid. http://avantilipids.com/index.php?option=com_content&view=article&id=410&Itemid=124&catnumber=100500

25. Mileykovskaya, E.; Dowhan, W. *Biochim. Biophys. Acta -Biomembrane* **2009**, *1788*, 2084–2091.

26. Hristova, K.; Selsted, M.; White, S.H. *J. Biol. Chem.* **1997**, *272*, 24224-24233.

27. Domenech, O.; Francius, G.; Tulkens, P.M.; van Bambeke, F.; Dufrene, Y., Mingeot-Leclercq, M.P. *Biochim. Biophys. Acta,* **2009**, *1788*, 1832-1840.

28. Van den Bogaart, G.; Guzman, J.V.; Milka, J.T.; Poolman, B. *J. Biol. Chem.* **2008,** *283*, 33854-33857.

29. Magzoub, M.; Oglecka, K.; Pramanik, A.; Eriksson, L.E.G., Graslund, A. *Biochim. Biophys. Acta* **2005**, *1716*, 126-136.

30. Epand, R.M., Rotem, S., Mor, A., Berno, B., Epand. R.F. *J. Am. Chem. Soc.* **2008**, *130*, 14346-14352.

CHAPTER 5

INVESTIGATING THE EFFECT OF POINT MUTATION ON THE SECONDARY STRUCTURE AND MEMBRANE INTERACTION OF ANTIMICROBIAL PEPTIDE ANOPLIN

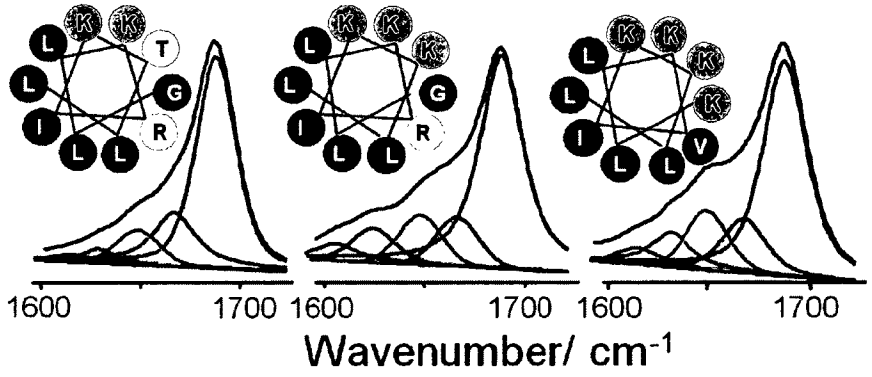

5.1 INTRODUCTION

Modification of peptide primary structure (amino acid substitutions) involving changes in the character of the side chain (charge, hydrophobicity and surface area) affect other peptide properties such as hydrophobic moment, hydrophobicity, and the size of the polar/hydrophobic domains, as well as charge and charge distribution.[1-4] Effect of variation in these properties on the activity of AMPs has previously been extensively studied using a number of natural and model peptides.[1-8] It is well established that electrostatic interactions between the cationic peptides and mostly anionic bacterial cell membranes are responsible for initial interactions between the molecules and therefore for selective toxicity. Hydrophobicity, amphipathicity and helicity appear to affect hemolytic activity in a more significant manner than antibacterial activity. At the same time, the effect of those parameters on antibacterial activity is not direct and is superimposed with peptide/lipid electrostatic interactions.[1-4] Modification of one parameter (for example charge), however, often leads to a change in the other (such as hydrophobic moment), thus making direct correlation between certain physicochemical properties and peptide activity challenging.[1-4] In addition, structural studies of AMPs rely heavily on the CD technique which is known to have limited sensitivity for short helical sequences.[9] Finally, the hydrophobic moment of a peptide is usually calculated assuming 100% helicity, which is incorrect, especially for short peptides.[2,10,11] Therefore, the structure/activity relationship of short antimicrobial peptides requires additional approaches. In this respect UVRR spectroscopy offers a significant advantage as a technique that allows the probing of conformation of short peptide sequences and selective unfolding of the peptide interior versus terminal parts.[12]

Short AMPs attract attention due to the potentially lower cost of their production. A number of such short antimicrobial peptide have recently been isolated.[13-18] Among these anoplin is one of the shortest amphipathic peptides occuring naturally.[19] Isolated from the venom sac of solitary spider wasp, *Anoplius samariensis,* α-helical anoplin (GLLKRIKTLL-NH_2) has a broad spectrum activity against both Gram-positive and Gram-negative bacteria while exhibitimg low hemolytic activity towards human erythrocytes and thus has great potential for further development. Correlation between the structure and the activity of anoplin was previously studied.[19,20] Among the 37 derivatives, two were found with increased antibacterial and low hemolytic activities, namely anoplin-8K (Ano8K, GLLKTIKKLL-NH_2) and anoplin-1K5V8K (Ano1K5V8K, KLLKVIKLL-NH_2).[20] Additional positive charge and amphipathicity changes were suggested to be the main factors for the increased selectivities of Ano8K and Ano1K5V8K towards bacteria, respectively. However, detailed structural studies of these derivatives were unsuccessful, likely due to the limitations of CD. Therefore, in this work we applied UVRR spectroscopy in combination with the Langmuir monolayer technique and vesicle leakage assay to correlate the activities of three anoplin derivatives with their secondary structure and surface activity.

5.2 RESULTS AND DISCUSSION

5.2.1 Single and multiple amino acid substitutions change surface/membrane activity of anoplin

Point mutation of natural AMPs is a widely used technique to improve their potential therapeutic properties.[1-4] This approach helps identify key amino acids in the primary

sequence, replacement of which can increase bactericidal activity and/or decrease cytotoxic effects. Upon these modifications, certain physicochemical properties of peptides change, such as secondary structure, charge, hydrophobicity and hydrophobic moment, leading to alteration of biological activity. To sufficiently exhibit antimicrobial activity, peptides need to be soluble in an aqueous phase to transport efficiently, which requires low hydrophobicity; nonetheless, to interact with the hydrophobic lipid tails and disturb the membrane structure and permeability, high hydrophobicity is needed.[21] Therefore, hydrophobicity and amphipathicity are often found as factors determining hemolytic and antibacterial activity of the peptides.[1-3]

Having only 10 amino acids, anoplin is one of the shortest natural AMPs.[19] In the previous detailed structure/function study, Ano8K (replacement of threonine to lysine at position 8) and Ano1K5V8K (replacement of glycine to lysine, arginine to valine and threonine to lysine at positions 1, 5 and 8, respectively) retained low or no hemolytic activity while having increased lytic activity towards both Gram-positive and Gram-negative bacteria (Table 5.1).[20] Additional positive charge and amphipathicity changes were suggested to be the main factors for increased selectivity of Ano8K and Ano1K5V8K towards bacteria, respectively. The amphipathicity of a peptide is determined by the value of its mean hydrophobic moment.[1-3] If a peptide adopts an α-helical conformation, such as anoplin, helical wheel or helical net diagrams can provide straightforward examination of the peptide's amphipathicity (Fig 5.1). Calculations of hydrophobic moment show that Ano8K has the highest amphipathicity followed by Ano1K5V8K and the wild type anoplin assuming the peptides fold into a 100% helix (Table 5.1). The former assumption is however never correct, and for short peptides like

anoplin the highest a-helical content can only be 50-60 % due to the terminal effects.[10, 11] Therefore, in this work several physicochemical techniques were used in order to determine relative helicities and amphipathicities of anoplin derivatives and to correlate these with peptide biological activities.

Table 5.1: Properties of anoplin and derivatives.

peptide	Q[a]	<H>[a]	μ_H[a]	MIC / μg/ml[a]		EC_{50}[a]/	π at CMC/	CPI / mN/m	
				S. aureus	*E. coli*	μg/ml	mN/m	DPPC	DPPG
anoplin	+3	-0.113	0.366	13	26	-	19.4	28.5	54.0
Ano8K	+4	-0.205	0.455	5	10	-	18.1	29.5	68.5
Ano1K5V8K	+4	-0.101	0.438	9	6	231	22.2	27.5	85.0

[a] Charge Q, mean hydrophobicity <H>, hydrophobic moment μ_H, MIC, and EC_{50} are from reference 20.

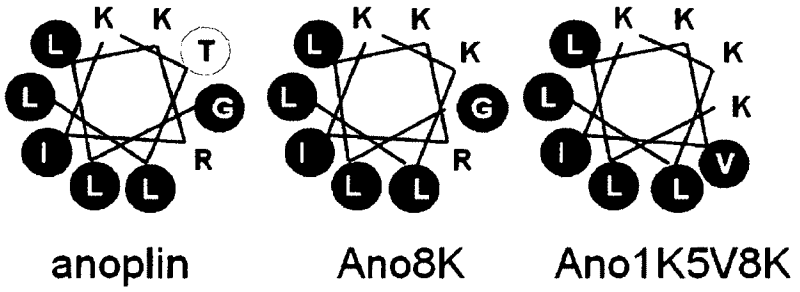

Amino Acid	Hydrophobicity Index*	Color
ILE	0.73	
VAL	0.54	
LEU	0.53	
GLY	0.16	
THR	-0.18	
LYS	-1.1	
ARG	-1.8	

Figure 5.1: Helical wheel diagram of anoplin, Ano8K, and Ano1K5V8K. Eisenberg consensus hydrophobicity scale was used. (*Eisenberg, D.; Weiss, R.M.; Terwilliger, T.C.; Wilcox, W *Faraday Symp. Chem. Soc.* **1982**, *17*, 109-120).

Monolayers at the air-water interface are commonly used to mimic cell membranes while controlling parameters such as molecule lateral packing and curvature.[21,22] At the interface, AMPs adopt a conformation similar to that in a biological membrane thus

becoming amphipathic.[21,23] At CMC, the air/water interface is saturated completely with surfactant molecules, or peptide in this case, such that micelles form upon any further peptide addition.[23] The lower the CMC, the more surface-active the peptide is, thus reflecting peptide amphipathicity.[23] By measuring the surface tension as a function of peptide concentration, we were able to determine the saturation surface pressure for anoplin and its two derivatives (Figure 5.2). The values obtained are 18.1 mN/m, 19.4 mN/m, and 22.2 mN/m, for Ano8K, anoplin, and Ano1K5V8K respectively. The sequence correlates with the overall hydrophobicity of the peptides rather than their amphipathicity (Table 5.1). The concentration at which the saturation occurs, the CMC, was found to be about 1.2 μg/ml for all three peptides, irrespective of the calculated hydrophobic moment. Thus according to the CMC data, there was no considerable difference between the peptides in terms of amphipathicity. This result disagreed with the calculations (Table 5.1) and partly reflected the fact that the peptides do not completely fold at the interface.

Peptide affinity to a cell membrane can be determined by measuring the CPI.[23] If a monolayer of phospholipid is prepared at the air/water interface at a certain surface pressure and a peptide is injected beneath the monolayer, the lipid film surface pressure will increase as peptide molecules bind to and insert into the lipid monolayer at constant area.[23] The degree of pressure increase depends on the lipid type, initial film surface pressure, peptide surface activity and concentration used. CPI is essentially the lipid monolayer surface pressure that prevents the peptide from inserting into the monolayer and can be determined by extrapolating the initial pressure (π_i) as a function of pressure changes ($\Delta\pi$), to a pressure increase that is equal to zero.[23] All three peptides were found

to possess similar affinities to the zwitterionic phospholipid monolayer DPPC (Fig 5.3 A). CPI values for Ano8K, anoplin and Ano1K5V8K were determined to be between 27.5 and 29.5 mN/m with little difference between the peptides (Table 5.1). Since the lateral packing of the biological membrane is believed to be in the range of 25-35 mN/m,[21-24] it is likely that all three peptides have a limited effect on the zwitterionic membrane and thus should have little toxic effect on mammalian cells. This is consistent with the results of biological assays.[19,20]

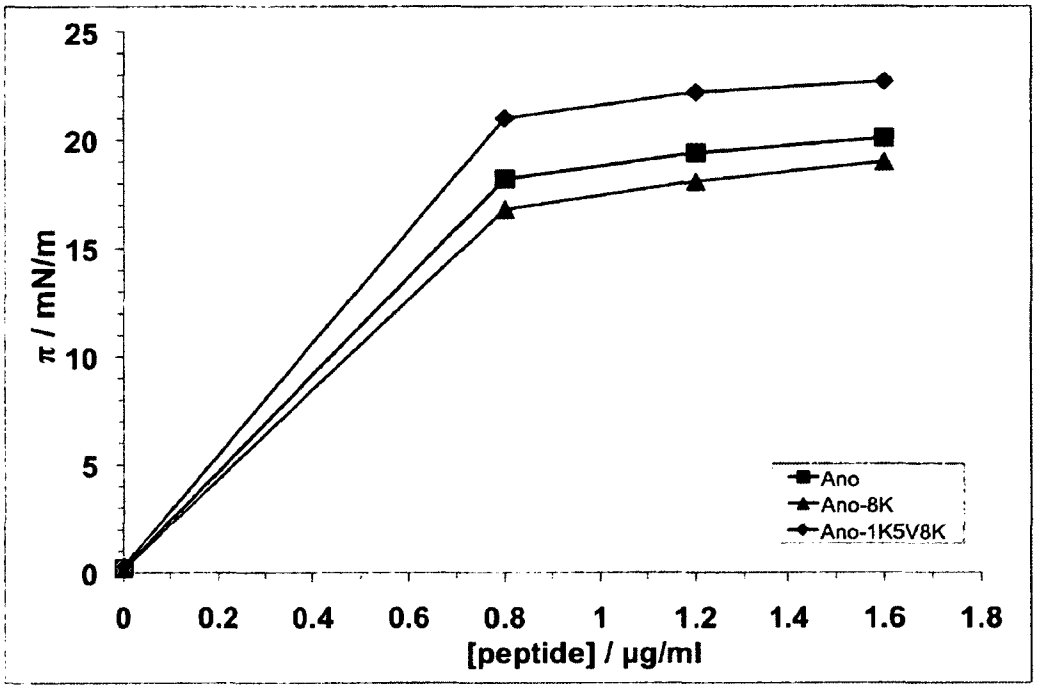

Figure 5.2: Peptide-induced pressure changes as a function of peptide concentration in the subphase for anoplin derivatives.

When a monolayer of anionic DPPG was used, CPI values and therefore affinity of all three peptides were considerably higher (Fig 5.3 B). We determined the CPI for Ano1K5V8K, Ano8K and anoplin to be 85.0 mN/m, 68.5 mN/m and 54.0 mN/m, respectively. These values are substantially greater than with DPPC, indicating the

importance of electrostatic interactions for all three peptides for their recognition and binding affinities for cell membranes. This is also consistent with the fact that the wild type anoplin has lower overall charge and also the lowest CPI in DPPG. At the same time, since CPI for Ano1K5V8K is higher than for Ano8K, despite the same charge, overall hydrophobicity and amphpathicity of the peptides likely contribute. The data suggest that at the interface Ano1K5V8K is more amphipathic. This can be achieved if the peptide adopted a more helical conformation than Ano8K.

To determine the kinetics of peptide binding and association with the cell membrane change with peptide physicochemical properties, a time course of the surface pressure increase was monitored after the peptide was injected into the subphase under the phospholipid monolayers with surface pressure kept in the range of biological membrane pressure, which is believed to be in the rage of 25-35 mN/m.[22-24] Fig 5.4 data clearly show the difference between zwitterionic and anionic membranes. All three peptides inserted into DPPC monolayers in a substantially smaller degree than into the DPPG monolayer. There were little changes of the surface pressure observed for DPPC monolayers. In the case of inserting into DPPG monolayers, both Ano8K and Ano1K5V8K increased the initial film pressure by approximately 10 mN/m, whereas the increase due to anoplin was ~8 mN/m. There was no visible difference in the time of insertion, and already after ~200 seconds, the process of peptide insertion was completed for all three peptides. The slow decrease in pressure with time for Ano8K in the DPPG monolayer could attribute to membrane destabilization due to disruption at a specific peptide accumulation.[24]

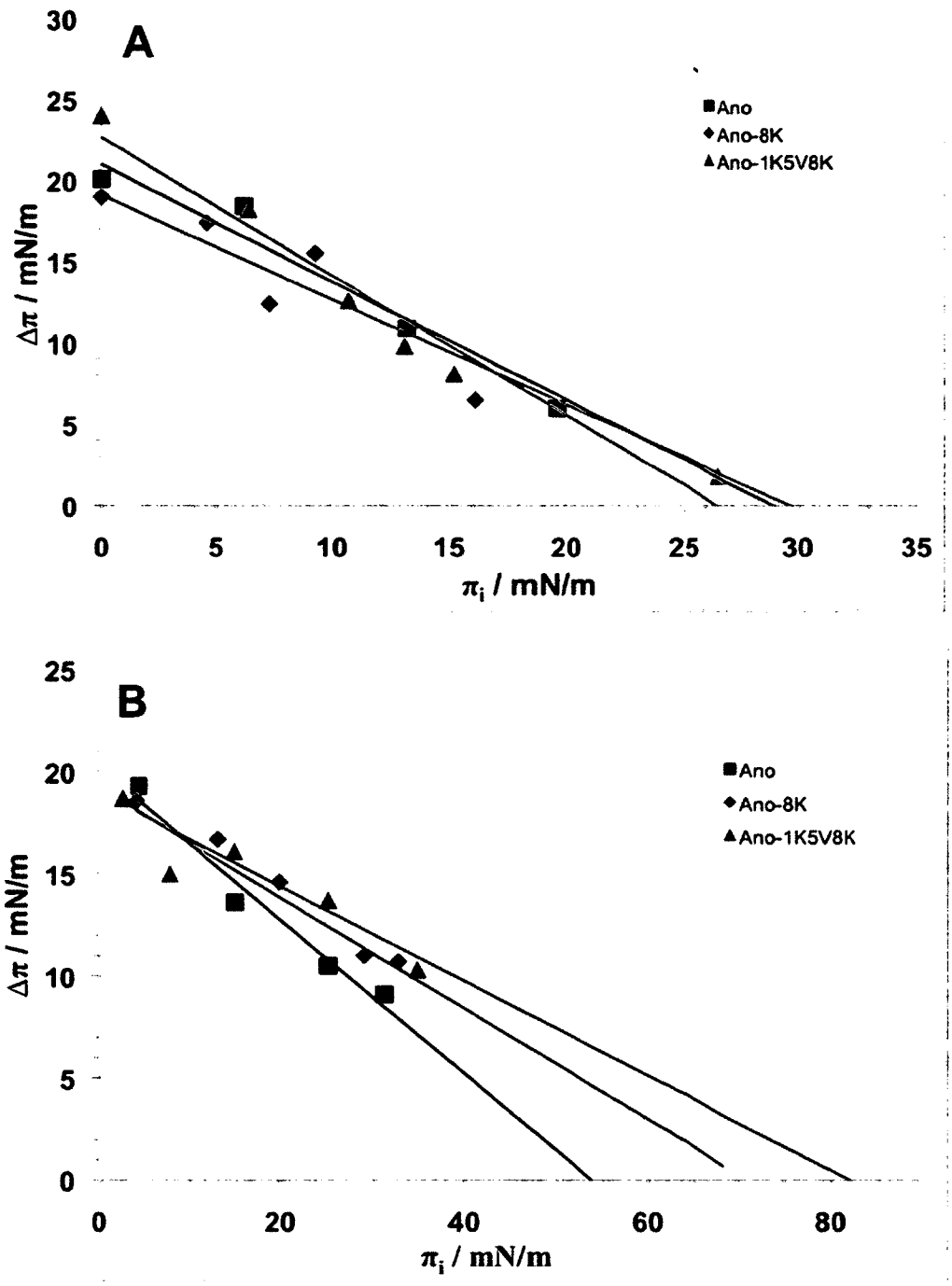

Figure 5.3: Insertion of anoplin derivatives into (A) DPPC and (B) DPPG monolayers. Extrapolation to zero change in pressure ($\Delta\pi$=0) gives the critical pressure of insertion.

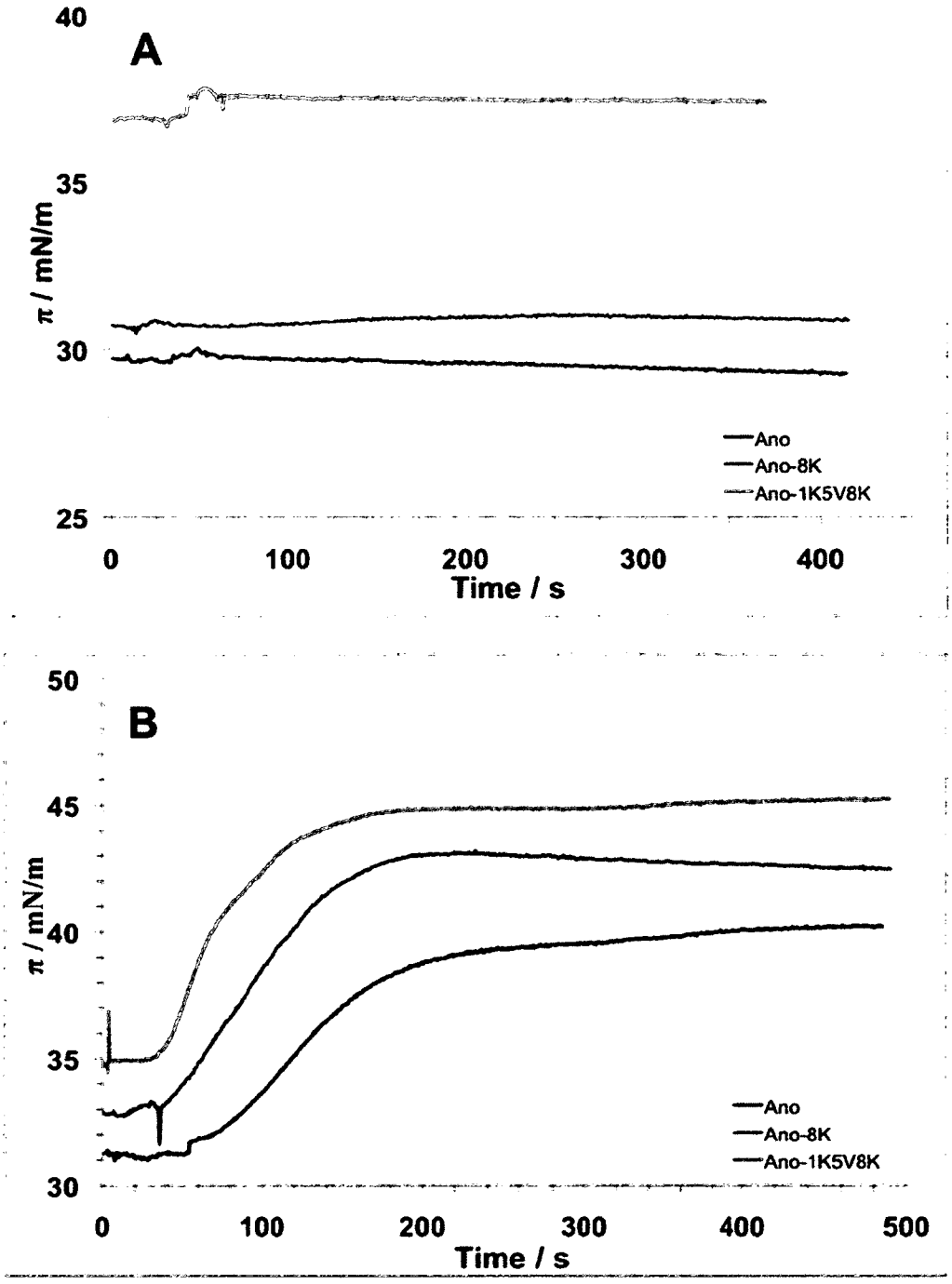

Figure 5.4: Relative increase of the pressure of (A) DPPC and (B) DPPG monolayers after inserting anoplin derivatives.

5.2.2 UVRR spectroscopy probes conformational difference of anoplin derivatives

There is a certain correlation between the conformation and amphipathicity of AMPs, and conformational studies can often help deduce the mechanism of action or toxicity.[1-3] For short peptides, however, such studies become more challenging.[1-3] For example, CD spectroscopy was used to determine that anoplin adopts a random coil-like conformation in aqueous buffer and a preferentially α-helical conformation in a membrane mimicking environment.[13,19,20,25] However, results from various studies were conflicting. Percentage of helical content was found to be between 24 and 77 %.[13,19,20,25] The discrepancy in the calculated secondary structure is likely due to poor sensitivity of CD spectroscopy to the conformation of short peptides.[9] Besides, CD spectroscopy was unable to detect any difference in the secondary structure of anoplin, Ano8K, and Ano1K5V8K.[20] Therefore, UVRR spectroscopy was used as a more sensitive method to discriminate between different conformations of short peptides.

UVRR spectroscopy is a powerful technique to study structure/function relationships of proteins. Three amide bands present in the Raman spectra of proteins are used to extract structural information: amide I, II, and III.[26-30] The position and relative intensities of these bands are particularly sensitive to the peptide's conformation. Conformational information can be extracted by performing spectral deconvolution using pure secondary structure reference spectra (for example α-helix, β-sheet, etc.) to identify the quantity of that particular secondary structure.[30-34] This approach is useful for larger peptides/proteins, where contribution from the terminal residues is negligible. Alternatively, a peak fitting procedure can be performed where several individual bands

are placed into a complex amide band region.[26, 35] Such an approach is more appropriate for short peptides like anoplin.

Raman spectroscopic studies of AMPs are usually concerned with the structural changes in aqueous versus membrane mimicking environments, such as TFE, in order to elucidate the conformational change and dynamics of peptide/membrane binding.[9,12,36,37] TFE aids peptide folding by creating a hydrophobic environment and removing solvent hydrogen bonding.[37] In this work, TFE was used to determine the changes that anoplin UVRR spectra undergo when the peptides fold. However, due to interference from TFE Raman bands, the amide III region could not be reliably used to determine the peptide secondary structure change (Fig 5.5-5.7). Therefore, in the present work the amide I band was used to extract the structural information of anoplin and its derivatives. Analysis was facilitated by the lack of aromatic amino acids in the primary structure of anoplin derivatives.

The amide I region of a peptide Raman spectrum can occasionally be properly fit with 3 peaks located at 1650-1656 cm^{-1}, 1664-1670 cm^{-1} and 1680 cm^{-1} corresponding to the α-helix, β-sheet and random coil/PPII structures respectively.[38,39] However, we could not satisfactorily model the anoplin amide I region using only three peaks. Instead, five peaks were selected in the amide I region similar to a study of a number of short peptides with KL repeating sequences.[35] Fig 5.5 to 5.7 show results of peak fitting and Table 5.2 shows the optimized locations of the bands for all three derivatives. The consistency of the locations of peaks across three different peptides in two different solvents supports the choice of this fitting method. In comparison to the 1615, 1635, 1651, 1664, 1679 cm^{-1} peaks found by Guiffo-Soh et al., the average peak locations for all three peptides were

determined to be 1612, 1631, 1650, 1668 and 1687 cm^{-1} (Table 5.2).[35] Except for the first (1612 cm^{-1}), the peaks were assigned to α-helix, β-sheet, β-strand and random coil/PPII secondary structural components, respectively.

Visually, anoplin and its two derivatives show a clear shoulder appearing to the left of the main amide I band in TFE (Fig 5.5-5.7). These results are very similar to previous experiments concerning anoplin, deamidated anoplin and fully D-amino acid substituted anoplin.[36] Peak fitting was performed to get a better idea of what secondary structure the anoplin derivatives are adopting. Table 5.3 summarizes these results reported as each band's percentage area contribution to the total amide I area (not the total percent of a particular secondary structure).

According to the results of peak fitting, the proportion of the amide I peak corresponding to the α-helical conformation of anoplin and Ano8k in PBS buffer is equal to ~7% of total amide I area whereas for Ano1K5V8K this number increases to 10% (Table 5.3). The α-helical content of each anoplin rises in 50% TFE. The increase is 28% for the wild type anoplin and ~60% for both substituted derivatives (Table 5.2). The final α-helical area as a percentage of total amide I area after folding in 50% TFE is 9%, 11% and 17% for the wild type anoplin, Ano8K, and Ano1K5V8K, respectively (Table 5.3).

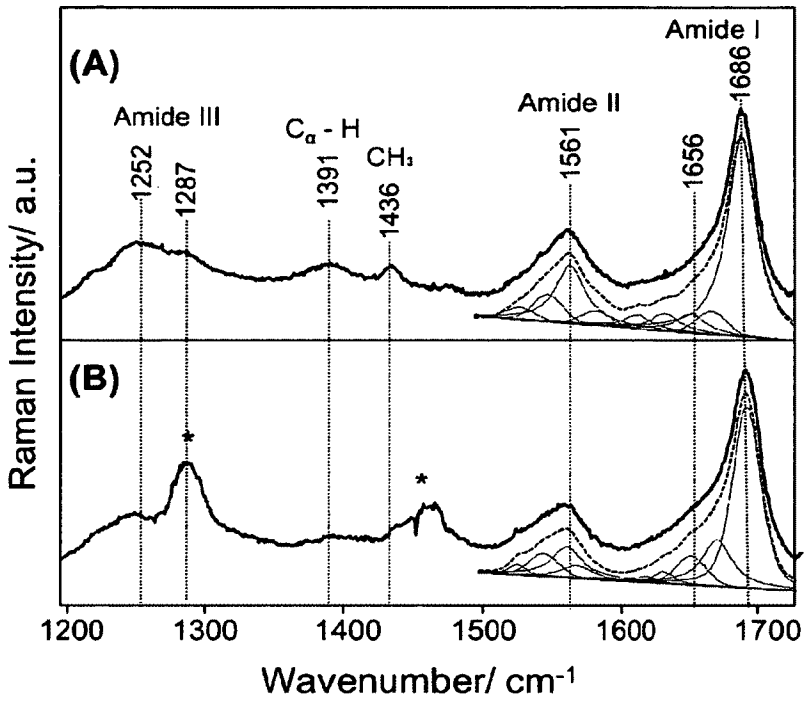

Figure 5.5: Peak fitting of UVRR spectra of anoplin in (A) PBS and (B) 50% TFE. Original spectrum (thick) is shown on top of the fitted trace (dashed) with individual fitted peaks (thin) and baseline (flat) below. TFE contributions are marked by asterisks.

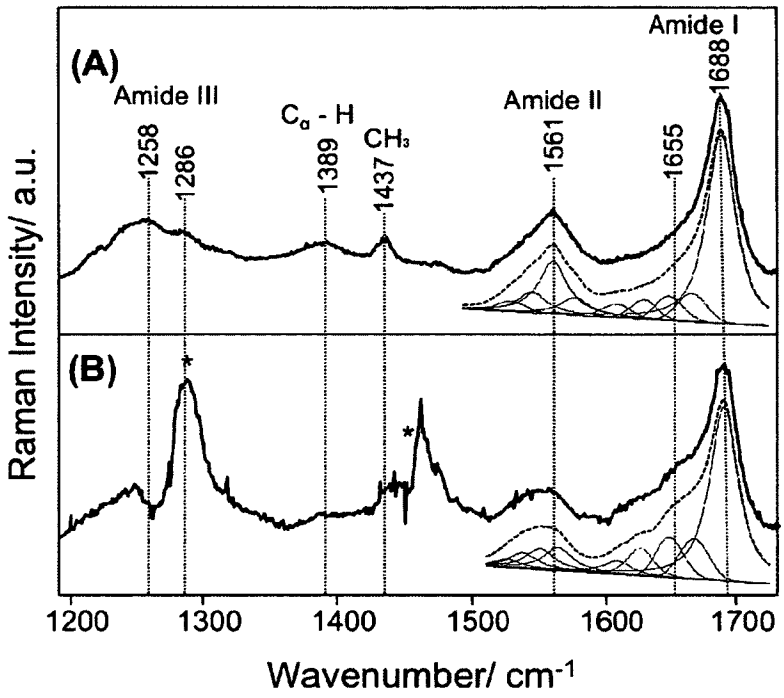

Figure 5.6: Peak fitting of UVRR spectra of Ano-8K in (A) PBS and (B) 50% TFE. Original spectrum (thick) is shown on top of the fitted trace (dashed) with individual fitted peaks (thin) and baseline (flat) below. TFE contributions are marked by asterisks.

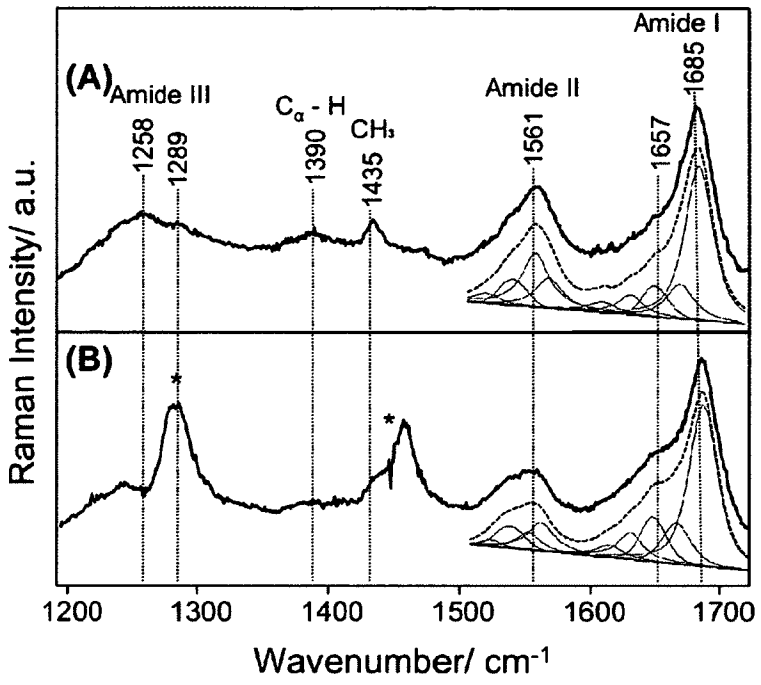

Figure 5.7: Peak fitting of UVRR spectra of Ano1K5V8K in (A) PBS and (B) 50% TFE. Original spectrum (thick) is shown on top of the fitted trace (dashed) with individual fitted peaks (thin) and baseline (flat) below. TFE contributions are marked by asterisks.

The substantial increase in the α-helical content in 50% TFE supports other literature findings that anoplin adopts a mostly α-helical secondary structure when folded.[19,40] It appears that although both substituted derivatives have a higher but approximately equal tendency to adopt α-helical structures in TFE compared to the wild type anoplin, they do not have a similar final α-helical content. In fact, as the wild type anoplin received one and then three substitutions, the TFE α-helix content steadily increased (Table 5.3). A likely explanation for this trend is the preference of certain residues for specific secondary structures.[41-43] It is well known and generally accepted that lysine prefers to adopt α-helical structures. Therefore, by substituting a lysine in place of a threonine (favours a β-sheet structure) for Ano8K and replacing an additional glycine (favours a disordered structure) for Ano1K5V8K, it is only natural that the substitutions would increase the peptide's preference for α-helical structure.[41] It also appears that the two lysine substitutions in Ano1K5V8K were influential enough to even increase the α-helical content in PBS (Table 5.3).

The β-sheet content was approximately equal for the wild type anoplin and Ano8K at 6% and 7% of total amide I area, while Ano1K5V8K had higher β-sheet content at 10% of total amide I area (Table 5.3). The β-sheet content of the wild type anoplin and Ano1K5V8K remained the same in 50% TFE but rose for Ano8K by 67% (Table 5.3). This increase for Ano8K brought its β-sheet content up to the same amount as Ano1K5V8K (10%) compared to the wild type anoplin in TFE (7%, Table 5.2). The higher β-sheet content in Ano1K5V8K is likely due to the addition of a β-sheet favoring valine in place of an arginine, which has no secondary structure preference.[41] The lack of change in β-sheet content for the wild type anoplin and Ano1K5V8K in 50% TFE

compared to PBS also gives evidence that anoplin adopts an α-helical structure when folded.

The random coil content of the wild type anoplin in PBS was 73% of total amide I area and decreased to 69% and 61% in Ano8K and Ano1K5V8K, respectively (Table 5.3). The random coil content of each peptide dropped in 50% TFE. The decrease was approximately the same for the wild type anoplin and Ano1K5V8K at 12% and 11% respectively, but it was greater for Ano8K at 17% (Table 5.3). The final level of random coil structure after folding in 50% TFE gradually decreased from the wild type anoplin to Ano8K and Ano1K5V8K, similarly to the random coil levels in PBS (Table 5.3). The random coil content is inversely related to the α-helix content of each peptide and is explained by the same concept. As the substitutions of inserted residues that favor α-helices and as the amount of α-helical content increased, the random coil content decreased. The trend also continued once the peptides were in the membrane mimetic TFE solvent where the α-helix content increased in TFE as the random coil content decreased.

Table 5.2: Assignment of the UVRR amide bands of anoplin derivatives in PBS and 50% TFE.

	anoplin		Ano8K		Ano1K5V8K		
Raman band	PBS	TFE	PBS	TFE	PBS	TFE	assignment[a]
Amide I	1609[b]	1616	1608	1613	1611	1616	
	1631	1631	1628	1628	1632	1635	β-sheet
	1653	1650	1645	1651	1652	1651	α-helix
	1665	1668	1665	1668	1672	1667	β-strand
	1686	1688	1687	1688	1687	1688	random coil
Amide II	1522	1521	1524	1529	1523	1529	α-helix
	1540	1540	1544	1542	1541	1543	α-helix
	1560	1557	1561	1555	1561	1553	random coil
	1582	1567	1578	1563	1583	1562	β-sheet

[a] From Guiffo-Soh et al.[35]
[b] Position of peak maximum measured in cm^{-1}.

Table 5.3: Relative area of the peaks corresponding to α-helix, β-sheet, and random coil in anoplin, Ano8K and Ano1K5V8K as percentages of total amide I area in PBS and 50% TFE.

	α-helix		β-sheet		random coil	
	PBS	TFE	PBS	TFE	PBS	TFE
anoplin	7%	9%	6%	6%	73%	65%
Ano8K	7%	11%	7%	10%	69%	59%
Ano1K5V8K	11%	17%	10%	10%	61%	55%

The amide II region is not often used for peptide secondary structure determination due to its lower sensitivity and low analyzability. However, some work has been done to determine amide II band shifts due to secondary structure.[26] In this work, the anoplin amide II region appeared to undergo a change in 50% TFE compared to PBS buffer and attempts were made to fit the region to support amide I results. Four bands were used to fit the amide II region based on the 1511, 1550, 1554, 1564 cm^{-1} bands (corresponding to α-helix, α-helix, β-sheet and unordered structures respectively) found by JiJi et al.[26] The locations of the peaks for each sample are shown in Table 5.2. Similarly to amide I peaks, the amide II peaks of all peptides showed good consistency amongst themselves and compared to the results of JiJi et al.[26] Although results of amide II fitting appeared promising based on peak locations, the quality of results declined once quantitative and comparative analysis was attempted. Consistent peak fitting results could not be produced to support or oppose amide I findings. No clear patterns or trends were found in amide II fitting results. The lack of success was deemed to be due to low sensitivity of amide II to peptide secondary structure and difficulty in fitting of the amide II region.

Overall UVRR spectroscopy was very effective in discriminating the conformation of the three anoplin derivatives. The data indicate that Ano8K and Ano1K5V8K are more helical in a membrane mimicking environment than is the wild type peptide. As a result, amphipathicities of these peptides are likely greater than that of the wild type anoplin, and do not follow the same trend as the calculated average hydrophobic moment (Table 5.1). The increased amphipathicity in addition to the increased charge contribute to the higher antimicrobial activity of the two derivatives. Since the tri-substituted anoplin

Ano1K5V8K has the highest helicity among the three peptides, it is likely the most amphipathic. This explains the higher hemotoxicity of the peptide (Table 5.1).

5.2.3 Membrane lytic activity of anoplin derivatives

Finally, the ability of all three anoplin derivatives to rupture model cell membranes was determined using dye leakage experiments. When encapsulated inside the lipid vesicles at high concentration, carboxyfluorescein fluorophore self-quenches.[44] Upon peptides' addition and binding, rupture of the lipid vesicles releases the entrapped fluorophore and thus leads to and increase in fluorescence intensity. Membrane lytic activity can be measured relative to the activity of nonionic surfactants such as Triton X-100, which completely rupture the vesicles. Six different model cell membranes were tested in this work: single saturated phospholipids (DPPC and DPPG) and four model mixtures with unsaturated phospholipids mimicking mammalian, Gram-negative bacterium *E. coli*, and Gram-positive bacteria *S. aureus* and *B. subtilis.*

As we observed in the monolayer experiments, anoplin had a much higher affinity for anionic DPPG than for the zwitterionic DPPC monolayer due to electrostatic attraction (Fig 5.3). In that respect, two derivatives Ano8K and Ano1K5V8K had even greater binding selectivity due to the additional positive charge. The selectivity did not however simply extrapolate to membrane rupturing activity thus showing non-additivity of electrostatic and hydrophobic interactions.[1-3]

All three anoplin derivatives demonstrated similar poor activity to zwitterionic DPPC and mammalian model membranes (Fig 5.8 A, C) consistent with poor binding of the peptides to neutral membranes (Fig 5.3 A). Upon addition of pure buffer to mammalian

model membranes, a small fluorescence intensity increase (<5%) was detected, possibly due to osmotic shock.[45] However, upon addition of the peptides into a mammalian model membrane, a small decrease of fluorescence intensity was detected (Fig 5.8 C). It has previously been shown that model membranes composed of several different types of lipids with different transition temperatures contain more membrane defects and allow spontaneous diffusion of carboxyfluorescein.[45] Therefore, the fluorescence signal intensity decrease observed for the mammalian model could be attributed to the binding of anionic fluorophore to the cationic peptides with the formation of a signal quenching fluorophore-peptide complex.[46-48]

All three anoplin derivatives were found to induce similar leakage from DPPG vesicles (Fig 5.8 B). We detected a small percentage of released dye at low peptide to lipid ratio. As the relative concentration of the peptide increased, up to 25% of the dye was released. When bacterial model cell membranes were used, however, we noticed a difference in peptide activity, with Ano1K5V8K being the most active, followed by Ano8K and the wild type anoplin (Fig 5.8 D-F). For both Gram-positive models Ano1K5V8K induced almost complete dye leakage at higher peptide/lipid ratio, indicating total vesicle disruption (Fig 5.8 E, F). Ano8K and anoplin were found to be considerably less active, especially against the *B. subtilis* model. Both Ano1K5V8K and Ano8K had lytic activities higher than anoplin against the *E. coli* model (Fig 5.8 D).

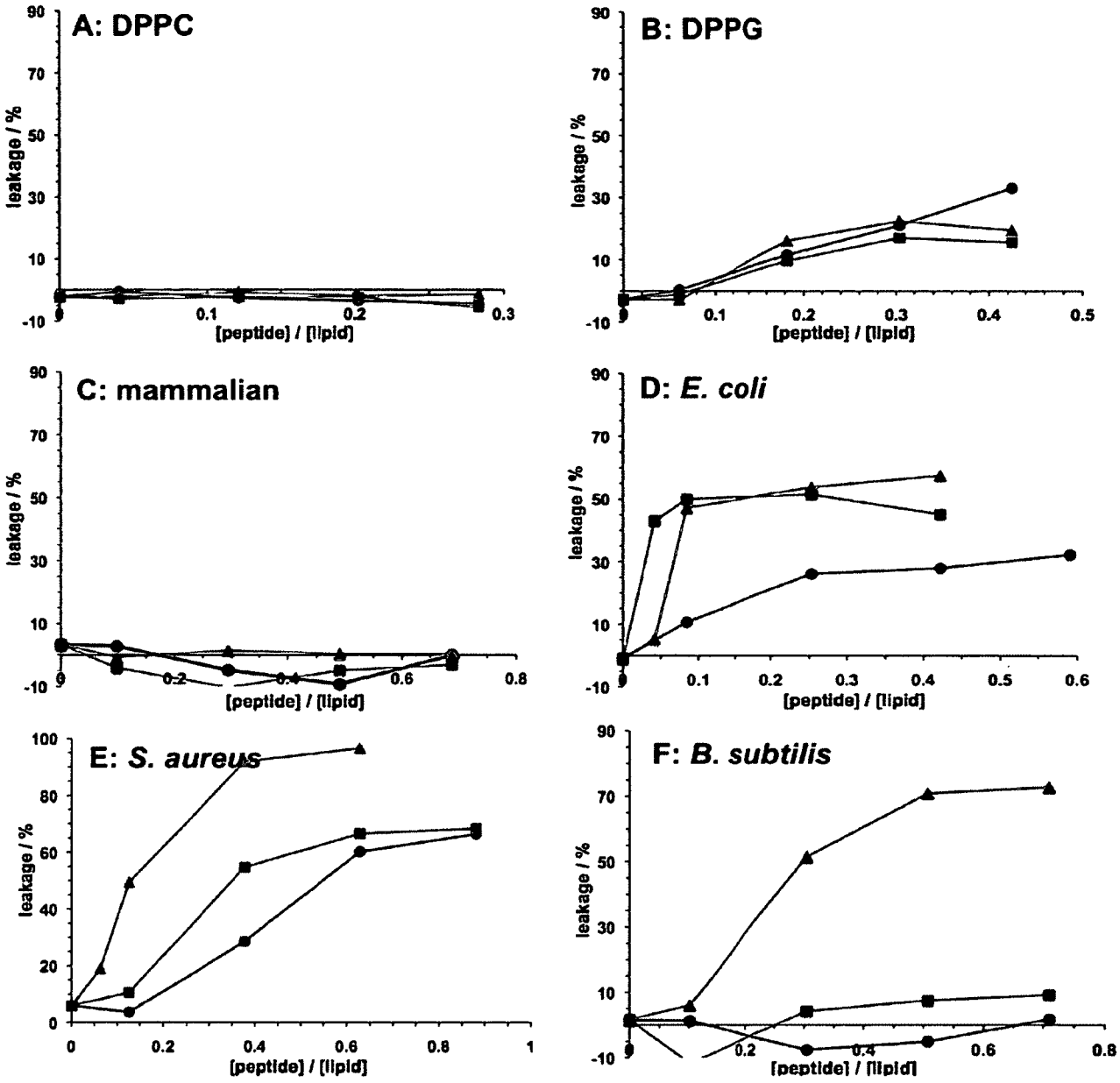

Figure 5.8: CF fluorescence signal increase after the addition of anoplin derivatives (Ano – black circles; Ano8K – grey squares; Ano1K5V8K – beige triangels) into (A) DPPC, (B) DPPG, (C) mammalian model, (D) *E. coli* model, (E) *S. aureus* model, and (F) *B. subtilis* model vesicles.

Overall the data indicate that the two derivatives have on average higher lytic activity than the wild type anoplin against all model cell membranes used. Although the higher lytic activity of the derivatives correlates with a greater charge, and as a result greater initial interaction and peptide/lipid binding, difference in the activity between the two derivatives Ano1K5V8K and Ano8K points at a more complex mechanism of membrane disruption. Degrees of helicity and amphiphathicity were previously reported as being important parameters in peptide antimicrobial activity.[3,49] According to UVRR spectroscopy, Ano1K5V8K has the greater percent of helical content in TFE, followed by Ano8K and anoplin. Therefore, it is reasonable that Ano1K5V8K, with the greatest helicity is the most amphipathic among the three peptides in a cell membrane environment, leading to higher antimicrobial activity of the peptide, as well as higher hemolytic activity.[1,5,8] Another explanation of the higher membrane lytic activity of the tri-substituted peptide against bacterial model membranes comes from the fact that it likely has a narrower polar face than anoplin and Ano8K (Fig 5.1). As a result, it destabilizes the bilayer to a greater degree. It has to be mentioned however, that due to relatively low helicity of the peptides, the whole concept of polar angle might not be appropriate for such short peptides.

5.3 CONTRIBUTIONS

Special thanks to Stahs Pripotnev and Annamaria Ruscito on NSERC USRA work in UVRR and monolayers measurements, respectively.

5.4 REFERENCES

1. Toke, O. *Biopolymers.* **2005**, *80*, 717-735.
2. Sathe, M.; Wieprecht, T. *Biochim. Biophys. Acta-Biomembrane.* **1999**, *1462*, 71-87.
3. Yeaman, M. R.; Yount, N. Y. *Pharm. Rev.* **2003**, *5*, 28–56
4. Chen, Y.; Mant, C.T.; Farmer, S.W.; Hancock, R.E.W.; Vasil, M.L.; Hodges, R.S. *J. Biol. Chem.* **2005**, *280*, 12316–12329.
5. Dathe, M.; Wieprecht, T.; Nokplenko. H.; Handel, L.; Maloy W.L.; MacDonald, D.L.; Beyermann, M.; Bienert M. *FEBS Letters*, **1997**, *403*, 208-212.
6. Giangaspero, A.; Sandri, L.; Tossi, A. *Eur. J. Biochem.* **2001**, *268*, 5589-5600.
7. Tachi, T.; Epand R.F.; Epand R.M.; Mastsuzaki K. *Biochemistry* **2002**, *41*, 10723-10731.
8. Fernandez-Vidal, M.; Jayasinghe, S.; Ladokhin A.S.; White, S.H. *J. Mol. Biol.* **2007**, *370*, 459-470.
9. Ozdemir, A.; Lednev, I.K.; Asher, S.A. *Biochemistry.* **2002**, *41*, 1893-1896.
10. Wallace, J.; Daman, O.A.; Harris, F.; Phoenix, D.A. *Theor. Biol. Med. Modelling.* **2004**, *1*, 5.
11. Phoenix, D.A.: Harris, F.; Daman, O.A.; Wallace, J. *Curr. Protein Pept. Sci.* **2002**, *3*, 201
12. Ianoul, A.; Mikhonin, A.; Lednev, I.K., Asher, S.A. *J. Phys. Chem. A.* **2002**, *106*, 3621-3624.
13. Konno, K.; Rangel, M.; Oliveira, J.S.; Cabrera, M.P.S.; Fontana, R.; Hirata, I.Y.; Hide, I.; Nakata, Y.; Mori, K.; Kawano, M.; Fuchino, H.; Sekita, S.; Neto, J. R. *Peptides.* **2007**, *28*, 2320-2327.

14. Fontana, R.; Mendes, M. A.; de Souza, B. M.; Konno, K.; César, L. M. M.; Malaspina, O.; Palma, M. S. *Peptides.* **2004**, *25*, 919-928.

15. Gao, B.; Sherman, P.; Luo, L.; Bowie, J.; Zhu, S. *FASEB J.* **2009**, *23*, 1230-1245.

16. Prates, M. V.; Sforca, M. L.; Regis, W. C. B.; Leite, J. R. S. A.; Silva, L. P.; Pertinhez, T. A.; Araujo, A. L. T.; Azevedo, R. B.; Spisni, A.; Bloch Jr, C. *J Biol. Chem.* **2004**, *279*, 13018-13026.

17. Jin, L. L.; Li, Q.; Song, S. S.; Feng, K.; Zhang, D. B.; Wang, Q. Y.; Chen, Y. H. *Comp. Biochem. Physiol. B Biochem. Mol. Biol.* **2009**, *154*, 174-178.

18. Abbassi, F.; Lequin, O.; Piesse, C.; Goasdoue, N.; Foulon, T.; Nicolas, P.; Ladram, A. *J. Biol. Chem.* **2010**, *285*, 16880-16892.

19. Konno, K.; Hisada, M.; Fontana, R.; Lorenzi, C. C.; Naoki, H.; Itagaki, Y.; Miwa, A.; Kawai, N.; Nakata, Y.; Yasuhara, T.; Ruggiero Neto, J.; de Azevedo Jr, W. F.; Palma, M. S.; Nakajima, T. *Biochim. Biophys. Acta - Protein Struc. Mol. Enzymol.* **2001**, *1550*, 70.

20. Ifrah, D.; Doisy, X.; Ryge, T.S.; Hansen, P.R. *J. Peptide Sci.* **2005**, *11*, 113-121.

21. Maget-Dana, R. *Biochim. Biophys. Acta – Biomembranes.* **1999**, *1462*, 109-140.

22. Brockman, H. *Curr. Opin. Struct. Biol.* **1999**, *9*, 438-443.

23. Eiriksdottir, E.; Konate, K.; Langel, U.; Divita, G.; Deshayes, S. *Biochim. Biophys. Acta – Biomembranes.* **2010**, *1798*, 1119-1128.

24. Ambroggio, E. E.; Separovic, F.; Bowie, J.; Fidelio, G. D. *Biochim. Biophy. Acta – Biomembranes.* **2004**, *1664*, 31-37.

25. Cabrera, M.P.D.S; Arcisio-Miranda, M.; de Costa, L.C.; de Souza, B.M.; Costa, S.T.B.; Palma, M.S.; Neto, J.R.; Procopio, J. *Arc. Biochem. Biophys.* **2009**, *486*, 1-11.

26. JiJi, R. D.; Balakrishnan, G.; Hu, Y.; Spiro, T. G. *Biochemistry*. **2006**, *45*, 34-41.

27. Ianoul, A.; Boyden, M. N.; Asher, S. A. *J. Am. Chem. Soc.* **2001**, 123, 7433– 7434.

28. Chi, Z.; Chen, X. G.; Holtz, J. S.; Asher, S. A. *Biochemistry.* **1998**, *37*, 2854–28 64

29. Huang, C.-Y.; Balakrishnan, G.; Spiro, T. G. *J. Raman Spectrosc.* **2006**, *37*, 277–282.

30. Xu, M.; Shashilov, V. A.; Ermolenkov, V. V.; Fredriksen, L.; Zagorevski, D.; Lednev, I. K. *Protein Sci.* **2007**, *16*, 815-832.

31. Xu, M.; Ermolenkov, V. V.; Uversky, V. N.; Lednev, I. K. *J. Biophotonics.* **2008**, *1*, 215-229.

32. Williams, R. W.; Dunker, K. *J. Mol. Biol.* **1981**, *152*, 783–813.

33. Williams, R. W. J. Mol. Biol. **1983,** *166*, 581–603.

34. Williams, R. W. *Methods Enzymol.* **1986**, *130*, 311–331.

35. Guiffo-Soh, G.; Hernandez, B.; Coic, Y., Boukhalfa-Heniche, F.; Fadda, G.; Ghomi, M. *J. Phys. Chem. B.* **2008**, 112, 1282-1289.

36. Pripotnev, S.; Won, A.; Ianoul, A. *J. Raman Spectrosc.* **2010** *in press.*

37. Buck, M. *Q. Rev. Biophys.* **1998**, *31*, 297-355.

38. Apetri, M. M.; Maiti, N. C.; Zagorski, M. G.; Carey, P. R.; Anderson, V. E. *J. Mol. Biol.* **2005**, *355*, 63-71.

39. Maiti, N. C.; Apetri, M. M.; Zagorski, M. G.; Carey, P. R.; Anderson, V. E. *J. Am. Chem. Soc.* **2004**, *126*, 2399-2408.

40. Cabrera, M.P.D.S; Arcisio-Miranda, M.; Costa, S.T.B.; Konno, K.; Ruggiero, J.R.; Procopio, J.; Neto, J.R. *J. Pept. Sci.* **2008**, *14*, 661-669.

41. Chou, P.Y.; Fasman, G.D. *Biochemistry.* **1974**, *13*, 222-245.

42. Chakrabartty, A.; Baldwin, J. A.; Baldwin, R. L. *Nature*. **1991**, *351*, 586-588.

43. Li, S.-C.; Deber, C.M. *Nature Struct. Biol.* **1994**, *1*, 368-373.

44. Schwarz,G.; Robert, C.H. *Biophys. J.* **1990**, *58*, 577-583.

45. Hays, L.; Crowe, J.H.; Wolkers, W.; Rudenko, S. *Cryobiology.* **2001**, *42*, 88-102.

46. Magzoub, M.; Oglęcka, K.; Pramanik, A.; Eriksson, L.E.G.; Gräslund, A. *Biochim. Biophys. Acta – Biomembranes.* **2005**, *1716*, 126-136.

47. Ringstad, L.; Kacprzyk, L.; Schmidtchen, A.; Malmsten, M. *Biochim. Biophys. Acta – Biomembranes.* **2007**, *1768*, 715-727.

48. van den Bogaart, G.; Guzmán, J.V.; Mika, J.T.; Poolman, B.; *J. Biol. Chem.* **2008**, *283*, 33854-33857.

49. Dathe, M.; Wieprecht, T. *Biochim. Biophys. Acta* **1999**, *1462*, 71-87.

CHAPTER 6
INVESTIGATING THE HINGE PROPERTY OF LATARCIN 2A ON LIPID MODEL MEMBRANES

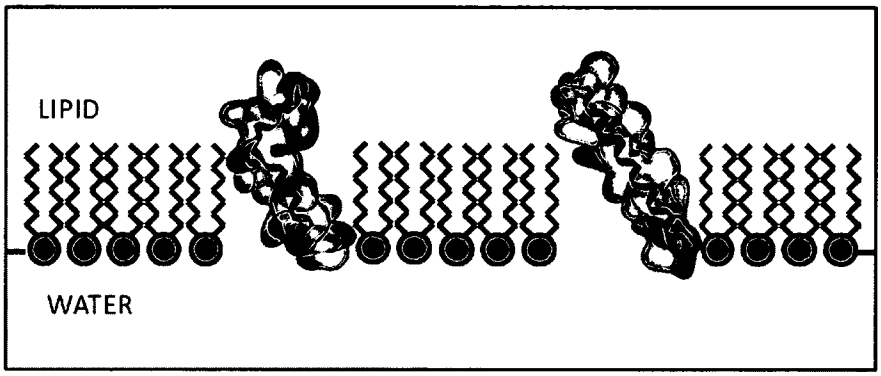

Reproduced with permission from

- Idiong, G.; Won, A.; Ruscito, A.; Leung, B.O.; Hitchcock, A.O.; Ianoul, A. Investigating the effect of a single glycine to alanine substitution on interactions of antimicrobial peptide latarcin 2a with a lipid membrane. *European Biophysical Journal* **2011**, *40*, 1087-1100. Copyright 2011 Springer.

- Won A.; Ruscito A.; Ianoul A. Imaging the membrane activity of bioactive peptide latarcin 2a. *Biochimica et Biophysica Acta – Biomembrane* **2012**, *1818*, 3072-3080. Copyright 2012 Elesvier.

6.1 INTRODUCTION

Latarcins are a new family of antimicrobial peptides that was purified from the venom gland of the Central Asian spider *Lachesana tarabaevi.*[1] There are seven structurally unrelated groups of short linear cysteine-free membrane-active peptides that are found to be lytic to Gram-positive and Gram-negative bacteria, erythrocytes, and yeast at micromolar concentrations and share little homology with other known peptides.[1] The two latarcins that have been studied extensively so far are ltc1 and ltc2a.

Ltc1 (SMWSGMWRRKLKKLRNALKKKLKGE-COOH) is a 26 amino acid residue peptide that has a net charge of +10, strong antibacterial activity — MIC value in the 0.5-5 μM range against Gram-positive and Gram-negative bacteria — and moderate hemolytic activity — EC_{50} value of 80 μM against rabbit erythrocytes.[10] The peptide was found to form a single amphipathic helix in membrane mimicking environments, with a narrow shaped hydrophobicity surface and no hydrophobicity gradient along the axis.[12] It was suggested that in the cell membrane, ltc 1 adopts a transmembrane orientation and forms variable sized lesions.[12]

Ltc2a is a 26 amino acid residue peptide that has a net charge of +9 and broad-spectrum antibacterial activity against Gram-positive and Gram-negative bacteria with MIC values in the 0.4 -7 μM range while having moderate hemolytic activity toward human erythrocytes, with EC_{50} in the 3 to 6 μM range.[1,2,3] Both molecular dynamics (MD) simulation and NMR data indicate ltc2a adopts a helix-hinge-helix structure in a small micelle with the N-terminus helix (residues 3 – 9) embedded in the micelle and C-terminus (residues 13 – 21) lying on the membrane.[4,5] In a larger micelle, however, MD simulation showed that the two helices of ltc2a are angled 150 ° apart and lie peripherally

on the membrane.[5] The two helices of the peptide are connected by glycine — a helix disrupting amino acid residue — and differ in their hydrophobic organization. The N-terminal helix is strongly amphiphilic with the side chains of hydrophobic (Phe3, Leu6, Ile7) and hydrophilic (Lys5, Lys8, and Lys9) amino acids divided and on opposite sides (Fig 6.1).[6,7] The C- terminal helix is less amphiphilic, with a narrow hydrophobic segment composed of Ile15, Val19, and Ala22 (Fig 6.1). Unlike ltc1, ltc2a was suggested to act by the carpet-like mechanism.[1] The difference in the hemolytic activity between the two peptides is suggested to result from the different secondary structure and organization of hydrophobic domains within the folded peptides.[4-6] An effort was made to modify the structure of ltc2a in such a way as to alter the hydrophobicity pattern and minimize the cytotoxicity.[3] Of particular interest are modifications within the hinge region of ltc2a.

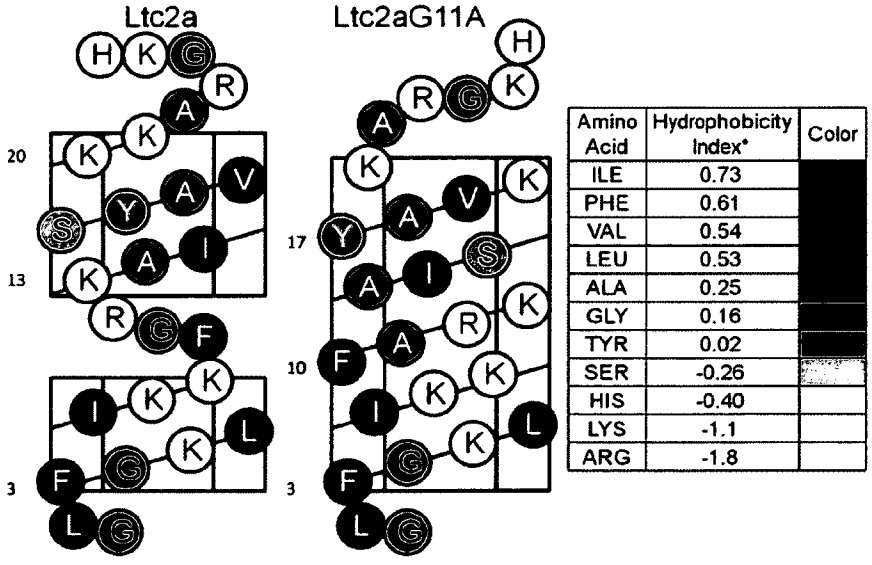

Figure 6.1: Helical net diagrams for ltc2a and lytc2aG11A. Eisenberg consensus hydrophobicity scale was used (* retrieved from reference 16).

The helix-hinge-helix structure of ltc2a is often found in cationic AMPs that are longer than 20 amino acid residues. One of the helices is commonly found to enter the membrane while the other helix is positioned parallel to the membrane surface with the help of some hydrophobic residues, such as Phe or Trp, to anchor the peptide to the membrane.[9-14] Small modifications in the hinge region were found to have a dramatic effect on the peptide's activity.[3,10-14] This effect is primarily due to the loss of conformational flexibility, which in turn prevents the peptides from binding and penetrating the bilayer deeper. For example, the helix-hinge-helix structural feature is crucial in the activity of a hybrid peptide incorporating cecropin and magainin 2 residues — since the hinge deletion resulted in a single α-helical structure without amphiphilicity that dramatically decreased bactericidal and tumoricidal activities.[9] The helix-loop-helix was found to be an important prerequisite for the antimicrobial activity of an internal peptide within hen lysozyme.[10] Two of the three glycines in clavanin A were demonstrated to be important in facilitating membrane insertion.[11] The antibiotic activity of caerin 1.1 decreased dramatically when two hinge forming proline residues were replaced with alanines — resulting in single helix formation with no clear hydrophobic face suggested to cause the derivative to be less active.[12] Replacement of two glycine amino acids with alanines in a single helix antimicrobial peptide piscidin 1 increased the hydrophobic moment of the peptide and as a result was shown to increase both antibacterial and hemolytic activity of the peptide.[14] However, when only one glycine was replaced with proline —breaking the helix to form a helix-hinge-helix structure — the derivative showed a considerably higher selectivity towards bacterial cells than the

original piscidin demonstrating the hinge region as a critical factor for bacterial cell selectivity.[14]

Several analogues with point mutations in ltc2a were proposed to change the hydrophobic properties of the N-terminal helix.[3] For several derivatives, the selective toxicity towards bacterial cells was improved. One derivative with the replacement of leucine with glycine in position 11 (ltc2aG11L) appeared to possess similar antibacterial properties as the wild type ltc2a. At the same time it was shown to be considerably more toxic to mammalian cells. In membrane mimicking environments, leucine is known to be a helix forming amino acid.[15] Replacement of Gly11 with leucine was shown to notably alter the hydrophobic properties of the peptide, which lead to the increase of the overall peptide toxicity.[3] To investigate the hinge property of ltc2a in this study, glycine was replaced with alanine that only slightly increases the peptide's overall hydrophobicity as the hydrophobicity indexes for the two amino acids are close (Fig 6.1).[16] Moreover, alanine has a much higher propensity to form a helix in membrane environments than glycine — due to a more restricted set of dihedral angles for alanine than for glycine.[15-20] Thus, it is reasonable to assume derivative ltc2aG11A adopts a single helix conformation with a single hydrophobic segment extending from Phe3 to Ala22 with a stronger hemolytic activity than ltc2a.

In the present study, the wild type ltc2a and ltc2aG11A, a derivative obtained by replacing the glycine in position 11 (the hinge region) with alanine, were compared in their ability to bind and rupture model cell membranes. As alanine favors the helix conformation, it is expected that the modified ltc2aG11A adopts a single helix structure (GLFGKLIKKF**A**RKAISYAVKKARGKH-COOH). We used LB monolayer techniques

combined with AFM and X-PEEM to investigate the role of the hinge region for latarcin interactions with phospholipid mono- and bi-layers as model cell membranes. Carboxyfluorescein leakage assay was used to determine the difference in the membrane rupturing activity between peptides. Results of this work demonstrate the effect of point mutations on the physicochemical and membrane binding properties of AMPs.

6.2 RESULTS AND DISCUSSION

6.2.1 Single amino acid replacement changes surface activity of latarcin 2a

In a membrane mimicking environment, ltc2a adopts a helix-hinge-helix structure, with the first (residues 3-9) and the second (residues 13-21) helical regions connected by glycine, a poorly ordered fragment containing a helix disrupting amino acid.[4] The two helices of the peptide differ in their hydrophobic organization. The N-terminal helix is strongly amphiphilic. The side chains of hydrophobic (Phe3, Leu6, Ile7) and hydrophilic (Lys5, Lys8, and Lys9) amino acids are divided and are on opposite sides (Fig 6.1).[6,7] The C- terminal helix is less amphiphilic, with a narrow hydrophobic segment composed of Ile15, Val19, and Ala22 (Fig 6.1). It is of interest to investigate the hinge property of latarcin2a. The replacement of glycine with alanine at position 11 only slightly increases the peptide's overall hydrophobicity since Eisenberg hydrophobicity indexes for the two amino acids are similar.[16] However, this replacement modifies the peptide's overall conformation since alanine has a much higher propensity to form a helix in membrane environments than glycine.[15] Therefore, it is expected that in membrane mimicking environments the derivative ltc2aG11A adopts a single helix conformation with a single hydrophobic segment extending from Phe3 to Ala22 (Fig 6.1).

The air-water interface has been suggested to be a useful membrane mimicking system where air is more hydrophobic than water.[21,22] Deposition of peptides at the interface, therefore, cause them to adopt a conformation similar to that in cell membranes.[21,23] Parameters, such as CMC and CPI can be used to evaluate the surface activity of a peptide.[23] The CMC is the concentration where micelle formation in the solution is thermodynamically favoured than at the air-water interface — in other words, added peptide molecules saturate the interface initially followed by micelle formation in solution.[24] Fig 6.2A shows that a saturation surface pressure of 20 mN/m was observed for both ltc2aG11A and ltc2a at peptide concentrations of ~1 μg/mL, and that indicates a similar affinity of the two peptides to the air/water interface. The removal of the hinge therefore has no effect on the surface activity of ltc2a.

The peptide's affinity to the cell membrane can be studied with a monolayer of phospholipid that is deposited at the interface prior to peptide injection.[23] A portion of the peptide molecules will bind to and insert into the deposited lipid monolayer thus affecting surface pressure or area of the lipid film at a constant area or pressure, respectively. The degree of the pressure change depends on the initial film pressure, type of the lipid used, surface activity and concentration of the peptide. Fig 6.2B shows the result of the pressure changes, $\Delta\pi$, after the peptide addition as a function of the initial lipid film pressure, π_i. The dependencies, $\Delta\pi(\pi_i)$, were found to be slightly different for the two peptides.

In the case of zwitterionic DPPC, the CPI were found to be around 35 mN/m for ltc2aG11A, and 28 mN/m determined for ltc2a. These values are slightly greater than the saturation pressures of both peptides (Fig 6.2 A) suggesting preferential incorporation of

the peptides into the lipid film and emphasizing the role of hydrophobic interactions. The higher CPI found for ltc2aG11A is likely due to its structure, and as a result, the difference between their amphiphilicities. The natural cell membrane is believed to have a surface pressure in the range of 25 mN/m and 35 mN/m[25], suggesting that of the two latarcin 2a derivatives, ltc2aG11A is more likely to spontaneously insert into the zwitterionic cell membrane and should therefore be more toxic to mammalian cells.

In the peptides' binding to anionic lipid DPPG, however, the CPI was found to be around 55 mN/m for ltc2aG11A and about 60 mN/m for ltc2a. These pressures are substantially greater than for DPPC, indicating the importance of electrostatic interactions of the peptides and cell membrane. The wild type ltc2a appears to have a slightly greater effect on the anionic lipid monolayer than ltc2aG11A.

Another interesting observation can be made from Fig 6.3 presenting the time course of the surface pressure change, measured specifically after peptide injection into the subphase under the lipid films with surface pressure maintained constant between 20 mN/m to 30 mN/m. Both graphs indicate that a fast association step occurs where surface pressure increases, followed by a slow step where the surface pressure decreased with time. This second step can be attributed to slow lipid solubilization by the associated peptide molecules, formation of micelles and loss of the lipid into the subphase. Such a trend is more pronounced for ltc2aG11A in DPPG at higher pressure. This behavior is characteristic of the carpet mechanism of action for antimicrobial peptides[25] and is consistent with the previously proposed model of action for ltc2a; the same mechanism of action can be attributed to ltc2aG11A.

Based on the results of the experiments described so far, the conformational change associated with the replacement of Gly11 with Ala11 in ltc2a led to a peptide ltc2aG11A that is capable of interacting and disrupting lipid monolayers via a carpet mechanism and is more active against the zwitterionic monolayers than the wild type peptide.

6.2.2 Single amino acid replacement changes molecular surface area and lipid/peptide monolayer morphology

Isotherms of the pure DPPC and DPPG — which have identical hydrophobic acyl chains but different hydrophilic head groups — are similar and show a transition from the liquid-expanded to the liquid-condensed phase at ~7 mN/m for DPPC and at ~10 mN/m for DPPG (Fig 6.4, 6.5 A).[26-29]

The first compression isotherm for ltc2a showed two small but clearly distinguishable transition shoulders at ~7 mN/m and ~19 mN/m (Fig 6.4, 6.5 B). The area per molecule determined from the isotherm was ~180 $Å^2$. Two small and less defined transition shoulders at 12 mN/m and ~20mN/m were also shown in the first compression isotherm of ltc2aG11A (Fig 6.4, 6.5 B). The area occupied by a single ltc2aG11A molecule was found to be considerably larger, at ~290 $Å^2$. The structural difference mentioned above — ltc2a forms a helix-hinge-helix conformation and ltc2aG11A forms a single helix at the interface — most likely attributes to the difference in the monolayer properties. In the gas phase, peptide molecules adopt a horizontal orientation at the interface — with the hydrophilic region facing the subphase. When the monolayer is compressed, repulsive forces — electrostatic and Van der Waals — due to the close proximity between peptide molecules, cause their orientation to be completely or partially

perpendicular to the surface.[21,30] Since ltc2aG11A forms a single helix, the transition from parallel to the interface orientation to perpendicular was straightforward, resulting in a relatively simple compression isotherm. On the other hand, the hinge region of ltc2a makes its overall structure more flexible.[9] As a result upon compression various helix orientations are possible resulting in a complex isotherm with more defined shoulders.

For a perfect α-helical conformation of a 26 amino acid residue peptide, the length is predicted to be around 40.0 Å — 1.5 Å of axial rise per residue[25] — that is the expected full length of the peptide ltc2aG11A. In the case of ltc2a, the length of the N-terminal helix is around 15.0 Å and the C-terminal helix is calculated to be 24.0 Å. With the estimated diameter of an average alpha helix 15 Å — 5 Å for the helix core plus 5 Å for the side chains surrounding the core[25] — the area occupied by a single ltc2aG11A molecule in orientation parallel to the surface should be around 600 $Å^2$. The area is ~180 $Å^2$ if the molecule is perpendicular to the interface.[31] Based on these calculations and the measured area per molecule of ltc2aG11A we can propose that its axis was oriented at a ~65° angle relative to the interface, with the C terminus inserted in the aqueous phase due to greater hydrophilicity.

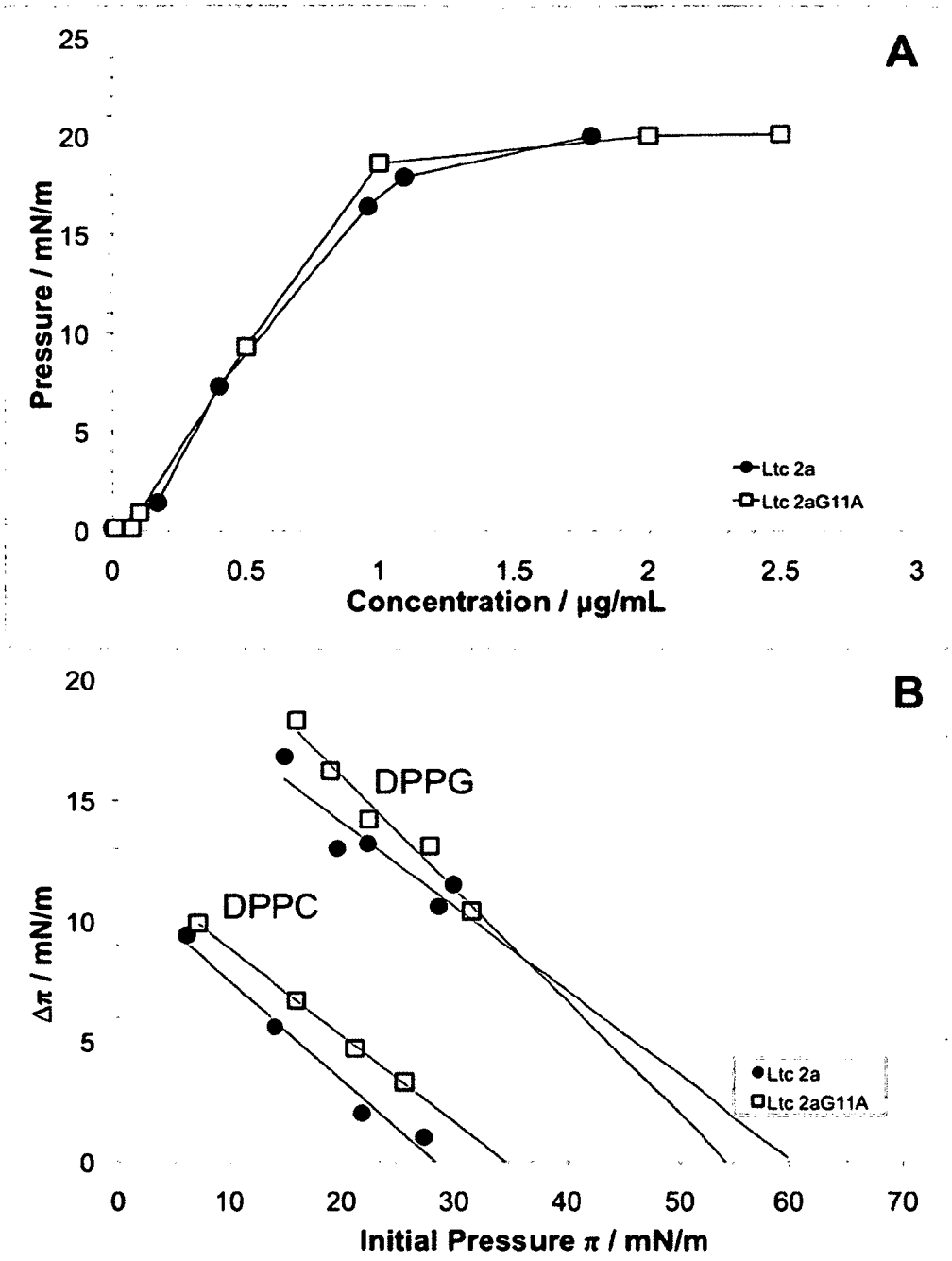

Figure 6.2: (A) Peptide induced variations of the surface pressure as a function of peptide concentration in the subphase for ltc2a derivatives. (B) Insertion of ltc2a derivatives into DPPC (left) and DPPG (right) monolayers. The surface pressure increase of the lipid monolayer ($\Delta\pi$) is presented as a function of the initial pressure (π_i). Extrapolation to zero $\Delta\pi$ gives the CPI. Peptide concentrations were 1.9 mg/ml (ltc2a) and 1.7 mg/ml (ltc2aG11A).

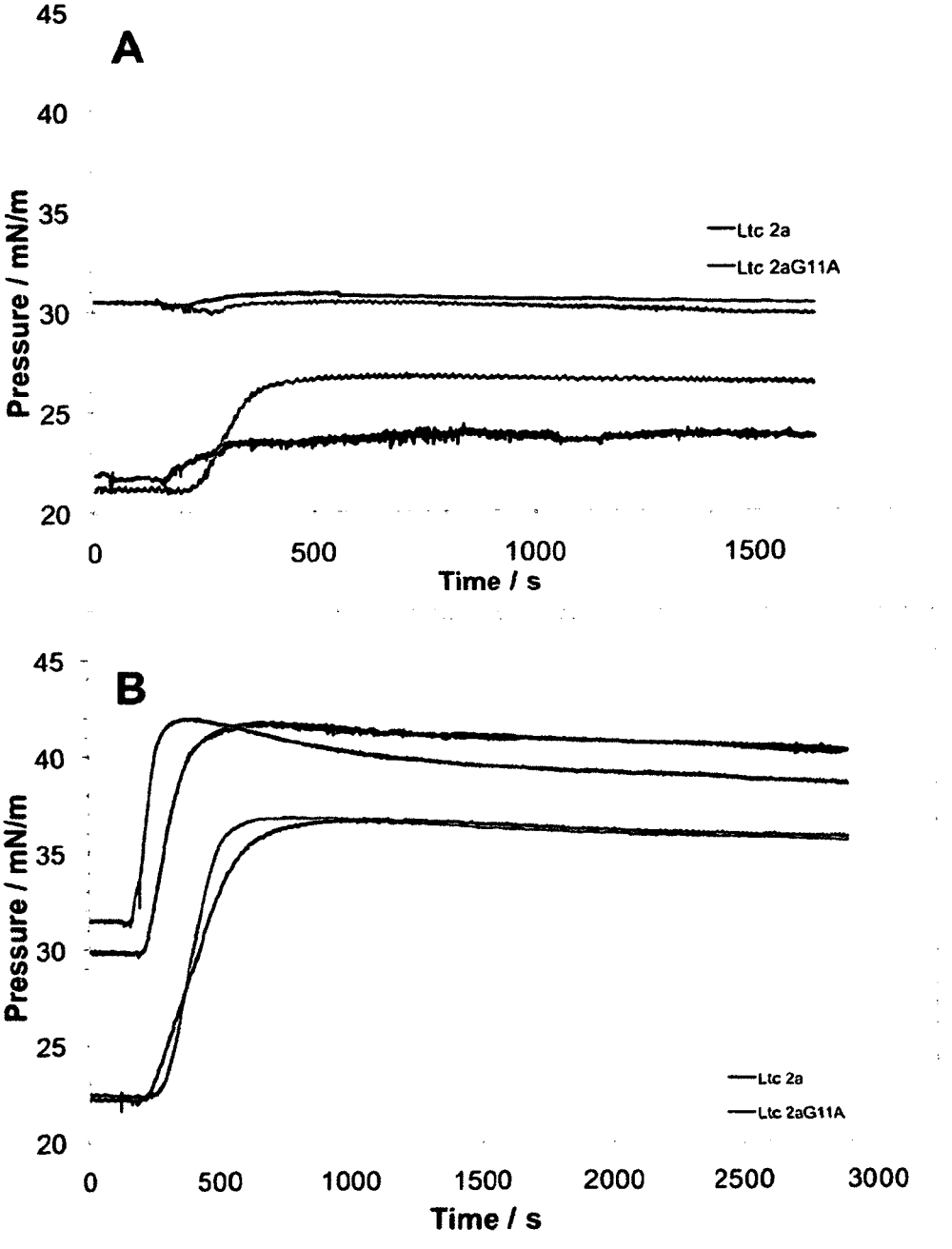

Figure 6.3: Kinetics of ltc2a derivatives inserting into (A) DPPC and (B) DPPG monolayers at different initial pressure. Peptide concentrations were 1.9 mg/ml (ltc2a) and 1.7 mg/ml (ltc2aG11A).

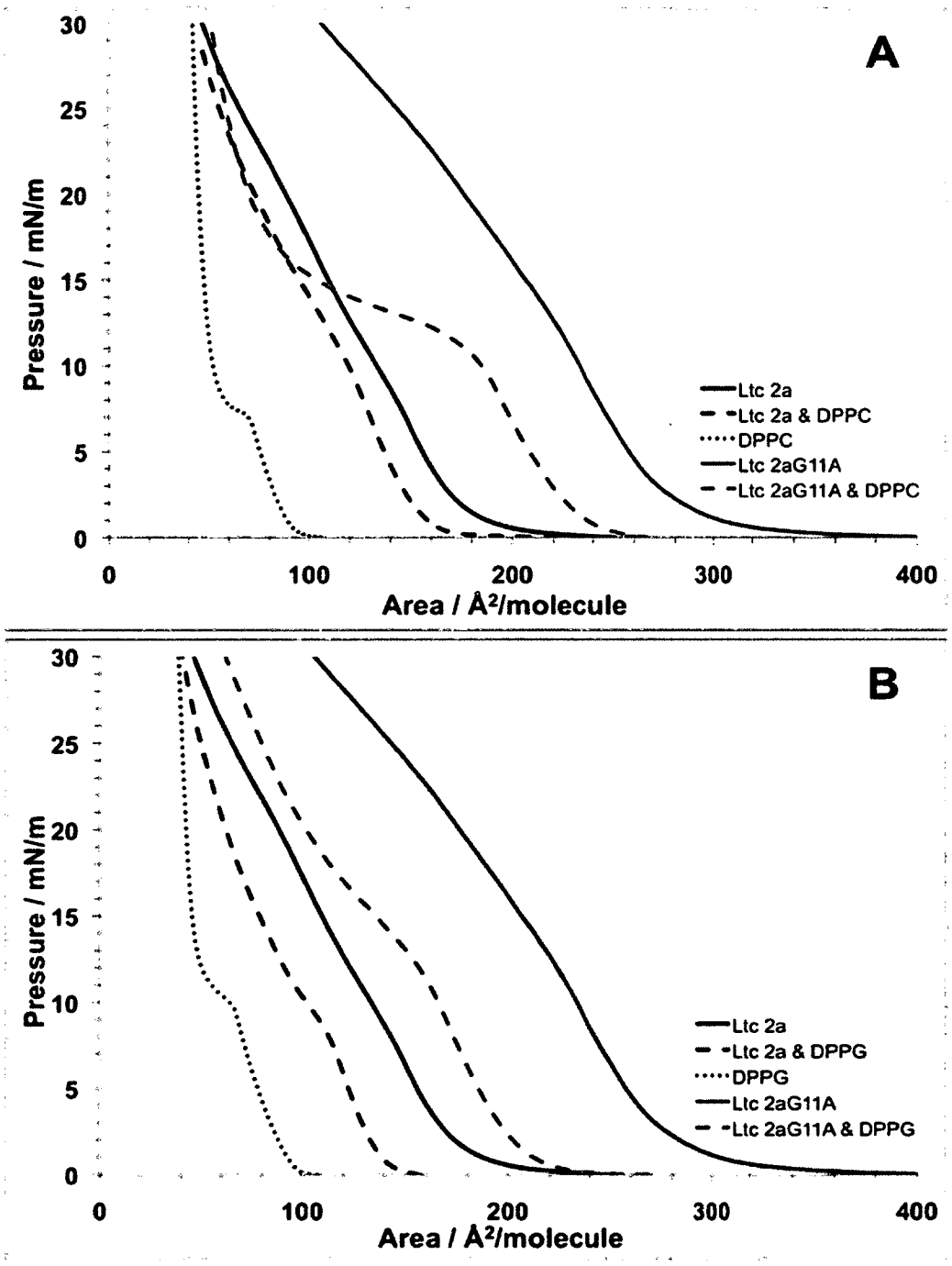

Figure 6.4: Compression isotherms for ltc2a derivatives and 50:50% molar ratio mixtures with (A) DPPC and (B) DPPG.

Areas occupied by the two helices of ltc2a are estimated to be around 190.0 $Å^2$ for the N-terminal helix and ~290 $Å^2$ for the C-terminal helix. The length of the N-terminal helix is closer to the measured area per single ltc2a molecule in the monolayer, 180 $Å^2$, thus suggesting that the peptide rearranges itself during the compression so that the N-terminal helix is parallel to the interface and the C-terminal is either pointing upwards to the air or downwards in the subphase. Such geometry, however, contradicts the proposed orientation of ltc2a observed in SDS micelles with NMR and MC simulation, where the C-terminal helix was found to be parallel to the interface.[4] Therefore, another orientation of ltc2a was suggested where the N-terminal helix is perpendicular to the interface and the C-terminal helix is tilted slightly to account for the smaller area. This orientation is also supported by the hydrophobicity gradient in the C-terminal helix, which should contribute to helix tilting.

The first compression isotherms for the 50/50 peptide/lipid molar ratio mixtures each showed a noticeable shoulder, suggesting either partial immiscibility or reorientation of the peptides during the compression (Fig 6.4, 6.5 C, D).[32] The area per molecule of the mixtures being smaller than the pure form and smaller area per molecule in the monolayer containing DPPG suggested preferential interactions of both peptides with DPPG.

Detailed investigations of the peptide/lipid interactions are usually supported by calculations of the free energy of mixing: the excess Gibbs free energy or the excess Helmholtz free energy.[21 33] In the case of latarcins and lipids 50/50 molar ratio mixtures, however, a hysteresis between the compression and expansion isotherm was observed with a decrease of area per molecule for all monolayer mixtures containing peptides (Fig

6.5 B-D) making the free energy of mixing calculation rather challenging. Stable monolayers composed of amphiphilic molecules exhibit little hysteresis, indicating similarity of organization and disorganization of molecules throughout different compression and decompression cycles as in the case of pure DPPC and DPPG (Fig 6.5 A).[34,35] The hysteresis appears when the monolayer is compressed above a pressure of around 20 mN/m, which is close to the CMC determined earlier. It appears that monolayers containing the peptides are not stable above pressures of ~20 mN/m.

Upon compression above a certain pressure, we observed not only a hysteresis but also the disappearance of certain features in the isotherms. For example, shoulders observed in the first compression no longer appeared in the second compression (Fig 6.5 C, D). The existence of a large hysteresis can sometimes be related to molecular reorganization, but it more often signals the loss of molecules from the air-water interface.[35,36] Comparison between the first compression and the corresponding expansion reveals that some of the peptide molecules were forced into the subphase during the compression.[37,38] In the course of the expansion, the peptide molecules can be reincorporated into the monolayer. However, the incomplete reincorporation can lead to a lower area per molecule on the second isotherm cycle as seen in latarcins and lipids 50/50 molar ratio mixture.[37,38]

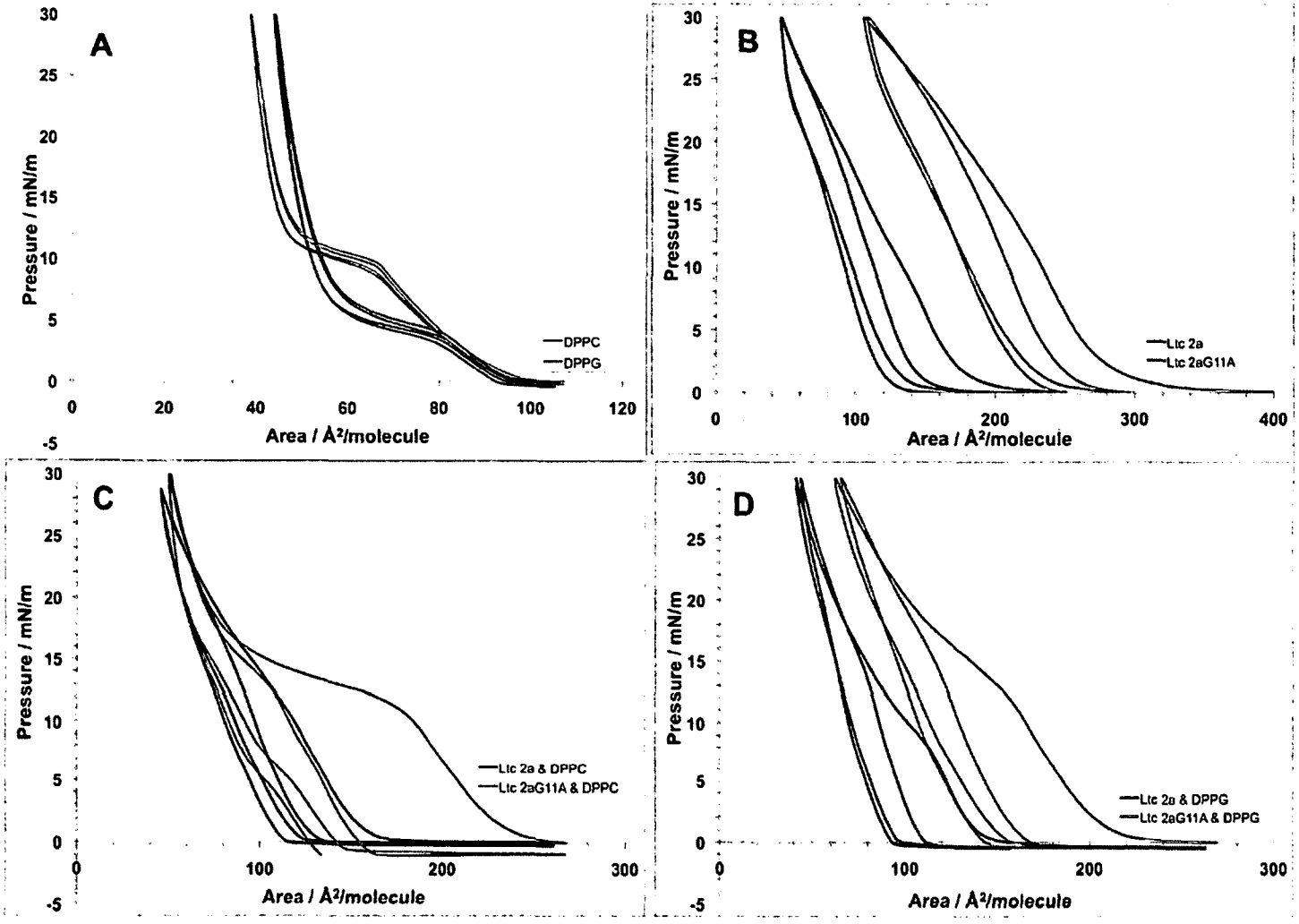

Figure 6.5: Compression and expansion isotherm cycles of (A) DPPC and DPPG, (B) ltc2a and ltc2a G11A, (C) DPPC and 50:50% molar ratio mixtures, and (D) DPPG and 50:50% molar ratio mixtures monolayers.

To probe the lateral organization of the two peptides in the absence and presence of lipid films, the monolayers were transferred onto mica for the topographies to be imaged by AFM. The peptide only monolayer did not reveal any aggregation of the peptides at the interface (Fig 6.6). However, there is a clear difference between peptides mixed with DPPC and DPPG (Fig 6.7). In the case of zwitterionic DPPC/peptide monolayers, we observed circular domains between 100 nm and 500 nm in diameter and 1.3 nm lower than in the rest of the sample (Fig 6.7 A, B). These domains are considerably smaller in size and height with ltc2aG11A as compared to ltc2a. In contrast, no clear circular domains can be detected in monolayers with DPPG (Fig 6.7 C, D). The monolayers are more homogeneous although some small clusters were observed. With DPPG, there was no significant difference between ltc2a and ltc2aG11A. Thus, AFM data indicated that both peptides mix better and prefer to interact with anionic DPPG than with zwitterionic DPPC, which is expected for cationic AMPs.

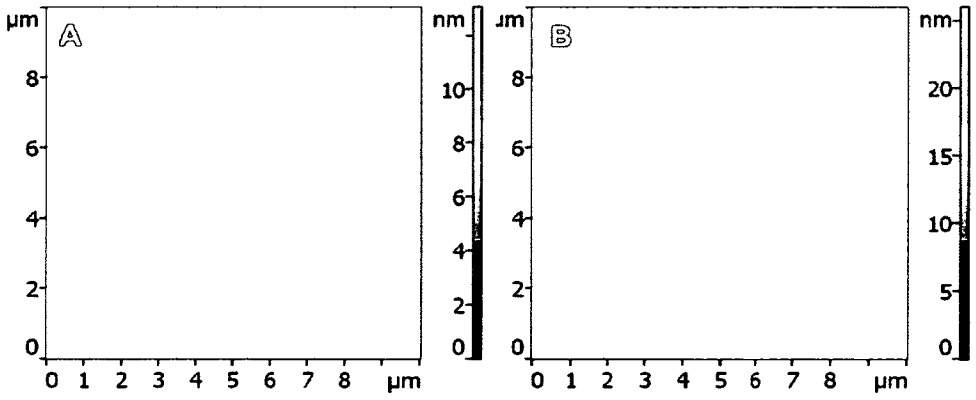

Figure 6.6: Selected AFM topography images of (A) ltc2a and (B) ltc2aG11A monolayer deposited at 30 mN/m.

To chemically identify the circular domains we further applied X-PEEM. Component maps and colour-coded composites showed that, as expected, anionic DPPG mixed homogeneously with cationic peptides (Fig 6.8). On the other hand, Fig 6.9 showed clear separation between the peptides and DPPC. The circular domains observed in AFM images were verified to be mainly composed of DPPC lipid whereas the surrounding area was mainly composed of the peptides. The difference in the size of the circular domains between the peptides can be attributed to a slightly higher affinity of peptide ltc2aG11A to the zwitterionic monolayer promoting the hydrophobic interactions with DPPC.

The length difference between a single DPPC or DPPG molecule (2.5 nm) and a single peptide (4.0 nm) corresponded well to the measured height difference between the peptides and lipid domains (1.3 nm). These measurements support the proposed peptides' orientation in the monolayers: with the N- and C-terminal helix of ltc2a perpendicular to the interface and slightly tilted, respectively, whereas the single helix ltc2aG11A is oriented ~65° to the interface.

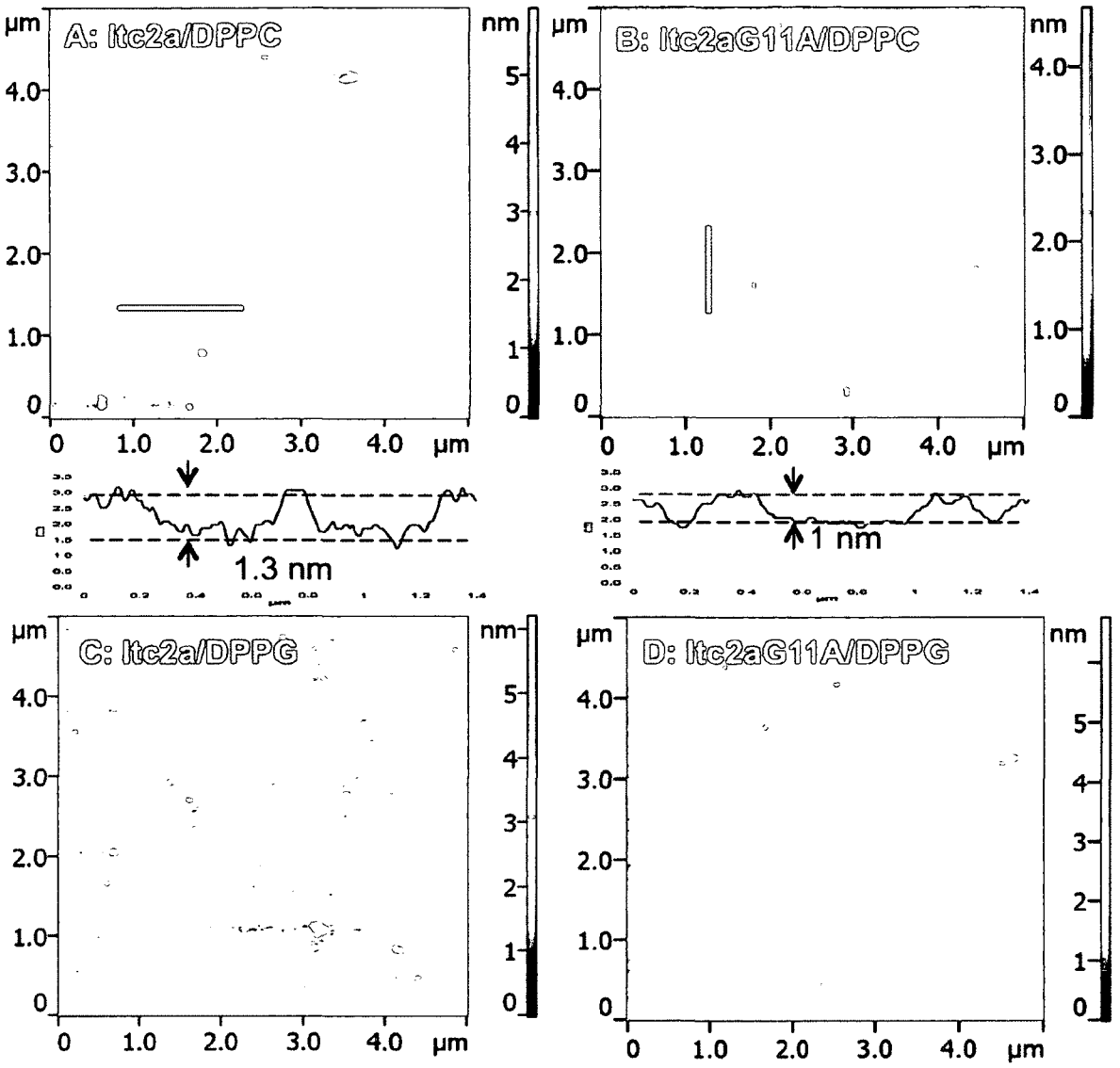

Figure 6.7: Selected AFM topography images and corresponding cross sections of 50:50% peptide/lipid molar ratio mixture monolayers deposited at 30 mN/m.

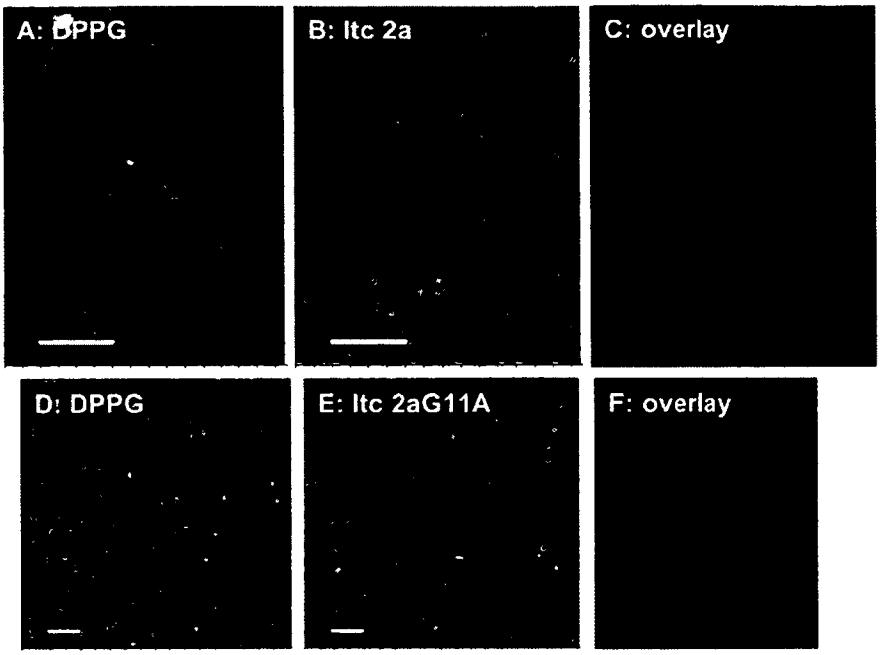

Figure 6.8: Selected X-PEEM images of (A-C) DPPG/ltc2a and (D-F) DPPG/ltc2a G11A 50/50 mol% mixtures. Scale bar is 5 mm.

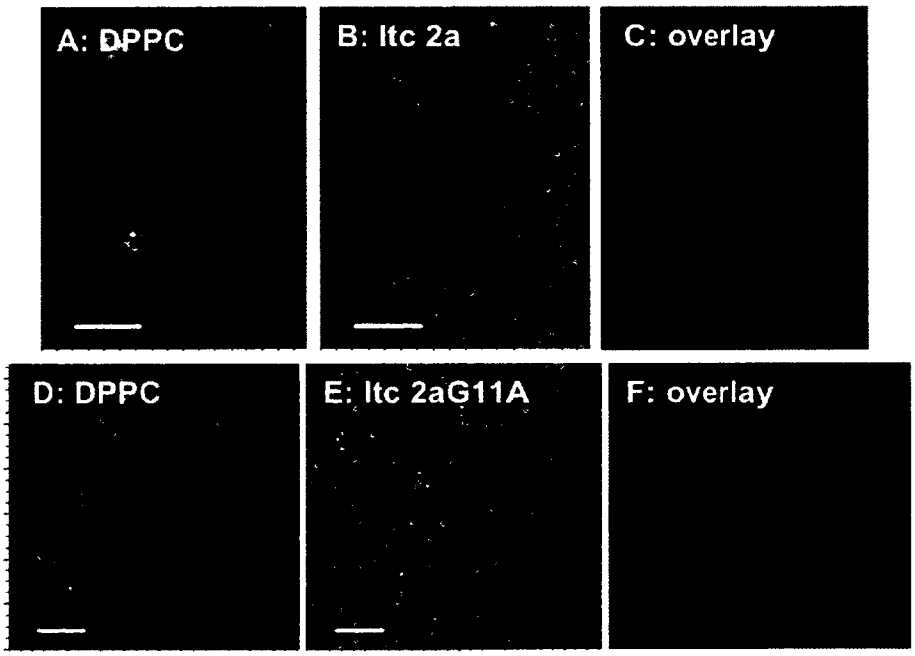

Figure 6.9: Selected X-PEEM images of (A-C) DPPC/ltc2a and (D-F) DPPC/ltc2a G11A 50:50 mol% mixtures. Scale bar is 5 mm.

6.2.3. Deletion of the hinge region does not affect membrane-rupturing activity

The membrane-rupturing activity of peptides was studied using the leakage assay. Both peptides were found to induce leakage on all seven model cell membranes used: DPPC, DPPG, mammalian, raft, *E. coli*, S. *aureus,* and *B. subtilis* model membranes. This was observed by an increase in fluorescence measured from the sample upon peptide addition, which infers fluorescent dye leakage from the ruptured lipid vesicles.

Moderate lytic activity to zwitterionic vesicles DPPC was observed for both peptides (Fig 6.10 A). This information is consistent with the relatively high hydrophobicity of the peptides and high hemolytic activity.[4-6] Surprisingly, both peptides were found to be less lytic towards DPPG than DPPC (Fig 6.10 B) as well as other types of vesicles studied, indicating that although electrostatic interactions are important for initial recognition and binding of latarcins to the cell membrane, hydrophobic interaction plays an important role in the lytic activity of peptides.

The mammalian model was chosen as a positive control, representative of human red blood cells, and the raft model was chosen to represent cancer cells, as cancer cells are more abundant in lipid rafts.[39,40] There was no notable difference between the activities of both peptides toward the raft model membrane (Fig 6.10 D). Yet, in comparison to the mammalian model, both peptides had greater lytic activity toward the raft model (Fig 6.10 C, D). This suggests that the presence of SM may have a stronger effect on the peptides activity than DOPE. As discussed later and observed in *in situ* AFM, SM promotes peptide aggregation and the formation of irreversible transmembrane pores, which could contribute to higher leakage in the raft model. At higher peptide/lipid ratios (>0.18), however, the rupturing activity of ltc2aG11A was greater than that of ltc2a

toward the mammalian model membrane. According to the scanning calorimetry and electron spin resonance results of Surewicz et al. three different, charged peptides altered the phase transition behavior of DMPC, leading to a transition point above and below the transition temperature of the lipid.[41,42] With increasing peptide concentration, the higher melting transition dominated which could increase the enthalpy of the transition.[41] It is possible that the peptide-lipid interaction brought about a similar alteration to the phase behavior of DOPC and lead to an increase in the enthalpy of the transition. Thus with more DOPC in the mammalian model membrane than in the raft, the potential for increase in enthalpy can lead to a more favourable peptide-lipid interaction. The combination of an increase in enthalpy, and ltc2aG11A being slightly more hydrophobic and having a greater CPI than ltc2a that was described earlier (section 6.2.1) could explain ltc2aG11A's greater activity toward the mammalian model than that of ltc2a at higher peptide/lipid concentrations.

When it comes to bacterial model membranes, the modified latarcin ltc2aG11A was found to be slightly more lytic to vesicles modeling Gram-positive bacteria *S. aureus* and *B. subtilis* membranes at lower peptide/lipid ratio but ltc2a was more lytic at higher peptide/lipid ratio — threshold values were 0.03 and 0.1 for *S. aureus* and *B. subtilis*, respectively (Fig 6.11 B, C). In the case of the Gram-negative bacteria *E. coli* model membrane, no difference in activity between the peptides was found until a threshold peptide/lipid ratio of 0.04, where ltc2aG11A became slightly more lytic (Fig 6.11 A). The peptide activity was found to correlate with the content of DOPE and/or CL; replacing glycine at position 11 with alanine does not lead to a decrease in amphipathicity but does result in a more rigid structure that interacts with zwitterionic model cell membranes

more efficiently, thus explaining higher activity (section 6.2.1). This was also shown with the peptide piscidin 1 when two glycines were replaced with alanines .[43] Thus suggesting that in addition to simple electrostatic interactions, local membrane curvature, fluidity and ability to form hydrogen bonds may play a considerable role in the activity of ltc2a.[44] The decreased leakage percentage in *S. aureus* and *B. subtilis* at a higher peptide/lipid ratio was found in previous studies.[45,46] This unusual quenching effect could be explained as the result of vesicle or dye aggregation in the presence of high peptide concentration.

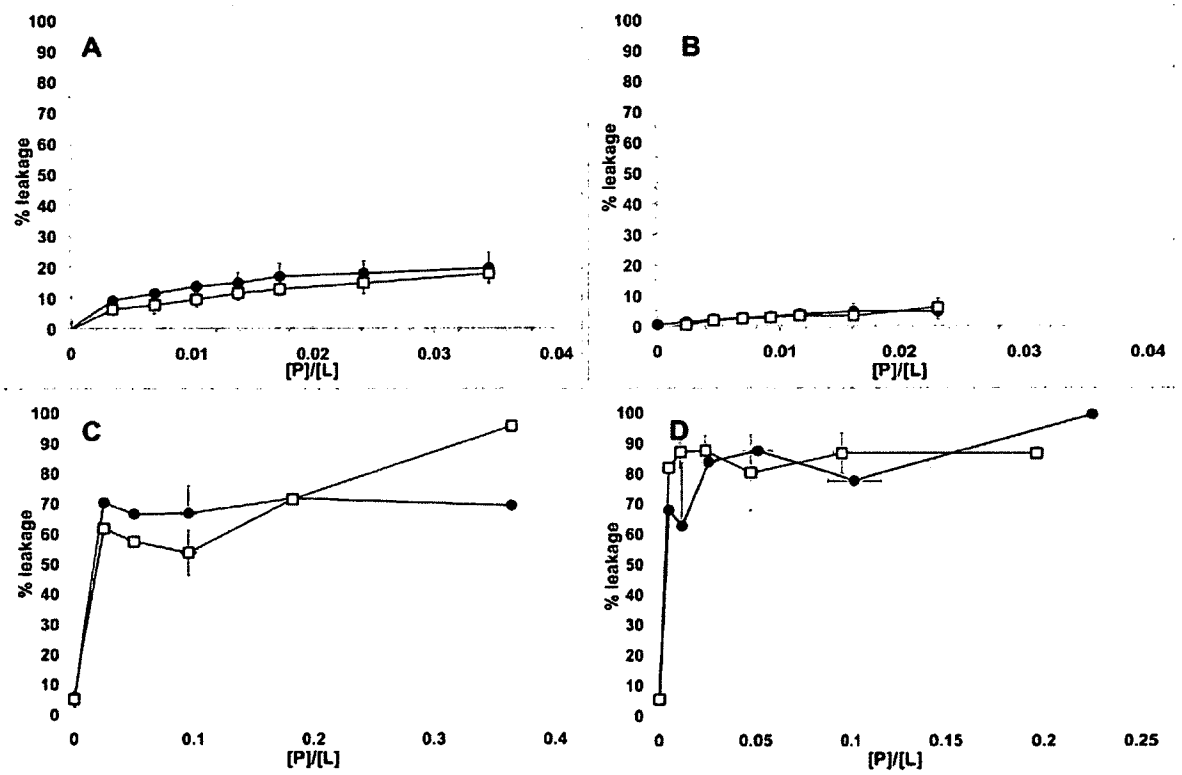

Figure 6. 10: CF fluorescence signal increase after the addition of ltc2a (solid circles) and ltc2a G11A (opened squares) in (A) DPPC, (B) DPPG, (C) mammalian model, and (D) raft model vesicles.

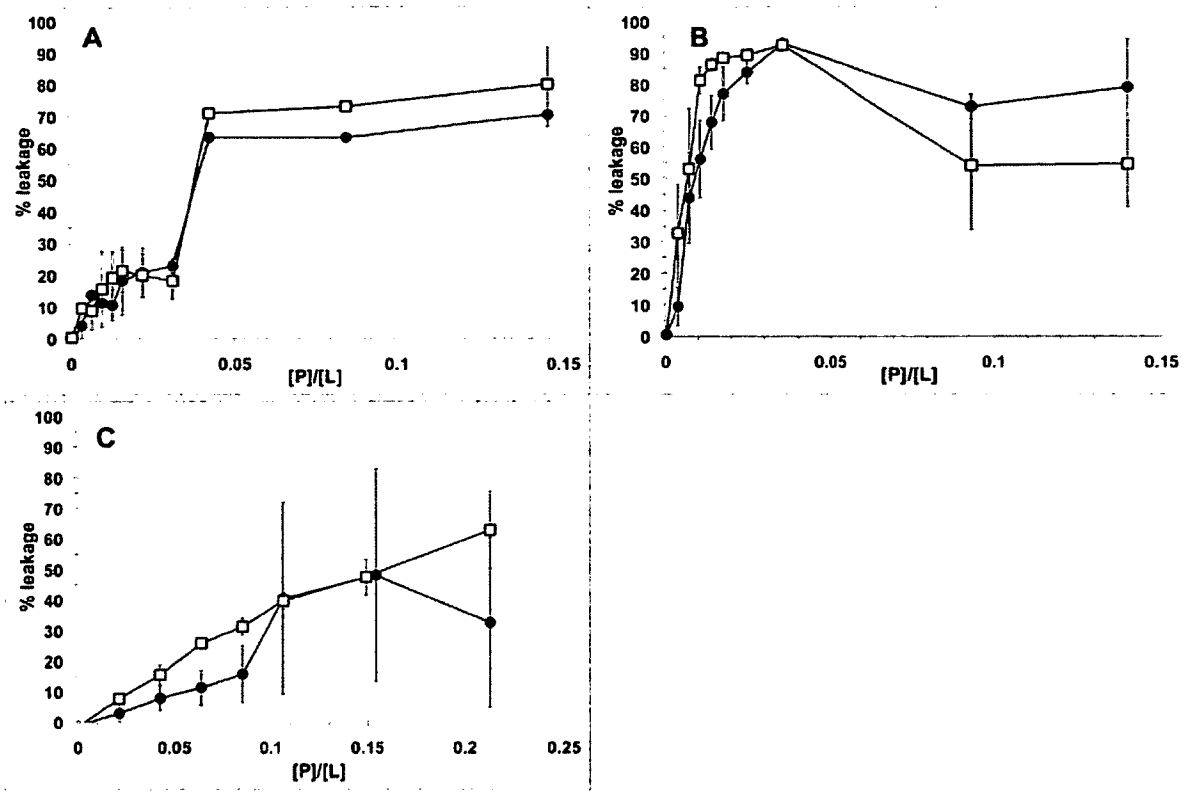

Figure 6. 11: CF fluorescence signal increase after the addition of ltc2a (solid circles) and ltc2a G11A (opened squares) in (A) *E. coli* model, (B) *S. aureus* model, and (C) *B. subtilis* model vesicles.

6.2.4 Supported lipid bilayers

6.2.4.1 Raft domains in supported lipid bilayers visualized by atomic force microscopy

Formation of microscale domains in the raft mixture has been extensively studied over the past decade. It is now well established that SM can form both inter- and intra-molecular hydrogen bonds with other lipids and Chol whereas PC lipid could only be the acceptor for hydrogen bonding.[47,48] In addition, intramolecular hydrogen bonding between SM molecules also limits the lateral diffusion and rotational motion of SM and indirectly strengthens the interaction with Chol.[49] Moreover, Chol preferentially interacts with SM and other sphingolipids due to their structure and the saturation of the

hydrocarbon chain.[51] As a result, when supported by freshly cleaved mica, SM/DOPC/Chol forms a phase separated SLB with SM and Chol in liquid ordered (L_o) phase that is 0.5 nm to 1 nm higher than DOPC in liquid disordered (L_d) phase (Fig 6.12).[47,51-54] The location and size of domains remain relatively constant over the 60 min period after the addition of 30 μL of deionized water or 150 mM NaCl solution. However the detergent resistant 5 nm domains were visualized after treatment with Triton X-100 at around 0.28 mM (Fig 6.12), consistent with previous studies.[52,55] Such SLBs therefore represent a convenient model to investigate the activity of various bioactive peptides, such as latarcins.

6.2.4.2 Peptides reduce line tension and reorganize morphology of the supported lipid bilayer

A number of studies have shown that peptides preferentially insert into loosely packed L_d phase rather than into L_o domains and change raft morphology.[53,56,57] For example, the addition of an antimicrobial peptide indolicidin and cell-penetrating peptide TAT remodeled raft SLBs (35 mol% SM/30 mol% Chol/35 mol% DOPC) by reducing the line tension and causing lipid association.[51] Binding and insertion of apoptosis regulator Bax-derived peptide to raft SLBs (DOPC/SM/Chol 1:1:0.67) released curvature stress at the domain interface with higher packing defects causing domain expansion.[56] The addition of a myristoylated cationic peptide for neuronal growth and plasticity NAP-22 caused the L_o domains to coalesce.[57]

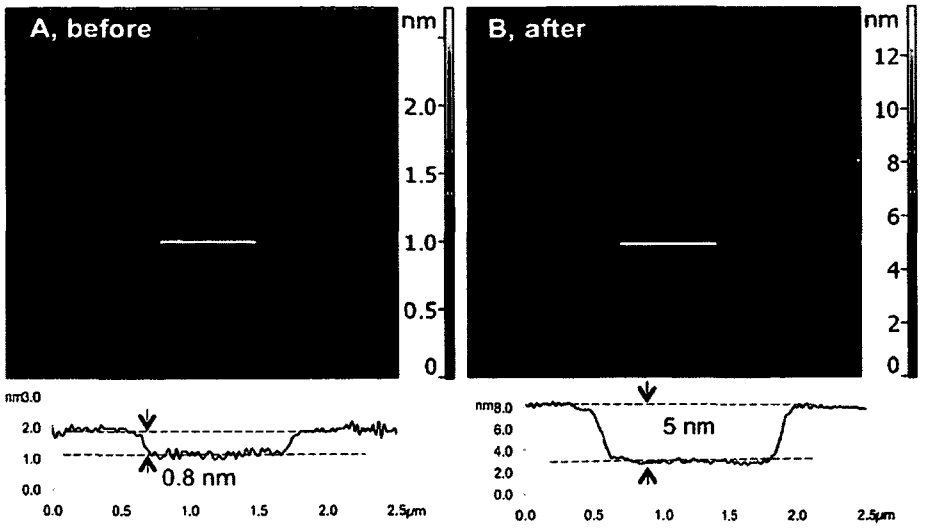

Figure 6.12: AFM images (10 × 10 μm^2) of raft SLBs composed of SM/DOPC/Chol 2:2:1 (A) before and (B) after the addition of 0.28 mM Triton X-100.

As ltc2a was shown to be toxic to human erythrocytes as well as to erythroleukemia K562 cells with EC_{50} values 3.4 μM and 3.3 μM, respectively, it can be considered an anticancer agent — under the class that is toxic to all cell types, including non-cancer mammalian cells.[2] The efficiency, however, should be enhanced by a larger surface area, higher fluidity, and the presence of anionic molecules (phosphatidylserine lipids and O-glycosylated mucins) of cancer cells.[57] The peptide demonstrated time and stage dependent erythrocyte membrane reorganization leading to the formation of pores 2 to 13 nm in diameter. In the case of cancer K562 cells, ltc2a insertion induced bleb formation and swelling accompanied by the formation of ~4 nm pores that then disintegrate the membrane.[2] Therefore, it was of interest to investigate the effect of both ltc2a derivatives on the raft SLBs.

The measurements were performed in deionized water and in 150 mM NaCl, since antimicrobial activity of some peptides was found to depend on salt concentration.[59-63]

Before peptide addition, raft SLBs contained small and circular L_o domains (Figs 6.13 to 6.16, A, E, and videos 1-8, initial frames) indicating presence of large line tension — the energy per unit length of the L_o boundary — which is the dominant factor among line tension, entropy, and electrostatic interaction.[64,65]

The peptide was then added to the SLB and sequential images were recorded. The first set of measurements was performed by incrementally increasing the peptide concentration in solution from 0.3 to 0.9 μM (Fig 6.13, 6.14, and videos 1-4). After the peptide addition, initially small aggregates or pores appeared in the L_d phase (Fig 6.14 B and F), subsequently L_o domains became irregular, expanded and coalesced (Figs. 6.13 D, G, Fig 6.14 C, F, and videos 1-4) suggesting the reduction of the line tension. The effect became more apparent with time and increasing peptide concentration. It also appeared that the morphology changes faster in deionized water (Figs 6.14 C, G, and video 2, 4) than in high salt medium (Figs 6.13 C, G, and video 1, 3) and for ltc2aG11A than for ltc2a. Association of the peptide caused an imbalance of uniformly distributed lipid molecules; therefore lipid bilayers reorganize to restore new equilibrium between the peptide and the lipid molecules.[51,66,67] Moreover, the inserted peptides increase positive curvature strain in the bilayers, which may facilitate more binding and insertion of peptides.

Bilayer morphology changes vary somewhat in high salt medium (150 mM NaCl). For example, in the case of ltc2aG11A, both cluster formation and disruption started from the L_d phase (Fig 6.14 F, G, and video 1) in deionized water but not in NaCl medium (Fig. 6.13 F, and video 3). It is known that NaCl compacts SLB with sodium ions tightly bound to the carbonyl oxygen of, on average, three lipid molecules.[66,68] This reversible

process has been observed in SLBs composed of various lipids such as PC, POPE, and *E. coli* lipid extract.[67] Previous studies have also showed that sodium ions strongly interact with the carbonyl oxygens in the peptide backbone and the carboxylate groups of amino acid side chains.[69,70] This decreases the hydrogen bonding of peptide with water and the peptide preferentially inserts into the hydrophobic environment. Thus in the presence of NaCl, peptides may deform, which can lead to the facilitation of complex formation with lipid molecules, followed by distortion and solubilization of SLBs.

Results of the present AFM experiments confirm membrane disintegration by ltc2a (Figs 6.13 D, H, Fig 6.14 G, and videos 1-4) observed before.[2] However no previously mentioned small pores were detected likely due to limitations of the AFM imaging.

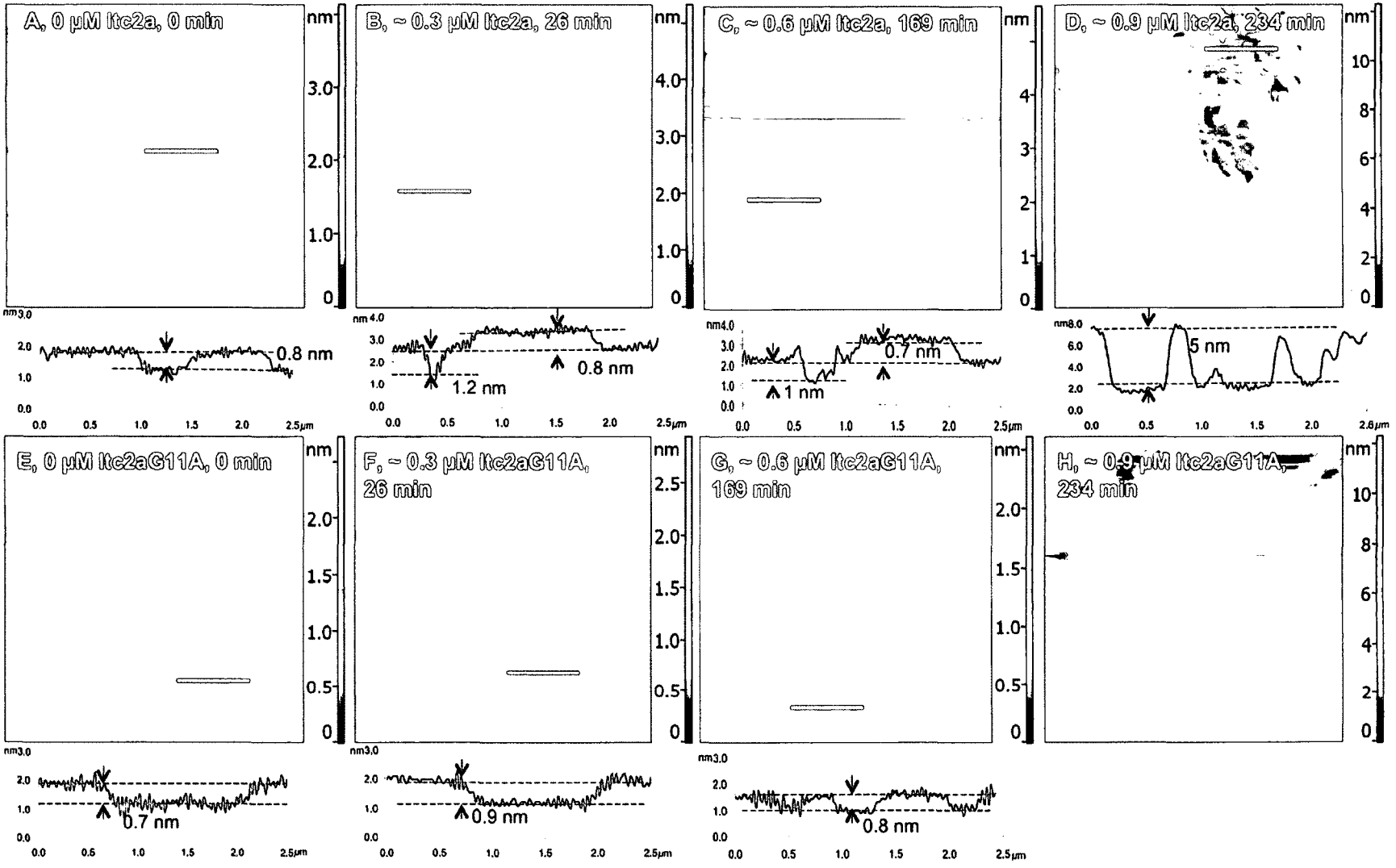

Figure 6.13: Representative AFM images (10 × 10 μm^2) of raft SLBs before and after the sequential addition of (A-D) Itc2a and (E-H) Itc2aG11A in 150 mM NaCl medium.

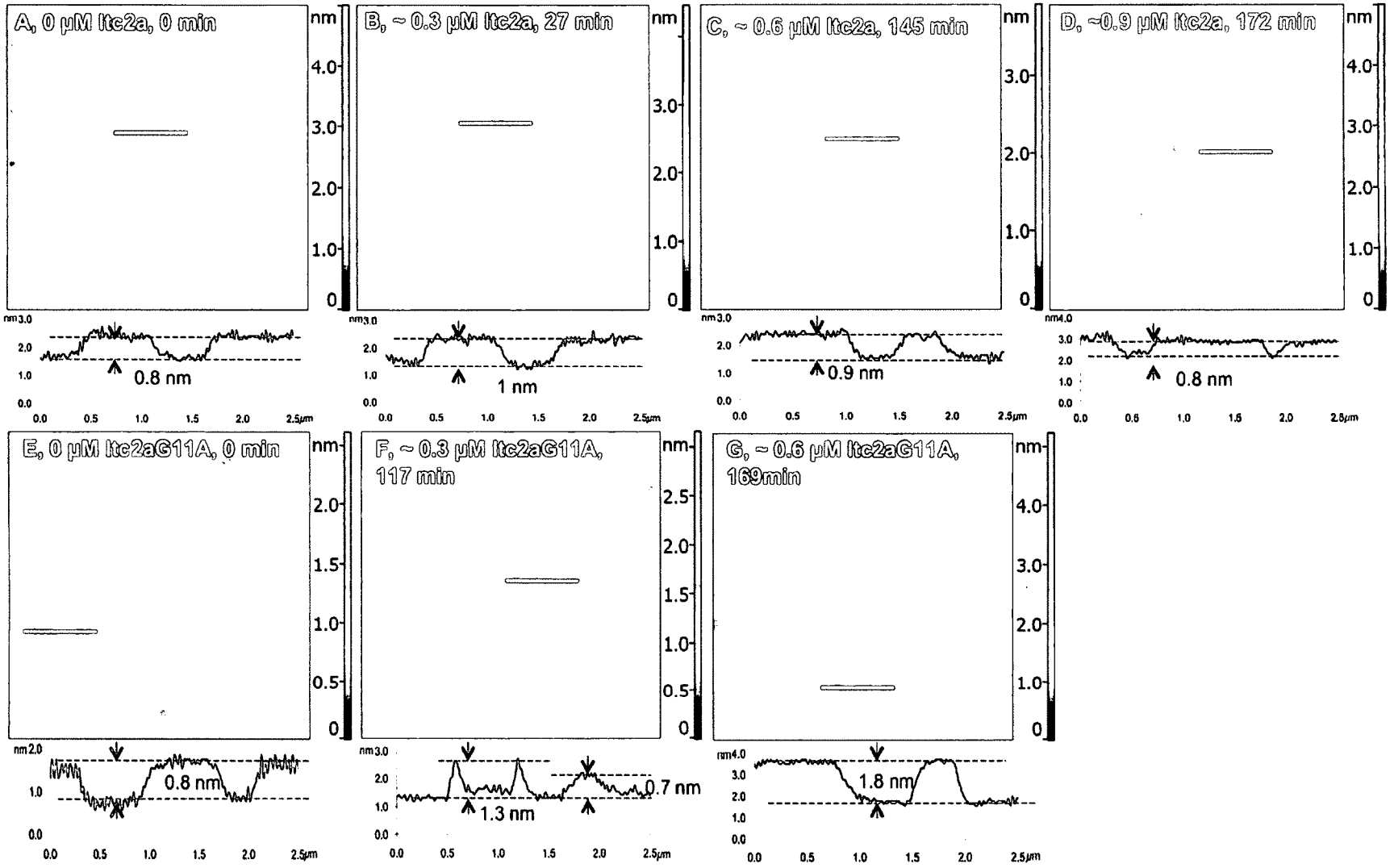

Figure 6. 14: Representative AFM images (10 × 10 μm^2) of raft SLBs before and after the sequential addition of (A-D) ltc2a and (E-G) ltc2aG11A in deionized water.

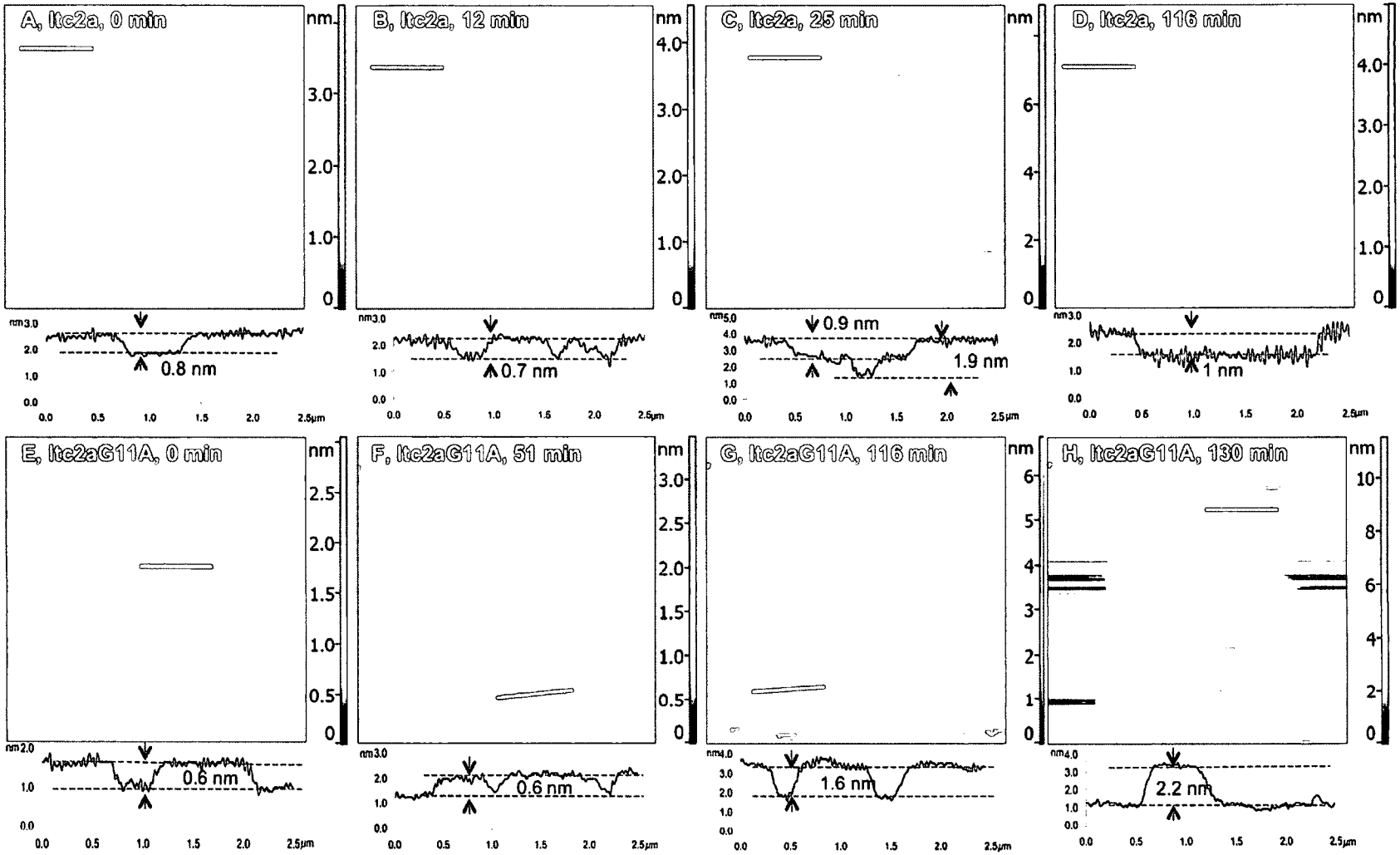

Figure 6.15: Representative AFM images (10 × 10 µm^2) of raft SLBs before and after the addition of (A-D) 0.6 µM Itc2a and (E-H) 0.6 µM Itc2aG11A in 150 mM NaCl medium. Time after the peptide addition as well as the concentration are indicated.

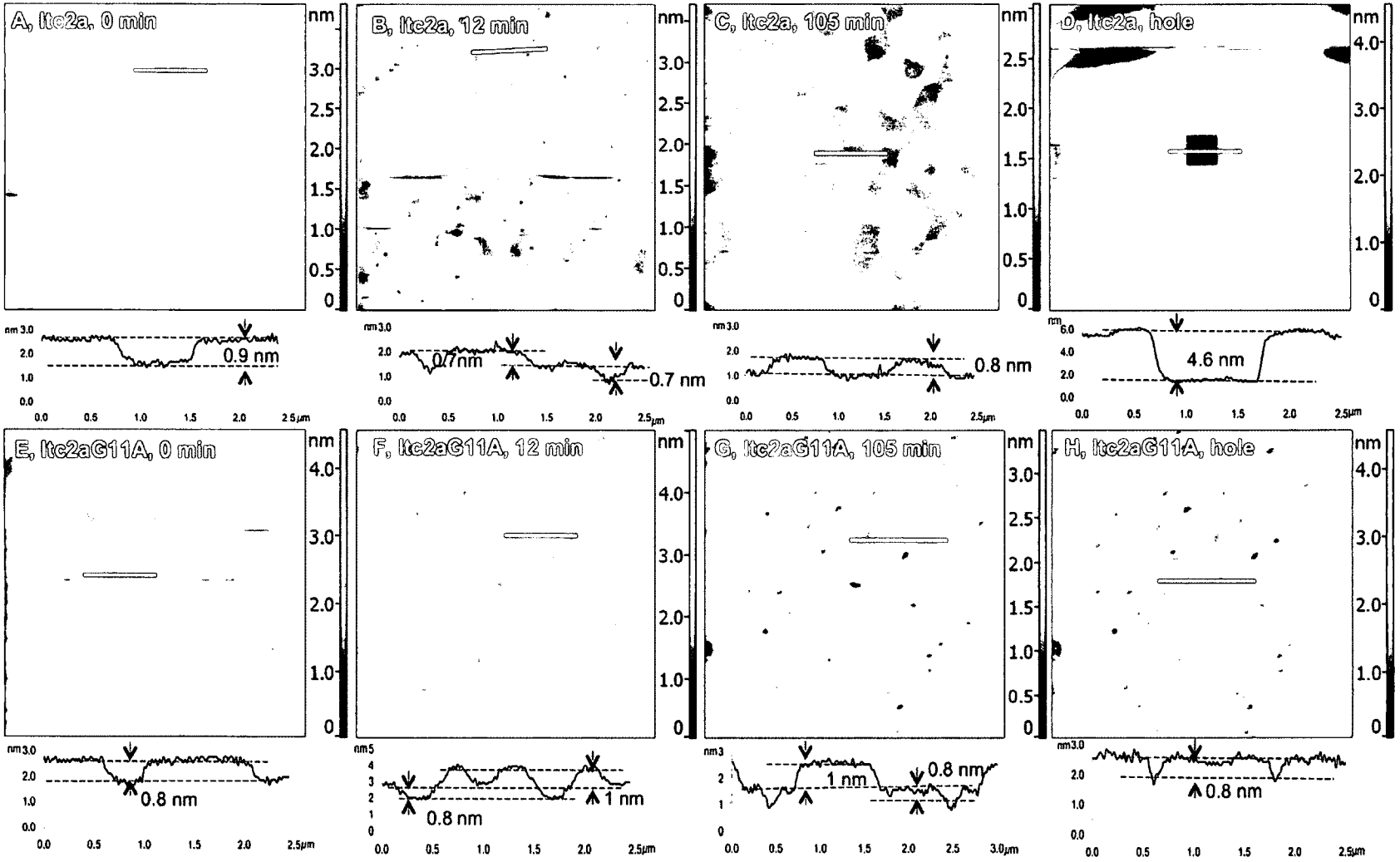

Figure 6.16: Representative AFM images (10 × 10 μm^2) of raft SLBs before and after the addition of (A-D) 0.6 μM ltc2a and (E-H) 0.6 μM ltc2aG11A in deionized water. Time after the peptide addition as well as the concentration are indicated.

6.2.4.3 Peptide oligomerization may contribute to the different mode of action

The second set of experiments was performed by adding the peptides to the bilayer in higher concentration (0.6 μM) (Fig 6.15, 6.16, and videos 5-8) to test the effect of potential latarcin oligomerization on the bilayer disruption. Such oligomerization was found to affect the selective binding of NAP-22 peptide to cholesterol rich domains.[71]

Upon the peptide addition, L_o domains expanded and coalesced both in NaCl (Fig 6.15, and videos 7, 8) and in deionized water (Fig 6.16, and videos 5, 6), similar to experiments with lower peptide concentrations. However, some differences between the two were observed.

In NaCl medium, ltc2a formed clusters in both L_o and L_d phases while the L_o phase expanded and coalesced around the clusters, followed by slow cluster dissociation and membrane solubilization (Fig 6.15 A-D, and video 8). A coarse-grained simulation study showed that magainin 2 induces spontaneous buckling and budding in DPPC bilayer system.[72] This was due to asymmetry of two leaflets after magainin 2 bound to the membrane, inducing positive curvature. The expanded and curved regions then eventually budded into vesicles. This may be the case for 0.6 μM ltc2a in the salt medium as the induced aggregates disappeared with time. It is also possible that repeated scanning of the same area contributed to the disappearance of the clusters. Without NaCl compacting SLBs, ltc2a formed defects and solubilized both L_d and L_o phases followed by slow L_o domain expansion and coalescence (Fig 6.16 A-C, and video 6). By scanning a 1×1 mm^2 area with high speed and high force, we were able to obtain a 5 nm deep hole for ltc2a/SLBs in deionized water indicating that ltc2a "freezes" the zwitterionic SLBs after peptide/lipid complex formation (Fig 6.16 D) as described by Polyansky et al.[3]

In comparison, ltc2aG11A in NaCl medium does not form pores or defects (Fig 6.15 E-H, and video 7), whereas in aqueous solution it immediately induced stable pore formation in L_d phase followed by rapid L_o domains expansion and coalescence (Fig 6.16 E-G, and video 5). It is qualitatively similar to the behavior of ltc2a in NaCl medium, although on a smaller scale. In the case of ltc2aG11A, the SLBs appeared to be more fluid as a 5 nm deep "hole" could not be obtained and was covered by expanded L_o phase (Fig 6.16 H).

In a separate set of experiments, morphologies of raft SLBs (DOPC/SM/Chol 1:1:1) were observed prior to and 30 mins subsequent to 0.6 μM peptide incubation in deionized water — instead of investigating *in situ* the morphology changes with peptide addition. Higher Chol content attributed to the larger size of L_o domains consistent with results of Sullan et al. (Fig 6.17 A).[47] Besides similar membrane reorganization and coalescence, comparable ltc2a-induced cluster formation and ltc2aG11A-induced stable pore formation were also observed (Fig 6.17 C-D). This corresponded to *in situ* experiments indicating morphology changes induced by ltc2a are independent of raft composition.

Thus, we observed that when the initial peptide concentration in solution is increased, some variations in the mechanism of action are detected suggesting potential initial peptide oligomerizaiton in solution followed by dissociation in a membrane.

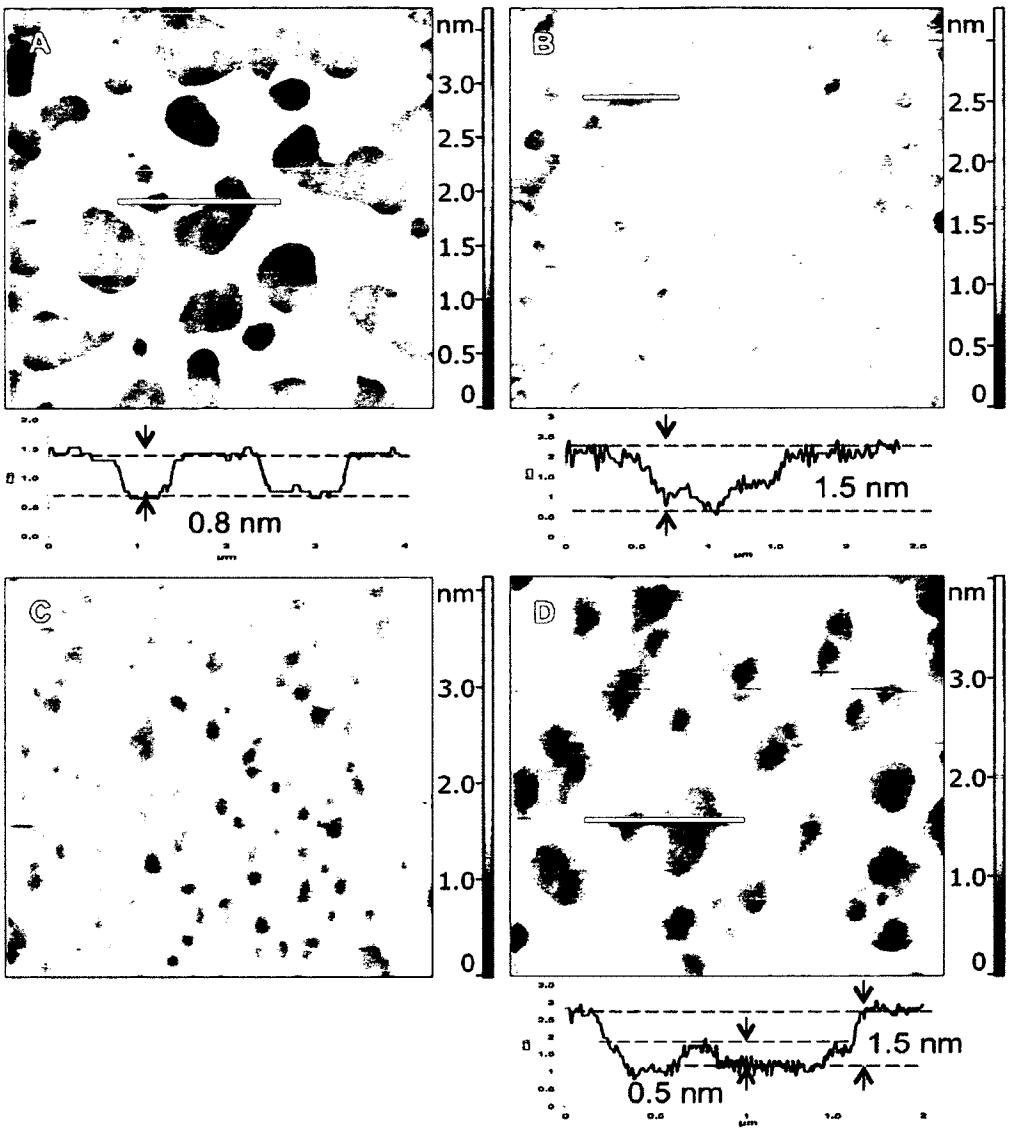

Figure 6.17: Representative AFM images (10 × 10 μm^2 expect 5 × 5 μm^2 for D) of raft SLBs (A) before and after the addition of (B) 0.6 μM ltc2a and (C, D) 0.6 μM ltc2aG11A in deionized water.

6.2.4.4 Ltc2aG11A induced membrane thinning

An interesting observation was made for ltc2aG11A. We detected the presence of nanometer-sized stable pores (50-100 nm) after the addition of ~ 0.6 μM ltc2aG11A to the raft SLBs in the deionized water *in situ* experiment (Fig 6.16 F–H, and video 5); and

submicron-sized pores in the 30 min incubation experiment (Fig 6.17 C, D). A reduction in the membrane thickness was also observed before complete membrane solubilization in all cases where SLBs were not rinsed with medium after peptide incubation (Fig 6.14 G, Fig 6.15 H, and video 1, 3, 7). After scanning a small area with high force for an extended period of time, for example following the Fig 6.14H image, we were unable to see any traces (unlike Figs. 6.16 D and H) suggesting that the lower phase is mica rather than the L_d phase of the lipid bilayer. Therefore, we concluded that after ltc2aG11A addition membrane thinning occurs followed by complete membrane solubilization.

The two-state model proposed by Huang suggests the incorporation of peptide into the outer leaflet of the membrane below the critical peptide/lipid ratio causes asymmetric area stretching and membrane thinning in a peptide concentration-dependent manner. Above the critical peptide/lipid ratio, peptides insert into lipid bilayers and induce pore formation while membrane thickness remains the same as before peptide addition.[73] The continuum theory described by Glaser et al. states that small metastable hydrophobic pores transition into large metastable hydrophilic pores after the critical radius and energy are reached, which then eventually leads to membrane rupture.[74] In the hydrophilic pores, lipid molecules reorient at the pore rim with the headgroups; on the other hand, lipid molecules remain in the lamellar orientation in order to allow small molecules to flow through in the hydrophobic pores.[74,75] We did not observe thickness reinstatement of SLBs prior to their solubilization by ltc2aG11A. However, 0.6 μM may be the threshold concentration for ltc2aG11A to induce metastable hydrophilic pores prior to membrane distintegration.

The thickness of the remaining L_o domains is in the range of 1.8 to 2.2 nm (Figs. 6.14 G, 6.15 H, and 6.17 D). This is more than the lipid head group (~0.9 nm) or a single helix (1.1 to 1.5 nm).[76,77] At the same time, it is less than a single monolayer of ~ 2.5 nm. Membrane thinning has been previously observed for various peptides: maganin 2, gramicidin, MSI-78, indolicidin, curcumin, and saposin C.[53,77-81] The underlying mechanism of peptide-induced membrane thinning includes membrane interdigitation, complex formation between a single leaflet and peptides, and peptide induced asymmetric bilayer formation by lipid flip-flopping.[54] It is unclear what mechanism is responsible for membrane thinning in the present study. However previous studies indicated membrane thickness to be 1.5 to 1.9 nm for interdigitated domains, suggesting this as the preferred mechanisms for ltc2aG11A.[78]

6.2.4.5 Cholesterol attenuated the effect of the peptides

Interactions between latarcins and bilayers composed of DOPC/SM 1:1 were investigated to observe the effect of Chol on ltc2a's activity. The morphology of the bilayer in the absence of peptide is similar to that observed previously.[82] When ltc2a was added in a final concentration of 0.6 μM, defects in the DOPC phase of the bilayer were observed (Fig 6.18 B). The size of the defects increased with time. SM domains coalesced and eventually were solubilized (Fig 6.18 C, D). In the case of ltc2aG11A, the peptide disrupted the DOPC/SM bilayer already at 0.3 μM. Chol is known to induce the formation of micrometer sized L_o phase domains with SM in the biological membrane. Previous studies have shown that Chol decreased the binding and insertion of some AMPs — and thus decreased their antimicrobial activities — even in the presence of

anionic lipids.[72,83,84] This could explain the disappearance of defects in raft SLBs (Fig 6.16B) while the defects in DOPC/SM SLBs formed and increased in size (Fig. 6.17 B). Bacterial membranes in the absence of sterols will be more susceptible to ltc2a, which demonstrates its antimicrobial activity.

6.2.4.6 Proposed mechanisms of action

The mechanisms of action of ltc2a and ltc2aG11A in NaCl medium and deionized water are proposed in Fig 6.19. Both peptides induce membrane reorganization through line tension reduction of L_o domains regardless of the imaging media — slower rate was observed in NaCl medium.

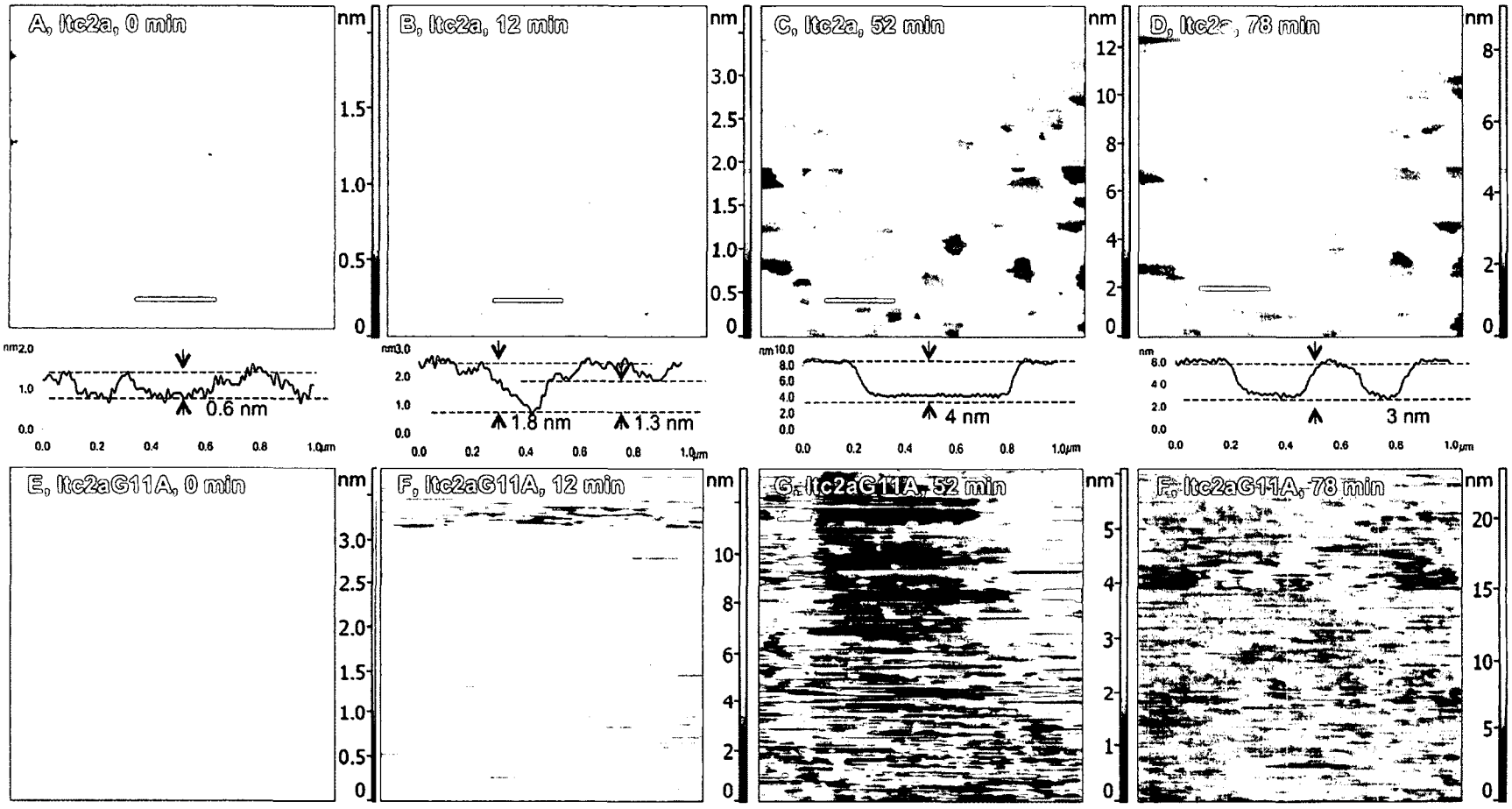

Figure 6.18: Representative AFM images (5 × 5 µm^2) of DOPC/SM 50/50 mol% SLBs before and after the addition of (A-D) 0.6 µM Itc2a and (E-H) 0.3 µM Itc2aG11A in deionized water. Time after the peptide addition as well as the concentration are indicated.

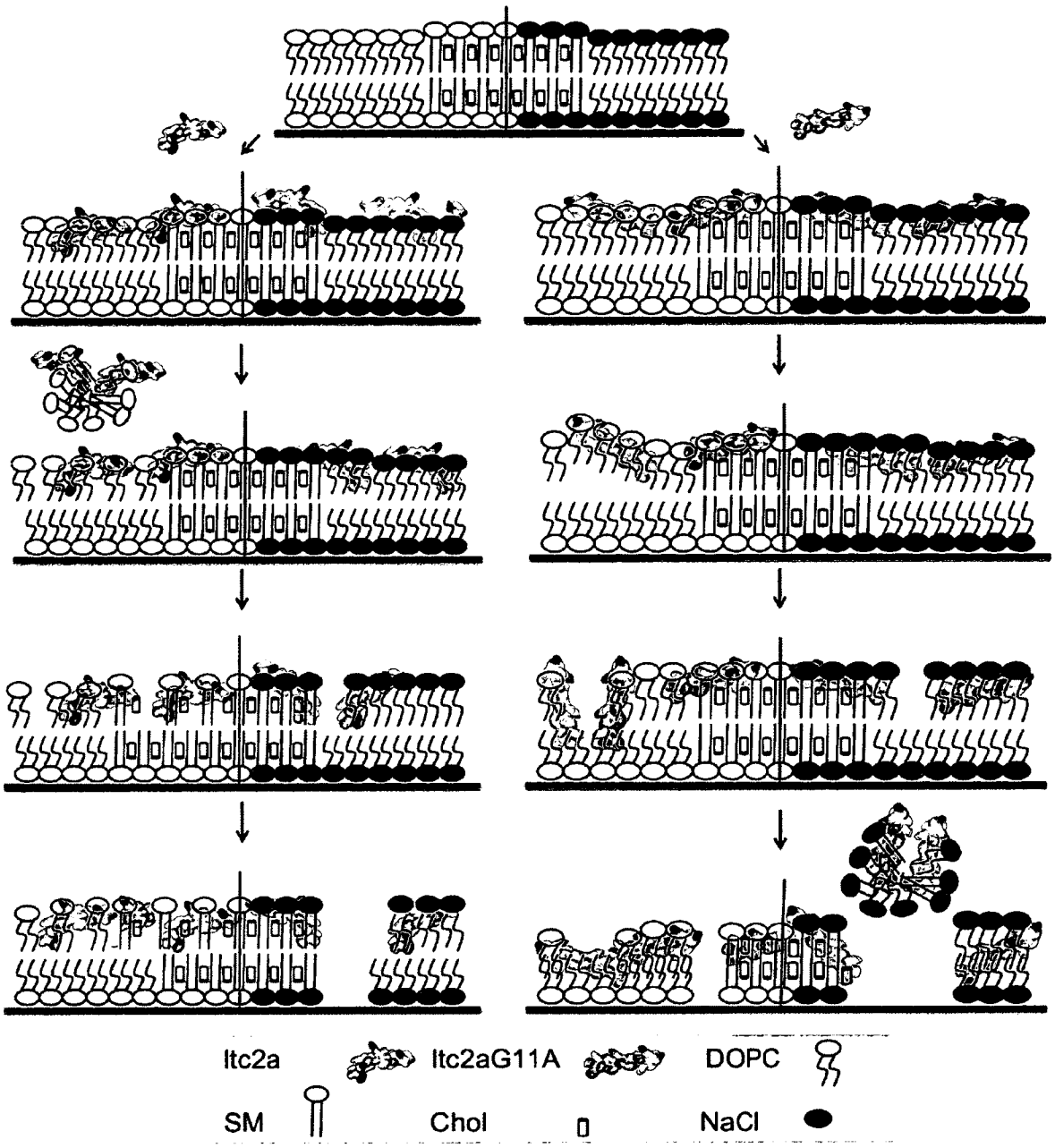

Figure 6.19: Proposed mechanisms of action of ltc2a (left) and ltc2aG11A (right) in deionized water (white head groups) and in 150 mM NaCl solution (blue head groups). Ltc2a solubilized both L_o and L_d phase after adsorbing SLBs in deionized water. Remaining ltc2a and lipid molecules reached the equilibrium as ltc2a reduced line tension and L_o domains increased in size. In NaCl solution, L_o domains also coalesced with addition of ltc2a, but followed by membrane disintegration. Ltc2aG11A induced coalescence of L_o domains in both deionized water and NaCl solution followed by or

alongside with membrane thinning. At a critical peptide concentration, ltc2aG11A may form stable sub-micron sized pores.

6.3 CONTRIBUTIONS

Special thanks to Grace Idiong on her 4908 work in monolayer measurements using LB and AFM; Annamaria Ruscito on her NSERC USRA work in CPI, CMC and most of the leakage assay investigations; Dr. Bonnie O. Leung and Dr. Adam Hitchcock in X-ray spectromicroscopy measurements.

6.4 REFERENCES

1) Kozlov, S.A.; Vassilevski, A.A.; Feofanov, A.B.; Surovoy, A.Y.; Karpunin, D.V.; Grishin, E.V. *J. Biol. Chem.* **2006**, *281*, 20983-20992.

2) Vorontsova, O.B.; Egorova, N.S.; Arseniev, A.S.; Feofanov, A.V. *Biochimie* **2011**, *93*, 227-241.

3) Polyansky, A.A.; Vassilevski, A.A.; Volynsky, P.E.; Vorontsova, O.V.; Samsonova, O.V.; Egorova, N.S.; Krylov, N.A.; Feofanov, A.V.; Arseniev, A.S.; Grishin, E.V.; Efremov, R.G. *FEBS letters* **2009** 583, 2425-2428.

4) Dubovskii, P.V.; Volynsky, P.E.; Polyansky, A.A; Chupin, V.V.; Efremov, R.G.; Arseniev, A.S. *Biochemistry* **2006**, *45*, 10759-10767.

5) Polyansky, A.A.; Volynsky, P.E.; Efremov, R.G. *J. Bioinform. Comput. Biol.* **2007**, *5*, 611-626.

6) Dubovskii, P.V.; Volynsky, P.E.; Polyansky, A.A.; Karpunin, D.V.; Chupin, V.V.; Efremov, R.G., Arseniev, A.S. *Biochemistry*. **2008**, *47*, 3525-3533.

7) Chakrabartty, A.; Baldwin, J. A.; Baldwin, R. L. *Nature*. **1991**, *351*, 586-588.

8) Melo, M.N.; Ferre R.; Castanho, M. *Nat. Rev. Microbiol.* **2009**, *7*, 245-250.

9) Oh, D.; Shin, S. Y.; Lee, S.; Kang, J. H.; Kim, S. D.; Ryu, P.D.; Hahm, K.; Kim, Y. *Biochemistry.* **2000**, *39*, 11855-11864.

10) Ibrahim, H.R.; Thomas, U.; Pellegrini, A. *J. Biol. Chem.* **2001**, *276*, 43767-43774.

11) Van Khan, E.J.M.; van der Bent, A.R.; Demel, R.; de Kruijff, B. *Biochemistry.* **2001**, *40*, 6398-6405.

12) Pukala, T.L.; Brinkworth, C.S.; Carver, J.A.; Bowie, J.H. *Biochemistry.* **2004**, *43*, 937-944.

13) Pukala, T.L.; Boland, M.P.; Gehman, J.D.; Kuhn-Nentwig, L.; Separovic, F.; Bowie, J.H. *Biochemistry.* **2007**, *46*, 3576-3585.

14) Lee, S.-A.; Kim, Y.K.; Lim, S.S.; Zhu, W.L.; Ko, W.; Shin, S.Y.; Hahm, K.-S.; Kim, Y. *Biochemistry.* **2007**, *46*, 3653-3663.

15) Li, S.-C.; Deber, C.M. *Nature Struct. Biol.* **1994**, *1*, 368-373.

16) Eisenberg, D.; Weiss, R.M.; Terwilliger, Wilcox, W. *Faraday Symp. Chem. Soc.* **1982**, *17*, 109-120.

17) Chakrabartty, A.; Baldwin, J.A.; Baldwin, R.L. *Nature*. **1991**, *351*, 586-588.

18) Rohl, C.A.; Fiori, W.; Baldwin, R.L. *Proc. Natl. Acad. Sci. USA*. **1999**, *96*, 3682-3687.

19) Okamoto, Y.; Hansmann, U.H.E. *J. Phys. Chem.* **1995**, *99*, 11276–11287.

20) Javadpour, M.M.; Eilers, M.; Groesbeek, M.; Smith, S.O. *Biophys. J.* **1999**, *77*, 1609-1618.

21) Maget-Dana, R. *Biochim. Biophys. Acta – Biomembranes.* **1999**, *1462*, 109-140.

22) Brockman, H. *Curr. Opin. Struct. Biol.* **1999**, *9*, 438-443.

23) Eiriksdottir, E.; Konate, K.; Langel, U.; Divita, G.; Deshayes, S. *Biochim. Biophys. Acta.– Biomembranes.* **2010**, *1798*, 1119-1128.

24) Ingenito, E.P.; Mark L.; Morris, J.; Espinosa F.F.; Kamm, R.D.; Johnson, M. *J. Apply Physiol.* **1999**, *86*, 1702-1714

25) Ambroggio, E.E.; Separovic, F.; Bowie, J.; Fidelio, G.D. *Biochim. Biophy. Acta – Biomembranes.* **2004**, *1664*, 31-37.

26) Ohe, C.; Ida, Y.; Matsumoto, S.; Sasaki, T.; Goto, Y.; Noi, M.; Tsurumaru, T.; Itoh, K. *J. Phys. Chem. B.* **2004**, *108*, 18081-18087.

27) Mansour, H.; Wang, D.; Chen, C.; Zografi, G. *Langmuir.* **2001**, *17*, 6622-6632.

28) Kim, K.; Kim, C.; Byun, Y. *Langmuir.* **2001**, *17*, 5066-5070.

29) Vollhardt, D.; Fainerman, V.B.; Siegel, S. *J. Phys. Chem. B.* **2000**, *104*, 4115-4121.

30) Oishi, Y.; Takashima, Y.; Suehiro, K.; Kajiyama, T. *Langmuir.* **1997**, *13*, 2527-2532.

31) Won, A.; Ianoul, A. *Biochim. Biophys. Acta – Biomembranes.* **2009**, *1788*, 2277-2283.

32) Nakorn, P.N.; Meyer, M.C.; Flach, C.R.; Mendelson, R.; Galla, H.-J. *Eur. Biophys. J.* **2007**, *36*, 477-489.

33) Feng, S.-S.; Gong, K.; Chew, J. *Langmuir* **2002**, *18*, 4061-4070.

34) Nakahara, H.; Lee, S.; Sugihara, G.; Shibata, O. *Langmuir.* **2006**, *22*, 5792-5803.

35) Constantino, C. J. L.; Dhanabalan, A.; Oliveira, O. N. *Rev. Sci. Instrum.* **1999**, *70*, 3674-3680.

36) Pascholati, C.P.; Lopera, E.P.; Pavinatto, F.J.; Caseli, L.; Nobre, T.M.; Zaniquelli, M.E.D.; Viitala, T.; D'Silva, C.; Oliveira Jr., O. N. *Colloids Surf., B* **2009**, *74*, 504-510.

37) Majerowicz, M.; Waring, A.J.; Wen, S.; Bringezu, F. *J. Phys. Chem. B.* **2007**, *111*, 3813-3821.

38) Miñones Jr., J.; Dynarowicz-Latka, P.; Minones, J.; Rodrigez Patino, J.M.; Iribarnegaray, E. *J. Colloid Interface Sci.* **2003**, *265*, 380-385.

39) Churchward, M.A.; Rogasevskaia, T.; Brandman, D.M.; Khosravani, H.; Nava, P.; Atkinson, J.K.; Coorssen, J.R. *Biophys. J.* **2008**, *94*, 3976-3986.

40) Li, Y.C.; Park, M.J.; Ye, S.-K.; Kim, C.-W.; Kim, Y.-N. *Am. J. Pathol.* **2006**, *168*, 1107-1118.

41) Surewicz, W.K.; Epand, R.M. *Biochemistry*, **1985**, *13*, 3135–3144.

42) Giragossian, C.; Schaschke, N.; Moroder, L.; Mierke D.F. *Biochemistry*, **2004**, *43*, 2724-2731.

43) Lee, S.-A.; Kim, Y.K.; Lim, S.S.; Zhu, W.L.; Ko, W.; Shin, S.Y.; Hahm, K.-S.; Kim, Y. *Biochemistry*, **2007**, *46*, 3653-3663.

44) Domenech, O.; Francius, G.; Tulkens, P.M.; Van Bambeke, F.; Dufrene, Y.; Mingeot-Leclercq, M.P. *Biochim. Biophys. Acta. – Biomembranes.* **2009**, *1788*, 1832-1840.

45) Magzoub, M.; Oglecka, K.; Pramanik, A.; Eriksson, L.E.G.; Graslund, A. *Biochim. Biophys. Acta*, **2005**, *1716*, 126-136.

46) Mileykovskaya, E.; Dowhan, W. *Biochim. Biophy. Acta*, **2009**, *1788*, 2084-2091.

47) Sullan, R.M.A.; Li, J.K.; Hao, C., Walker, G.C.; Zou, S. *Biophys. J.* **2010**, *99*, 507-516.

48) Lonnfors, M.; Doux, J.P.F.; Killian, J.A.; Nuholm, T.K.M.; Slotte, J.P. *Biophys. J.* **2001**, *100*, 2633-2641.

49) Won, A.; Ianoul, A. *Biochim. Biophys. Acta –Biomembrane,* **2009**, *1788*, 2277–2283.

50) Chen, P.S.; Toribara, T.Y.; Warner Jr., H. *Anal. Chem.* **1956**, *28*, 1756-1758.

51) Pike, L. J. *J. Lipid Res.* **2009**, *50*, S323.

52) Rinia, H.A.; Snel, M.M.E.; van der Eerden, J.P.J.M.; de Kruijff, B. *FEBS Lett.* **2001**, *501*, 92-96.

53) Shaw, J.E.; Epand, R.F.; Hsu, J.C.Y.; Mo, G.C.H.; Epand, R.M.; Yip, C.M. *J. Struct. Biol.* **2008**, *162*, 121-138.

54) Shaw, J.E.; Alattia, J.-R.; Berity, J.E.; Prive, G.G.; Yip, C.M. *J. Struct. Biol* **2006**, **154**, 42-58.

55) El Kirat, K.; Morandat, S. *Biochim. Biophys. Acta - Biomembrane*, **2007**, *1768*, 2300-2309.

56) Garcia-Saez, A.J.; Chiantia, S.; Salgado, J.; Schwille, P. *Biophys. J.* **2007**, *93,* 103-112.

57) Puench, P.-H.; Borghi, N.; Karatekin, E.; Brochard-Wyart, F. *Phys. Rev. Lett.* **2003**, *90*, 128304-.

58) Li, Y.C.; Park, M.J.; Ye, S.-K.; Kim, C.-W.; Kin, Y.-N. *Am. J. Pathol.*, **2006**, *168*,1107-1118.

59) Konno K.; Hisada M.; Fontana R.; Lorenzi C.; Naoki H.; Itagaki Y.; Miwa A.; Kawai N.; Nakata Y.; Yasuhara T.; Neto J.R.; Azevedo W.F.; Palma M.S.; Nakajima T. *Biochim. Biophys. Acta*, **2001**, *1550*, 70-80.

60) Tuner, J.; Yoon, C.; Nhu-Nguyen, D.; Waring, A.J.; Robert, L.I. *Antimicrob. Agents Chemother.* **1988**, *42*, 2206-2214.

61) Tam, J.P.; Lu, Y.-A.; Yang, J.-L.; Chiu, K.-W. *Proc. Natl. Acad. Sci. USA*. **1999**, *96*, 8913-8918.

62) Travis, S.M.; Anderson, N.N.; Forsyth, W.R.; Espiritu, C.; Conway, B.D.; Greenberg, E.P.; McCray, P.B. Jr.; Lehrer, R.I.; Welsh, M.J.; Tack, B.F. *Infect. Immun.* **2000**, *68*, 2748-2755.

63) Friedrich, C.; Scott, M.G.; Karunaratne, N.; Yan, H.; Hancock, R.E.W. *Antimicrob. Agents Chemother.* **1999**, *43*, 1542-1548.

64) Kuzmin, P.I.; Akimov, S.A.; Chizmadzhev, Y.A.; Zimmerberg, J.; Cohen, F.S. *Biophys. J.* **2005**, *88*, 1120-1133.

65) Garcia-Saez, A.J.; Chiantia, S.; Schwille, P. *J. Biol. Chem.* **2007**, *282*, 33537-33544.

66) Oncins, G.; Garcia-Manyes, S.; Sanz, F. *Langmuir* **2005**, *21*, 7373-7379.

67) Garcia-Manyes, S.; Oncins, G.; Sanz, F. *Biophys. J.*, **2005**, *89*, 1812-1826.

68) Bockmann, R.A.; Hac, A.; Heimburg, T.; Grubmuller, H. *Biophys. J.*, **2003**, *85*, 1647-1655.

69) Aziz, E. G.; Ottosson, N.; Eisebitt, S.; Eberhardt, W.; Jagoda-Cwiklik, B.; Vacha, R.; Jungwirth, P.; Winter, B. *J. Phys. Chem. B* **2008**, *112*, 12567-12570.

70) Kalcher, I.; Horinek, D.; Netz, R.R.; Dzubiella, J. *J. Phys. Condens. Matter* **2009**, *21*, 424108-.

71) Shaw, J.E.; Epand, R.F.; Sinnathamby, K.; Li, Z.; Bittman, R.; Yip, C.M. *J. Struct. Biol.* **2006**, *155*, 458-469.

72) Mason, A.J.; Arnaud, M.; Burkhard, B. *Biophys. J.* **2007**, *93*, 4289-4299.

73) Huang, H.W. *Biochim. Biophys. Acta* **2006**, *1758*, 1292 -1302.

74) Glaser, R.W.; Leikin, S.K.; Chernomordik, L.V.; Pastushenko, V.F.; Sokirko, A.I. *Biochim. Biophys. Acta* **1988**, *940*, 275-287.

75) Fuertes, G.; Gimenez, D.; Esteban-Martin, S.; Samchez-Munoz, O.L.; Salgado, J. *Eur. Biophys. J.* **2011**, *40*, 399 - 415.

76) Idiong, G.; Won, A.; Ruscito, A.; Leung, B.O.; Hitchcock, A.P.; Ianoul, A. *Euro. Biophys. J.* **2011**, *40*, 1087-1100.

77) Mecke, A.; Lee, D.-K.; Ramamoorthy, A.; Orr, B.G.; Holl, M.M.B. *Biophys. J.* **2005**, *89*, 4043-4050.

78) You, H.X.; Qi, X.; Grabowski, G.A.; Yu, L. *Biophys. J.* **2003**, *84*, 2043-2057.

79) Huang, W.-C., Chen, F.Y.; Lee, C.-C.; Sun, Y.; Lee, M.-T.; Huang, H.W. *Biophys. J.* **2008**, *94*, 4331-4338.

80) Huang, H.W. *Biophys. J.* **1986**, *50*, 1061-1070.

81) Ludtke, S.; He, K.; Huang, H.W. *Biochemistry* **1995**, *34*, 16764-16769.

82) Rinia, H.A.; de Kruiff B. *FEBS Lett.* **2001**, *504*, 194-199.

83) Prenner, E.J.; Lewis, R.A.N.; Jelokhani-Niaraki, M.; Hodges, R.S.; McElhaney, R.N. *Biochim. Biophys. Acta* **2001**, *1510*, 83-92.

84) Nicol, F.; Nir, S.; Szoka Jr., F.C. *Biophys. J.* **1996**, *71*, 3288-3301.

CHAPTER 7 CONCLUSIONS AND FURTHER DIRECTION

7.1 CONCLUSIONS AND IMPLICATION

This thesis provides further evidence and insight as to how minute alterations — such as deamidation and single or multiple amino acid substitutions — in a peptide sequence greatly affect a peptide's activity. Moreover, the studies further demonstrated the important balance between various parameters such as charge, hydrophobicity, amphipathicity, and helicity in determination of peptide/lipid interactions.

Chapter 3 demonstrated importance of tryptophan in Lys 49 phospholipase A2 that the lytic activiy of pEM-2 is strongly dependent on the model membrane composition As expected, electrostatic interaction played a more important role in initial recognition indicated by monolayer studies. However, the interaction between peptide and lipid bilayer verified through leakage study showed the importance of hydrophobic interaction and the role of tryptophan with satureated lipids where more dye leaked out from DPPC than DPPG vesicles.

Chapter 4 confirmed the mechanism of action of anoplin as non-specific and revealed the importance of amidation. There was no notable structural change, antibacterial activity, or peptide/monolayer interactions between full L- and D- anoplin. The deamidation of anoplin did not affect its helical content, however, the antibacterial activity, membrane binding, and lytic activity were all obviously influenced by the introduction of a negative charge at the C-terminus. All three derivatives adopted a more α-helical structure in the presence of anionic lipids. The peptide activity was also found to be cell membrane dependent, which correlated with CL quantity.

Chapter 5 exihibited UVRR spectroscopy is more sensitive in structural determination than conventional method circular dichroism spectroscopy using small peptide anoplin and two different derivatives (Ano8K and Ano1K5V8K). Both derivatives had a higher tendency to fold into an α-helix in membrane mimicking environment, with trisubstituted Ano1K5V8K being the most defined one. As a result, the two derivatives were more amphipathic at the cell membrane, which led to higher antimicrobial and hemolytic activity.

Chapter 6 investigated the role of the hinge in ltc2a by comparing the activity with its derivative ltc2aG11A, which is believed to be a more rigid single helix. Both latarcin 2a derivatives induced membrane reorganization by reducing line tension of liquid ordered phase upon the association of peptides. Presence of salt did not notably decrease the peptide activity but slightly altered the mode of action to disintegrate the supported lipid bilayers. The importance of cholesterol was evidenced using *in situ* AFM by visualizing its role in attenuating peptide-induced membrane disruption. The studies collectively found that only the cytotoxic activity ltc2a are dependent on the hinge, where ltc2aG11A is more hemolytic toward eukaryotic cells.

7.2 SUGGESTIONS AND FUTURE DIRECTION

Antimicrobial peptides pEM-2 and ltc2a, both extracted from snake venom, have shown their potential anticancer properties. Interestingly, pEM-2 and ltc2a have higher net charge than anoplin but they are effective towards zwitterionic saturated vesicles. In an effort to further clarify the activity and understand the involved mechanism of action of ltc2a and pEM-2, future studies could incorporate lipids such as phosphatidylserine

(increased component in cancer cells) in supported lipid bilayers. Alongside of using *in situ* AFM, using techniques such as force microscopy, X-PEEM and tip enhanced Raman spectroscopy will provide chemical and structural details on peptides' actions.

Furthermore, peptide activity comparison between symmetric and asymmetric bilayers would be an interesting investigation, as the latter resembles living cell membranes. Asymmetric bilayers controllably fabricated by the Langmuir Blodgett technique would provide additional understanding of the effect of anionic lipids (phosphatidylserine), present in the inner leaflet of mammalian membrane on peptide toxicity.

Finally, thorough studies on the effect of salt and serum levels on pEM-2, anoplin, and ltc2a on membrane activity would assist development of peptide drugs.